

**STUDY OF URANIUM LUMINESCENCE IN  
BOROPHOSPHATE AND BORATE HOSTS**

*By*

**ANNAPURNA ROUT  
CHEM02201104010**

**Indira Gandhi Centre for Atomic Research  
Kalpakkam**

*A thesis submitted to the  
Board of Studies in Chemical Sciences*

*In partial fulfillment of requirements  
for the Degree of*

**DOCTOR OF PHILOSOPHY**

*of*

**HOMI BHABHA NATIONAL INSTITUTE**



**August, 2018**



# Homi Bhabha National Institute

## Recommendations of the Viva Voce Committee

As members of the Viva Voce Committee, we certify that we have read the dissertation prepared by **Annapurna Rout** entitled “**Study of Uranium luminescence in borophosphate and borate hosts**” and recommend that it may be accepted as fulfilling the thesis requirement for the award of Degree of Doctor of Philosophy.

---

Chairman – Dr. M. Joseph

**Date:**

---

Guide / Convener – Dr. B.S. Panigrahi

**Date:**

---

Examiner -

**Date:**

---

Member 1- Dr. N. Sivraman

**Date:**

---

Member 2- Dr. K. Sundararajan

**Date:**

---

Final approval and acceptance of this thesis is contingent upon the candidate's submission of the final copies of the thesis to HBNI.

I/We hereby certify that I/we have read this thesis prepared under my/our direction and recommend that it may be accepted as fulfilling the thesis requirement.

**Date:**

**Place:**

**Dr. B.S. Panigrahi**

**Guide**



## **STATEMENT BY AUTHOR**

This dissertation has been submitted in partial fulfillment of requirements for an advanced degree at Homi Bhabha National Institute (HBNI) and is deposited in the Library to be made available to borrowers under rules of the HBNI.

Brief quotations from this dissertation are allowable without special permission, provided that accurate acknowledgement of source is made. Requests for permission for extended quotation from or reproduction of this manuscript in whole or in part may be granted by the Competent Authority of HBNI when in his or her judgment the proposed use of the material is in the interests of scholarship. In all other instances, however, permission must be obtained from the author.

**Annapurna Rout**



## **DECLARATION**

I, hereby declare that the investigation presented in the thesis has been carried out by me. The work is original and has not been submitted earlier as a whole or in part for a degree / diploma at this or any other Institution / University.

**Annapurna Rout**



## List of Publications arising from the thesis

### Journal

1. “Photoluminescence properties of U in SrBPO<sub>5</sub> host: Effect of concentration and annealing temperature”, **Annapurna Rout**, M. Mohapatra, N. Suriyamurthy, B.S. Panigrahi, *Journal of Luminescence*, **2015**, 167, 45-50.
2. “Uranium speciation and its site occupancy in alkaline-earth Borophosphates”, **Annapurna Rout**, Bhabani Shankar Panigrahi, Chandrani Nayak, Dibeyndu Bhattacharyya, Shambhu Nath Jha, *Journal of American Ceramic Society*, **2017**, 100, 2921–2931.
3. “Synthesis, characterization and photo luminescence studies of uranyl doped SrBPO<sub>5</sub>” **Annapurna Rout**, N. Suriyamurthy, and B. S. Panigrahi, Citation: *AIP Conference Proceedings*, **2015**, 1665, 040019. Publisher: American Institute of Physics.

### Conferences

1. “Luminescence investigation on: SrBPO<sub>5</sub>: UO<sub>2</sub><sup>2+</sup>, Eu<sup>3+</sup>”, **Annapurna Rout**, B.S. Panigrahi, N.Suriyamurthy, presented at “Recent trends in Spectroscopy-2014”, 20-21 June, at IITM, Chennai.
2. “Optical properties of uranyl doped SrBPO<sub>5</sub>: A green phosphor”, **Annapurna Rout**, B.S. Panigrahi, N.Suriyamurthy, presented at “International Conference On Advancements in materials, health & Safety towards sustainable energy & Environment (MHS-2014)”, 7-8<sup>th</sup> August 2014, Chennai.
3. “Synthesis, characterization and photoluminescence studies of uranium doped SrBPO<sub>5</sub>”, **Annapurna Rout**, B.S. Panigrahi, N. Suriyamurthy, presented at “59<sup>th</sup> DAE-Solid state physics symposium”, 16-20 December, 2014, VIT University, Vellore, T.N., India.
4. “Investigation of uranium luminescence in BaBPO<sub>5</sub>”, **Annapurna Rout**, B.S. Panigrahi, N. Suriyamurthy, presented at “5<sup>th</sup> International Conference on luminescence & Its Applications”, 9-12 Feb., 2015, Bangalore, India.
5. A fluorimetric study of europium 7 uranium complexes of DTPA in aq. solution, **Annapurna Rout**, B.S. Panigrahi, N.Suriyamurthy, presented at “4<sup>th</sup> International Conference on Luminescence & its Applications, 7-10, February, 2012, Hyderabad, India.

6. Photo luminescence investigation of uranium in  $\text{BaAl}_2\text{B}_2\text{O}_7$ , **Annapurna Rout**, U. madhusoodan, B.S. Panigrahi, presented at “NUCAR-2017”, at KIIT University, BBSR, Odisha, 6-10 Feb., 2017.

### **Others**

1. Luminescence studies on photo stimuable phosphor  $\text{CsBr: Eu}^{2+}$ , N. Suriyamurthy, B. S. Panigrahi , K. Dukenbayev , **Annapurna Rout** , S. K. Sekatskii & G. Dietler, Radiation Effects and Defects in Solids: Incorporating Plasma Science and Plasma Technology, **2013**, *168*, 146–152.

### **Communicated paper**

1. “Investigation of Photo luminescence and site occupancy of uranium in  $\text{BaAl}_2\text{B}_2\text{O}_7$ ”, **Annapurna Rout**, S.K. Panda, B.S. Panigrahi, *Journal of Luminescence*, Ref No- LUMIN\_2018\_1458.

**Annapurna Rout**

Dedicated to.....

My beloved Parents

Mr. Artatran Rout, Mrs Sabitri Rout



## ACKNOWLEDGEMENTS

I express my sincere thanks and gratitude to my Ph. D supervisor **Dr. B. S. Panigrahi**, for his guidance, strong support, and valuable suggestions throughout the course of my Ph. D program.

I am pleased to express my deep sense of gratitude to my doctoral committee chairman, **Dr. M. Joseph**, and members **Dr. N. Sivaraman**, **Dr. K. Sundararajan**, for their valuable suggestions, constant encouragement and insightful comments provided throughout the course of my Ph. D program. I also want to express my heartfelt thanks to my Head of Division **Mr. P. Muralidaran** for his cooperation and concern during my PhD work. I wish to express my special thanks to **Dr. H. N. Jena** for his kind help in XRD experiments. My deeply thanks to **Dr. Manoj Mohapatra**, RCD, BARC and **Dr. N. Suriyamurthy** for their guidance and valuable suggestions during my PhD work. I take immense pleasure in thanking **Dr. S. Majhi**, **Dr Satendra Kumar** for their support in life time measurement experiments. I wish to thank **Ms. Dhanya**, **Mr. Harish**, for their help and support during sample preparation. I am very much thankful to my friends **Dr. Prasant Kumar Nayak**, **Dr. S. K. Gupta**, **Mr. Arun Kumar Panda**, **Mr. Sanjit Parida**, **Ms Soja**, **Mr. S. K. Panda**, **Mr. Nimai Pathak**, **Mr. Manmath Das**, **Mr. G. Yatish Kumar** and **Mr. Arnav Chakravorthy** for their kind support during my PhD work. I take immense pleasure in thanking **Mrs P. Krithika**, who was there always with a helping hand. I want to express my heartfelt thanks to **Mr Ranjib Kumar Padhi** for his constant moral support and help. My special thanks to **Mrs Swagatika Panigrahi** for her love, affection, support and kind help that really contributed a lot to finish this work.

Last but always at the close to heart, I am fortunate to have blessings, love, support and encouragement from **my parents**, who made me stable and studious at all odd and even happenings. My heartfelt thanks to **Ashish**, **Trupti** and **Soumya** for their emotional support, entertainment and being a great company all the time. I am gratefull to my **in-laws and family** for their moral support. I am very much lucky to have strong support from my better half **Dr. Balaram Mohapatra**, for being a constant source of inspiration and encouragement, without his support and keen contributions the work would have not been at its shape as it is now. Finally lot of thanks to my little Angel **Pihu** and her cute smile who made my days joyful and cherrishing.

*Above all I thank the almighty for enabling me to complete the task.*

**Annapurna Rout**



# CONTENTS

<b>Title</b>		<b>Page No.</b>
<b>Synopsis</b>		<b>i</b>
<b>List of Figures</b>		<b>x</b>
<b>List of Tables</b>		<b>xv</b>
<b>CHAPTER 1: Introduction</b>		
1.	General Introduction	4
1.1.	Introduction to Luminescence	4
1.2.	Photo physical processes in electronically excited molecules	6
	1.2.1. Absorption	7
	1.2.2 Non-radiative forms of energy dissipation	11
	1.2.2.1 Vibrational relaxation	11
	1.2.2.2 Internal conversion	11
	1.2.2.3 Intersystem crossing	12
	1.2.3 Radiative form of transitions	12
	1.2.3.1 Fluorescence	12
	1.2.3.2 Phosphorescence	13
1.3.	Luminescent Material	14
1.4.	Introduction to thesis	16
1.5	Luminescence of Uranium	17
	1.5.1 Uranyl luminescence	20
	1.5.2 Luminescence of octahedral uranate	26
	1.5.3 Uranium luminescence in solids	28
1.6	Motivation for the present study	30
1.7	Scope of the thesis	32

1.8	References	34
<b>Chapter 2: General Experimental Procedures and Technical Details</b>		
2.1	Introduction	44
2.2	Phosphor synthesis by solid-state reaction	44
2.3	Phosphor synthesis by co-precipitation	45
2.4	Phosphor synthesis by combustion synthesis	45
2.5	Pelletizer	46
2.6	Tubular furnace	47
2.7	Characterization of phosphors by XRD and SEM	48
2.8	Spectrofluorimeter and life time decay studies	48
2.9	EXAFS Analysis	50
2.10	References	66
<b>Chapter 3: Photoluminescence properties of U in SrBPO<sub>5</sub> host: Effect of concentration and annealing temperature</b>		
3.1.	Introduction	54
3.2.	Experimental	56
3.3.	Results and Discussion	57
	3.3.1 Crystal structure and Morphology	57
	3.3.2 PL investigations	62
	3.3.3 Evaluation of color coordinates	68
3.4.	Conclusion	70
3.5	References	70
<b>CHAPTER 4: Uranium speciation and its site occupancy in alkaline earth borophosphates</b>		
4.1.	Introduction	76
4.2.	Experimental	79
4.3	Results and Discussion	81

	4.3.1 Crystal structure and morphology	81
	4.3.2 PL studies on U doped MBPO <sub>5</sub>	85
	4.3.3 EXAFS analysis	91
4.4.	Conclusion	98
4.5.	References	99
<b>CHAPTER 5: Understanding the energy transfer mechanism from Uranium to Europium and Samarium in SrBPO<sub>5</sub> <i>stillwellite</i> host</b>		
5.1.	Introduction	106
5.2.	Experimental	107
5.3	Results and discussion	108
	5.3.1 Crystal structure analysis	108
	5.3.2 PL studies on Eu doped SBP	109
	5.3.3 PL studies on Sm doped SBP	111
	5.3.4 PL studies on U doped SBP	113
	5.3.5 Understanding the energy transfer process from Uranium to Europium	115
	5.3.6 PL decay time investigations	118
	5.3.7 Calculation of the efficiency of energy transfer (optimum concentration for maximum energy transfer)	121
	5.3.8 Mechanism for the energy transfer process	123
	5.3.9 Understanding the energy transfer from uranium to samarium	127
	5.3.10 Calculation of the efficiency of energy transfer (optimum concentration for maximum energy transfer)	130
	5.3.11 PL decay time investigations	133
5.4.	Conclusions	136
5.5.	References	137
<b>CHAPTER 6A: Luminescence approach on Speciation of uranium in Barium borate (BaB<sub>2</sub>O<sub>4</sub>)</b>		
6A.1	Introduction	142
6A.2	Experimental	142

6A.3	Results and discussion	142
	6A.3.1 Crystal structure	142
	6A.3.2 Morphology	143
	6A.3.3 Photo luminescence (pl) investigation	144
	6A.3.4 Evaluation of color coordinates	147
6A.4	Conclusion	149
6A.5	References	149
<b>CHAPTER 6B: Investigation of Photo luminescence and site occupancy of uranium in BaAl<sub>2</sub>B<sub>2</sub>O<sub>7</sub></b>		
6B.1	Introduction	152
6B.2	Experimental	153
6B.3	Results and discussion	155
	6B.3.1 Crystal structure and morphology	155
	6B.3.2 PL investigations	156
	6B.3.3 PL decay time studies	159
6B.4	EXAFS studies on BaAl <sub>2</sub> B <sub>2</sub> O <sub>7</sub> : U	160
	6B.4.1 Ba L <sub>3</sub> edge	160
	6B.4.2 U L <sub>3</sub> edge	163
6B.5	Conclusions	165
6B.6	References	165
<b>Chapter 7: Summary and conclusions</b>		
7.1	Introduction	170
7.2.	Summary and conclusions	170
7.3	Scope for the future studies	173
<b>Glossary</b>		174

## Synopsis

### **1. Introduction**

The present era is in demand of energy and especially clean energy and towards this perspective one of the suitable and sustainable option is nuclear power. The emergence of nuclear industries has helped improving the global energy scenario to a better extent but at the same time it has also raised serious safety and security issues due to radio activities from its fissile/fertile materials as well as fission products. The detection and estimation of radioactive heavy metal ions in trace level is an important requirement. To this end, fluorescence spectroscopy involving lanthanides and actinides is a promising technique owing to its high sensitivity. Of all the actinide ions, uranium has gained much attention owing to its multiple oxidation states. The fluorescence property of uranium is quite interesting as uranium shows strong fluorescence in aqueous solution, solid ceramic matrices as well as in glasses [1, 2, 3, and 4]. Uranium doped glasses and ceramics are used as internal actinometers in biological chemistry [5], as luminescent sensors [6] and in uranium detection assays [7].

At present, uranium incorporated solid matrices are active area of research. It has gained much interest in nuclear fuel cycle. The solid hosts are one of the suitable options for long term storage of radioactive nuclear waste. Uranium is considered as an intermediate-level radioactive waste and its isotopes impart long-term dose. The conventional method of storage of high-level radioactive waste (HLW) arising from spent nuclear fuel is immobilization of HLW in vitreous waste form in alkali boro silicate glass matrix [8]. Although it is a standardized regular practice but certain drawbacks exist. In long run, certain fission products prefer to reside in a crystalline

phase which may lead to devitrification and instability of the glass matrix is likely to take place. In this context, ceramics are better candidates as they show better chemical, radiation and thermal stability than glasses [9]. To be very particular, ceramics that mimics natural minerals may serve the purpose well, wherein the fission product elements can be constrained resulting in radioactive stability and restricted leaching. Uranium being a heavy element, its incorporation and stabilization in solid matrices is always challenging. In many matrices Uranium is not soluble and may undergo for a second phase formation. In some matrices though it is soluble, its interaction with surrounding ligand field results with no luminescence i.e. non-radiative decay is proactive and extraction of information about it becomes difficult. Thus, it is of great interest to find a suitable solid matrix for radioactive waste.

In this regard Phosphate based ceramics are of great interest. It has been found to be an excellent host to stabilize substantial quantities of nuclear waste for a long term purpose [10]. In our present study uranium doped in alkaline earth boro phosphate ( $MBPO_5$ ,  $M = Ca, Sr, Ba$ ) as well as in borate matrix ( $BaB_2O_4$ ,  $BaAl_2B_2O_7$ ) has been discussed from different perspectives.

## **2. Scope of the present study**

In present study we have investigated luminescence properties of uranium doped boro-phosphate solid matrices such as  $CaBPO_5$ ,  $SrBPO_5$ , and  $BaBPO_5$  and also uranium doped borate matrices such as  $BaB_2O_4$  and  $BaAl_2B_2O_7$ . Our study involves synthesis as well as characterization of the solid matrices. Here one of our prime objectives is to probe the oxidation state of uranium in different solid matrices. In addition to this, information regarding the form of stabilization of uranium is also quite interesting. In order to validate the matrix with respect to accommodating uranium the compatibility

with the host environment with its increased concentrations were also evaluated. The coordination behaviour with the surrounding ligand atoms present in host is an important fact to discuss as it gives an idea about uranium speciation depending on the host matrix and therefore, studies were carried out in that direction. Uranium being a green emitter is always known to be a good donor for red emitters, thus its behaviour towards a co-dopant like Eu/Sm were also investigated to probe possible energy transfer phenomenon.

### **3. Organization of the thesis**

#### **3.1. Chapter 1**

This chapter is an introductory chapter to the thesis. To start with a brief introduction to luminescence, its modern day applications and advantages have been discussed. In order to give a clear insight in to luminescence, its basic mechanisms are also described. Various luminescent materials and its application in different fields such as lighting, imaging and detection are highlighted. The emergence of different types of solid host matrices and varieties of dopant ions are also discussed. Followed by this a brief introduction to thesis has been given. This particular section mainly deals with basics of uranium luminescence. The electronic origin behind uranium luminescence is discussed. The luminescence behaviour of different forms of uranium i.e. uranyl, uranate is also discussed. Uranium luminescence in different solid host matrices is briefly noted here. Importance of analysis of uranium luminescence spectra to elucidate information about the matrix as well as uranium itself is also explained. Next to this the motivation towards present work i.e. incorporation of uranium in to solid ceramics has been highlighted followed by the scope of the thesis i.e. the brief representation of our thesis work has been discussed.

### **3.2. Chapter 2**

This chapter describes the experimental procedures of synthesis of phosphors through different routes and the analytical techniques used to characterize and study the luminescence properties of the phosphors. The conventional solid state, co-precipitation and combustion routes were followed for sample preparation whereas XRD and SEM were used for characterization of structure and morphology of samples respectively. Luminescence and life time decay were carried out for detailed photo luminescence study. EXAFS analysis was done for speciation and site occupancy studies of uranium.

### **3.3. Chapter 3**

This chapter is more about luminescence of uranium in Strontium borophosphate ( $\text{SrBPO}_5$ ) matrix. Strontium borophosphate (SBP) with and without uranium doped samples were synthesized through solid state reaction route in air atmosphere at different annealing temperatures. The dopant ion concentration was varied between 1 to 8 mole percent. X ray diffraction studies confirmed the formation of single phase compound in all the samples without any impurity phase up to 8 mol% of the dopant ion. The overall morphology and particle size was confirmed by scanning electron microscopic studies which suggested the presence of uneven, agglomerated particles with less than 1  $\mu\text{m}$  individual size. It was observed that upon annealing at higher temperatures, the particles get agglomerated more and more with smooth boundaries. Photoluminescence (PL) studies confirmed stabilisation of uranium as uranyl ion ( $\text{UO}_2^{2+}$ ) in the system. Based on the PL emission data concentration quenching was observed beyond 7 mol% of the dopant ion concentration. The critical distance ( $L_c$ ) was estimated to be 3 Å suggesting Dexter type of energy transfer mechanism

responsible for the quenching. The life time decay studies indicated the presence of two different types of environment around Uranyl ion. On annealing at temperatures beyond 900°C the PL emission and decay time reduced drastically. It was concluded that on annealing at temperatures beyond 900°C, defect centres get agglomerated around the metal ion providing non radiative pathways for the energy to get dissipated thereby reducing the PL emission and decay time. Color coordinates were evaluated for the 7 mol% uranium doped sample annealed at 900°C. The values suggested that the system can be used as a potential green emitting phosphor material.

### **3.4. Chapter 4**

This chapter mainly deals with Uranium luminescence and its speciation in a series of Alkaline earth (calcium, strontium and barium) boro phosphate matrices. In brief the alkaline earth (calcium, strontium and barium) boro phosphates doped with uranium (U) were prepared through conventional solid state reaction route. The form of stabilized uranium in these solid matrices was characterized and investigated using X-ray diffraction (XRD), photo luminescence (PL) and extended X-ray absorption fine structure (EXAFS). XRD measurements confirmed the single phase formation of uranium doped alkaline earth boro phosphate samples. The PL of uranium in calcium and barium borophosphate is studied for the first time. Photoluminescence studies indicated presence of uranium as Uranyl in SrBPO<sub>5</sub> and CaBPO<sub>5</sub> matrices whereas in case of BaBPO<sub>5</sub> the indication was for uranate species. The life time data corroborated presence of a different uranium species in SrBPO<sub>5</sub>, CaBPO<sub>5</sub> and BaBPO<sub>5</sub>. The site occupancy of uranium was further probed using EXAFS which confirmed that in case of BaBPO<sub>5</sub>, uranium enters the host as uranate whereas in case of SrBPO<sub>5</sub> and CaBPO<sub>5</sub>, uranium enters as Uranyl.

### **3.5. Chapter 5**

In this chapter an investigation of energy transfer phenomenon from Uranium to europium as well as samarium in Strontium borophosphate matrix was carried out. Often the f-f transition of the lanthanide ions suffers from poor (direct) excitation and emission cross section due to their forbidden nature. This can be overcome by the use of a suitable co-dopant ion which can transfer its energy to the lanthanide thereby increasing the overall efficiency of the system. In this context, SBP samples incorporated with Eu and co-doped with U were synthesized via solid state reaction route and the possible energy transfer mechanism was investigated using photoluminescence spectroscopy. It was observed that while 'Eu' was stabilised in its trivalent state, uranium was stabilised as the uranyl ion ( $\text{UO}_2^{2+}$ ) in this stillwellite host. In the co-doped system, uranyl to europium energy transfer was observed. Detailed mechanism for the observed energy transfer was studied using emission, excitation and photoluminescence decay time measurements. Similar studies were also carried out for SBP: U, Sm and here also energy transfer process was discussed.

### **3.6. Chapter 6**

This chapter deals with luminescence of uranium in barium borate ( $\text{BaB}_2\text{O}_4$ ) and  $\text{BaAl}_2\text{B}_2\text{O}_7$  host matrices. It includes synthesis, characterization, luminescence studies, life time decay studies, colour co-ordinate calculation. The uranium site occupancy and its speciation studies by EXAFS measurements were also reported here.

### **3.7. Chapter 7**

This chapter summarizes the results and conclusions obtained in the present work. This chapter also discusses about scope for the future work in this field.

### 3.8. References

1. Azenha MEDG, Burrows HD, Formosinho SJ, Mignel MGM, Daramanyan AP, Khudyakov V. On the Uranyl ion luminescence in aqueous solutions. *J Lumin.* 1991; 48–4:522-526.
2. Blasse G, Bleijenberg KC, Krol DM. The Luminescence of hexavalent uranium in solids. *J Lumin.* 1979; 18-19:57-62.
3. Mohapatra M, Rajeswari B, Kadam RM, et al. Investigation of uranium luminescence in SrB4O7 matrix by time resolved photoluminescence, thermally stimulated luminescence and electron spin resonance spectroscopy. *J Alloys Compd.* 2014; 611:74-81.
4. E. Rabinowitch, R.L. Bedford, *Spectroscopy and Photochemistry of Uranyl Compounds*, Pergamon Press, Oxford, 1964, pp. 112.
5. A Bucholtz, *Ann. Chim. Phys.* 56 (1805) 142; V. Gopal, J. Xavier, M.Z. Kamal, S. Govindarajan, M. Takafuji, S. Soga, T. Ueno, H. Ihara, N.M. Rao, *Bioconjugate. Chem.* 22 (2011) 2244.
6. D. Pestov, C.-C. Chen, J.D. Nelson, J.E. Anderson, G. Tepper, *Sens. Actuators B* 138 (2009) 134.
7. J. Liu, A.K. Brown, X. Meng, D.M. Crokek, J.D. Istok, D.B. Watson, Y. Lu, *Proc Natl. Acad. Sci. U.S.A.* 104 (2007) 2056; N.W. Hayes, C.J. Tremblett, P.J. Melfi, J.D. Sessler, A.M. Shaw, *Analyst* 133 (2008) 616.
8. D. Gombert, *Global Nuclear Energy Partnership-Materials Disposition And Waste Form Status, Report*, GNEP-WAST-AI-TR-2007-00013, 2007.
9. S.V. Stefanovsky, A.G. Ptashkin, O.A. Knyazev, S.A. Dmitriev, S.V. Yudintsev, B.S. Nikonov, *J. Alloys Compd.* 444–445 (2007) 438–442.

10. Raicevica S, Wrightb TJV, Veljkovic V, Conca JL. Theoretical stability assessment of uranyl phosphates and apatites: selection of amendments for in situ remediation of uranium. *Sci Total Environ.* 2006; 355:13-24.



## List of Figures

Figure No.	Title of the Figure	Page No.
1.1.	The foundation of a typical Jablonski diagram	6
1.2.	Possible absorption transitions from ground electronic state to higher electronic states	8
1.3.	Frank-Condon energy diagram	9
1.4.	A schematic Jablonski diagram presenting possible electronic transitions	10
1.5	Role of Elements in making phosphor	15
1.6	A comparison of f-state energies of 3+ lanthanide and actinide ions having the same number of f-electrons. The J value of the ground and predominant emitting f state is shown	18
1.7	Energy level diagrams for the trivalent actinide ions doped in LaCl <sub>3</sub> , illustrating the ground state and excited state energy levels	19
1.8	One electron MO's of a collinear O-U-O entity. The MO's are shown separated in to their component AO's for reasons of clarity	21
1.9	Deconvoluted spectra of uranyl absorption, 40.1mmol/L uranyl, 5 mmol/L nitrate ion	22
1.10	Schematic energies of Uranyl valence orbitals	23
1.11	Emission (solid line) and absorption (dashed line) spectrum of Uranyl ion in 0.1M NaClO <sub>4</sub> at 25 °C. Wavelengths given in nm	25
1.12	Emission spectrum of SrB <sub>4</sub> O <sub>7</sub> : U, at $\lambda$ excitation= 246 nm: representing UO <sub>6</sub> <sup>6-</sup> emission profile	27
1.13	Room temperature excitation spectrum of SrZrO <sub>3</sub> : U under $\lambda$ emission of 537 nm; representing excitation profile of UO <sub>6</sub> <sup>6-</sup>	28
2.1.	Combustion flame generated during combustion synthesis	46
2.2.	Schematic sketch of modified tubular furnace	48
2.3.	Shimadzu RF 5301pc spectrofluorimeter	49
2.4.	Image of solid sample holder	50
2.5.	Optical layout of BL-9	51
3.1.	(A) Shows the crystal structure of SrBPO <sub>5</sub> showing the 8 coordinated 'Sr' site; The figure 1 (B) shows the crystal structure with the two planes (2 0 0) and (1 0 4) (the shaded region) that show the highest intensity in XRD data.	58
3.2.	XRD patterns for SrBPO <sub>5</sub> doped with uranium as a function of dopant ion concentration (in mole %) A- 1 mole%, B- 4mole% C- 8 mole%; all samples are synthesized at 900°C	59

	annealing temp. The figure D indicates the standard pattern of the ICDD file no- 18-1270.	
3.3.	XRD patterns for SrBPO <sub>5</sub> doped with uranium as a function of annealing temperature	60
3.4.	SEM micrographs of the SBP samples as a function of annealing temperature; A-900, B-1000 and C-1100 °C.	62
3.5.	PL emission spectra of the SBP:U system as a function of dopant ion concentration; the inset figure shows the emission intensity values for the 520 nm peak as a function of Uranium concentration.	63
3.6.	Excitation spectrum for the 7 mol% uranium doped SBP system annealed at 900 °C	66
3.7	PL emission spectra for the U: SBP system as a function of annealing temperature	67
3.8	PL decay time data for the U: SBP system as a function of annealing temperature	68
3.9	CIE chromaticity diagram for the SBP: U (7 mol %) system annealed at 900 °C; The coordinates are demarked by an asterisk	69
4.1.	XRD pattern of undoped and uranium doped (a) CaBPO <sub>5</sub> (b) SrBPO <sub>5</sub> and (C) BaBPO <sub>5</sub>	82
4.2.	XRD Rietveld analysis of a) CaBPO <sub>5</sub> : U b) SrBPO <sub>5</sub> : U c) BaBPO <sub>5</sub> : U sintered at 900 °C, 3h	83
4.3.	Schematic presentation of crystal structure of MBPO <sub>5</sub> system; M= (Ca <sup>2+</sup> , Sr <sup>2+</sup> , Ba <sup>2+</sup> ).	84
4.4	SEM micrographs of the MBPO <sub>5</sub> : U samples; a) CaBPO <sub>5</sub> : U b) SrBPO <sub>5</sub> : U c) BaBPO <sub>5</sub> : U	84
4.5	Emission spectra of 1 mole% uranium doped in (a) SrBPO <sub>5</sub> (b) CaBPO <sub>5</sub> and (c) BaBPO <sub>5</sub> at 440 nm excitation wavelength. The inset shows a magnified (a)	85
4.6	Excitation spectra of 1 mole% uranium doped in (a) CaBPO <sub>5</sub> (b) SrBPO <sub>5</sub> and (c) BaBPO <sub>5</sub> at 519 nm emission wavelength. The inset shows a magnified (b)	86
4.7	Luminescence decay time profile of (a) BaBPO <sub>5</sub> : U (b) SrBPO <sub>5</sub> : U and (c) CaBPO <sub>5</sub> : U under 440 nm excitation and 519nm emission wavelength	89
4.8	XANES spectra of MBPO <sub>5</sub> : U along with UF <sub>4</sub> and UO <sub>2</sub> CO <sub>3</sub>	91
4.9	Normalized EXAFS spectra of U doped MBPO <sub>5</sub> , at U L3 edge	92
4.10	EXAFS spectra in L space for MBPO <sub>5</sub> : U	94

4.11	$\chi(r)$ vs $(r)$ at Sr K edge in SrBPO <sub>5</sub> : U sample	97
5.1.	(a) XRD patterns for the undoped SBP, (b) Eu (1 mol%) doped SBP, (c) U (1 mol%) doped SBP, (d) U and Eu co-doped SBP, (e) Standard (ICDD) pattern no-18-1270	109
5.2.	(a) XRD patterns for the undoped SBP, (b) Sm (1 mol%) doped SBP, (c) U (1 mol%) doped SBP, (d) U and Sm co-doped SBP, (e) Standard (ICDD) pattern no-18-1270	110
5.3.	PL (a) excitation and (b) emission spectra for the 0.1 mol% Eu doped SBP sample	111
5.4.	PL emission spectrum of SBP: Sm, at an excitation wavelength of 410 nm	112
5.5.	PL excitation spectrum of SBP: Sm, at an excitation wavelength of 596 nm	113
5.6.	PL a) excitation and b) emission data of uranium (1 mol %) doped SBP	114
5.7.	PL emission spectra of U, Eu and U-Eu co-doped SBP with $\lambda_{ex} = 440$ nm (corresponding to uranyl excitation)	116
5.8	PL emission spectra of Eu (fixed at 0.1 mol %) SBP co-doped with varying Uranium concentration	117
5.9.	PL emission spectra of Eu <sup>3+</sup> in U- Eu co-doped SBP at (a) $\lambda_{ex} = 440$ nm and (b) $\lambda_{ex} = 394$ nm	118
5.10.	Spectral overlap of a) excitation spectrum of SBP doped with Eu <sup>3+</sup> (0.1 mol %) and b) emission spectrum of SBP doped with U (0.1 mol%)	119
5.11.	PL decay time data for the U and Eu+U co-doped samples with $\lambda_{ex} = 440$ nm and $\lambda_{em} = 521$ nm (corresponding to the uranyl species)	121
5.12.	PL emission spectra of SBP doped with U (1.0 mol %) with varying Europium concentration	122
5.13.	Energy transfer efficiency ( $\eta_T$ ) of the SBP samples doped with UO <sub>2</sub> <sup>2+</sup> (1 mol %) and co-doped with varying Eu <sup>3+</sup> concentration	123
5.14.	Dependence of $I_s/I_{so}$ of uranyl on (a) $C_{U+Eu}$ , (b) $C_{U+Eu}^{6/3}$ (c) $C_{U+Eu}^{8/3}$ and (d) $C_{U+Eu}^{10/3}$	125
5.15	A schematic energy level diagram explaining the energy transfer process from uranium (UO <sub>2</sub> <sup>2+</sup> ) to europium (Eu <sup>3+</sup> ) in SBP host	126
5.16	PL emission spectra of U, Sm and U-Sm co-doped SBP at different $\lambda_{ex}$	127

5.17	PL emission spectra of Sm (fixed at 0.1 mol %) SBP co-doped with varying Uranium concentration at $\lambda_{ex} = 424$ nm	129
5.18	Spectral overlap of a) excitation spectrum of SBP doped with $Sm^{3+}$ (0.1 mol %) and b) emission spectrum of SBP doped with U (1 mol %)	130
5.19	Emission spectra of a) Sm (0.3 mol%) at $\lambda_{exc.}$ 401 nm b) U (1 mol%) + Sm (0.3 mol%) at $\lambda_{exc.}$ 424 nm c) U (1 mol%) + Sm (0.3 mol%) at $\lambda_{exc.}$ 401 nm d) U (1mol%) at $\lambda_{exc.}$ 424 nm.	131
5.20	Emission spectra of SBP: U, Sm at Constant U (1 mol%) varying Sm concentration from 0.1 mol% to 0.5 mol% at an excitation wavelength of 424 nm	132
5.21	Energy transfer efficiency vs mol% of Sm plot	133
5.22	Life time decay curves of SBP: U, Sm systems	134
5.23	Life time of Uranium with increased concentration of Samarium in SBP: U (1 mol %) + Sm (x mol %), x= 0.1, 0.3, 0.5	135
5.24	A schematic energy level diagram explaining the energy transfer process from uranium ( $UO_2^{2+}$ ) to Samarium ( $Sm^{3+}$ ) in SBP host	136
6A.1.	PXRD pattern of $BaB_2O_4$ , $BaB_2O_4$ : U, standard $BaB_2O_4$	143
6A.2	SEM image of $BaB_2O_4$ : U system, synthesized via co-precipitation route	144
6A.3.	PL emission spectra of $BaB_2O_4$ : U	145
6A.4.	PL excitation spectra of $BaB_2O_4$ : U	146
6A.5	Photoluminescence decay profile of $BaB_2O_4$ : U at $\lambda_{exc.} = 360$ nm	147
6A.6	CIE chromaticity diagram for the $BaB_2O_4$ : U system, the coordinates are demarked by an asterisk	148
6B.1	XRD patterns of undoped and uranium doped $BaAl_2B_2O_7$ with a reference of standard ICDD 86-2168 pattern	155
6B.2	Schematic presentation of crystal structure of $BaAl_2B_2O_7$ system	156
6B.3	PL emission spectra of the $BaAl_2B_2O_7$ : U system at an excitation wavelength of 285nm	158
6B.4	PL excitation spectra of the $BaAl_2B_2O_7$ : U system at an emission wavelength of 550nm	159
6B.5	PL decay curve of the $BaAl_2B_2O_7$ : U system at an $\lambda_{emission}$ of 550 nm and $\lambda_{excitation}$ of 285 nm	160
6B.6	XANES spectra of the $BaAl_2B_2O_7$ and U doped $BaAl_2B_2O_7$ samples at Ba $L_3$ edge	161
6B.7	$\chi(r)$ versus $r$ plots of $BaAl_2B_2O_7$ and U doped $BaAl_2B_2O_7$ samples at Ba $L_3$ edge	162
6B.8	XANES spectra of the U doped $BaAl_2B_2O_7$ sample at U $L_3$	163

	edge along with $\text{UO}_2\text{CO}_3$ standard	
6B.9	$\chi(r)$ versus $r$ plots (or FT-EXAFS spectra) of the U doped $\text{BaAl}_2\text{B}_2\text{O}_7$ sample at U $L_3$ edge	164

## List of Tables

<b>Table No.</b>	<b>Title of theTable</b>	<b>Page No.</b>
1.1	Types of luminescence	5
3.1.	X-ray diffraction data of SBP: U system	63
4.1	Life time decay values of MBPO5: U	90
4.2.	U L3 edge EXAFS results	95
4.3.	Sr K edge EXAFS results	96
5.1	PL decay time values for the U and Eu-U co-doped samples with 440 nm excitation and 521 nm emission.	120
5.2	Life time values of SBP: U, SBP: Sm and SBP: U, Sm systems	134
6B.1	EXAFS Results of Ba L <sub>3</sub> edge	163
6B.2	EXAFS Results of U L <sub>3</sub> edge	164



# **Chapter 1**

## **Introduction**



## **1. General Introduction:**

The field of luminescence has achieved a sustained growth both in fundamental aspects and applications in a highly interdisciplinary area like chemical sciences, physics, mineralogy, gemmology, biophysics, biochemistry as well as in biotechnology. This powerful tool has been proved to be sensitive enough to replace radioactive tracers for many biochemical measurements [1-6]. It is extensively used in flow cytometer, medical diagnostics, DNA sequencing, forensics and genetic analysis [7-13]. Fluorescence in situ hybridization (FISH) technology has brought advancement in determining the chromosomal assignment and sub chromosomal localization of cloned DNA sequences [14-19] Fluorescence resonance energy transfer (FRET) technology is an advanced process used to study protein interactions, detect specific nucleic acid sequences and used as biosensors [20-25]. It can also improve imaging of intracellular molecules, even at the level of single-molecule detection. This effective technique is also dominating in coal petrology and mineral oil exploration [26, 27]. At present in the global portfolio one of the best contribution of fluorescence spectroscopy is development of phosphor based white light emitting diodes (WLED) leading to significant conservation of energy [28-36].

### **1.1 Introduction to Luminescence:**

The word “Luminescence” is derived from a Latin word *lumen* which means light. In 1888 Eilhardt Wiedemann [37] a German physicist proposed the definition of luminescence as “for all those phenomena of light which are not solely due to the rise in temperature”. In general, a molecule placed at higher energy level is unstable and to attain stability it undergoes de-excitation process, loses energy and returns to ground state. Luminescence is a photo physical phenomena where the molecule gets excited to its higher electronic states

by non-thermal excitation and during de-excitation emits light in the visible or near visible region. Depending on the excitation source luminescence can be termed differently (Table 1.1).

**Table. 1.1 Types of luminescence**

<b>Type</b>	<b>Excitation source</b>	<b>Applications</b>
<b>Photoluminescence</b>	<b>UV photons</b>	<b>Fluorescent Lamps</b>
<b>X-Ray Luminescence</b>	<b>X-rays</b>	<b>X-Rays intensifier</b>
<b>Cathode luminescence</b>	<b>Electrons</b>	<b>TVs, monitors</b>
<b>Electro Luminescence</b>	<b>Electric field</b>	<b>LEDs, EL Displays</b>
<b>Thermo Luminescence</b>	<b>Heat</b>	<b>Age determination</b>
<b>Chemiluminescence</b>	<i>Chemical Reaction</i>	<b>Emergency Signals</b>
<b>Bioluminescence</b>	<b>Bio Chemical Reaction</b>	<b>Fireflies, Jelly fish</b>
<b>Sonoluminescence</b>	<b>Ultrasound</b>	-
<b>Mechanoluminescence</b>	<b>Mechanical Energy</b>	-

When the excitation source is electromagnetic radiation such as ultra violet or visible radiation the luminescence process is termed as ‘Photoluminescence’. Depending on the nature of excited states, luminescence can be divided into two categories, the fluorescence and phosphorescence. In fluorescence the transitions occur between singlet states, a spin allowed transition with radiative life time of  $10^{-7}$ – $10^{-8}$  s whereas in phosphorescence the emission is from triplet state, a spin forbidden transition with the life time of about  $10^{-3}$ – $10^{-4}$  s. The emitted wavelength is longer than incident wavelength and the difference between absorption and emission maxima is called Stokes [38] shift.

### 1.2 Photo physical processes in electronically excited molecules:

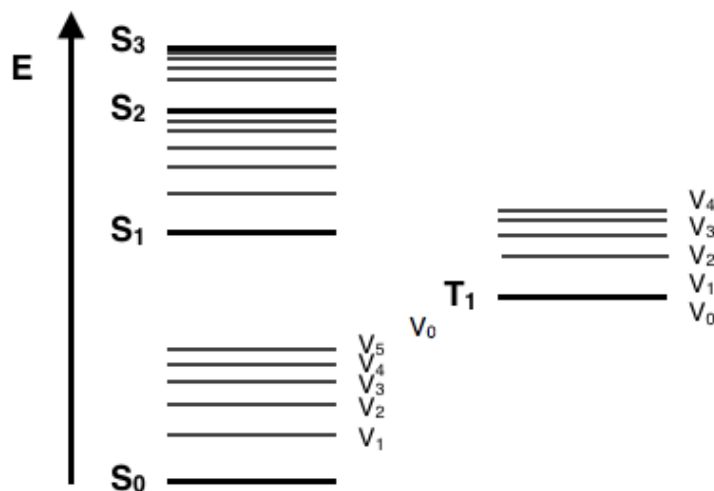


**Figure 1.1: The foundation of a typical Jablonski diagram [web ref.1]**

The Photo physical processes can be better explained by Jablonski Diagram proposed by Aleksander Jablonski, a Polish academic [39]. This represents (Figure 1.1) energy levels on a vertical axis.

The energy levels here are schematically represented and quantitatively denoted. Here for a particular molecule vertical columns are arranged and the columns represents specific spin multiplicity. The horizontal lines present in a column represents eigenstates for a particular molecule. Among the horizontal lines the bold one indicates the limits of electronic energy states. The electronic energy states are consist of several vibronic energy states. Irrespective of several possible vibrations, only a few of the vibrational eigenstates are taken in to consideration. Each vibrational energy state is again associated with rotational energy levels; however, typical Jablonski diagram does not consider rotational energy levels in details. According to classical mechanics, the difference in energy at higher electronic energy states becomes continually less, and slowly it becomes a continuum. In addition to this the vibronic energy levels are more prone to overlap with each other as the electronic energy levels get closer approximation. When a molecule get exposed to a particular wavelength, it absorbs some energy and depending on the absorbed energy transition happens. Throughout the diagram straight and curved lines are used to show different types of transitions between eigenstates. Here the conversion of energy of an electron in to a photon of light is shown by straight lines whereas curved lines represent transitions of electrons without any light emission.

### **1.2.1 Absorption:**

Jablonski diagram explains absorption as an electron excitation process. Here the electron excites from a lower energy level and falls in to a higher energy level (Figure 1.2). Absorbance takes place on the order of  $10^{-15}$  seconds and here it is indicated by a straight arrow line. The eigenstate to which the electron transition takes place is governed by the energy of the photon. The energy difference between two different eigen states are the only energies that can be absorbed. The most probable electronic transitions occurs from the lowest (ground) electronic state.

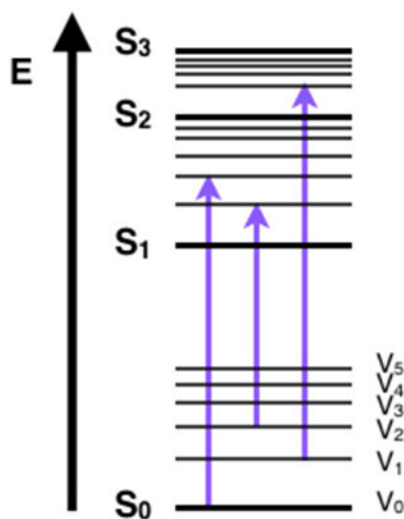


**Figure 1.2: Possible absorption transitions from ground electronic state to higher electronic states [web ref 2]**

The availability of electrons in the ground electronic state follows Boltzmann distribution law and it is a function of the Boltzmann's constant as well as the temperature of the system. The electrons present in the low lying ground state make transition to excited electronic states which are comprised of vibrational states. Although there are several electron transitions take place from the ground state but the most important i.e the most probable electronic transition during photon absorption is that, which originates from the center of

$v=0$  vibrational level. The time taken for an electronic transition is of the order of  $10^{-15}$ s, whereas the time period for vibration is about  $10^{-13}$  s which is nearly 100 times slow resulting in no change in inter-nuclear distances (Born-Oppenheimer approximation) during light absorption. Hence, the electron transition is represented by a vertical line which is parallel to the potential energy axis and originates from the lower potential curve to the upper excited state curve. According to Franck-Condon principle "Electronic transitions (on the order of  $10^{-15}$  s) are so fast when compared to the nuclear motion on the order of  $10^{-13}$  s that immediately after the transition, there is no relative change in the position and momentum of the involved nuclei. It expresses the difficulties of rapid conversion of electronic energy into vibrational kinetic energy. It has given importance to the conservation of momentum and position of the nuclei during electronic transitions.

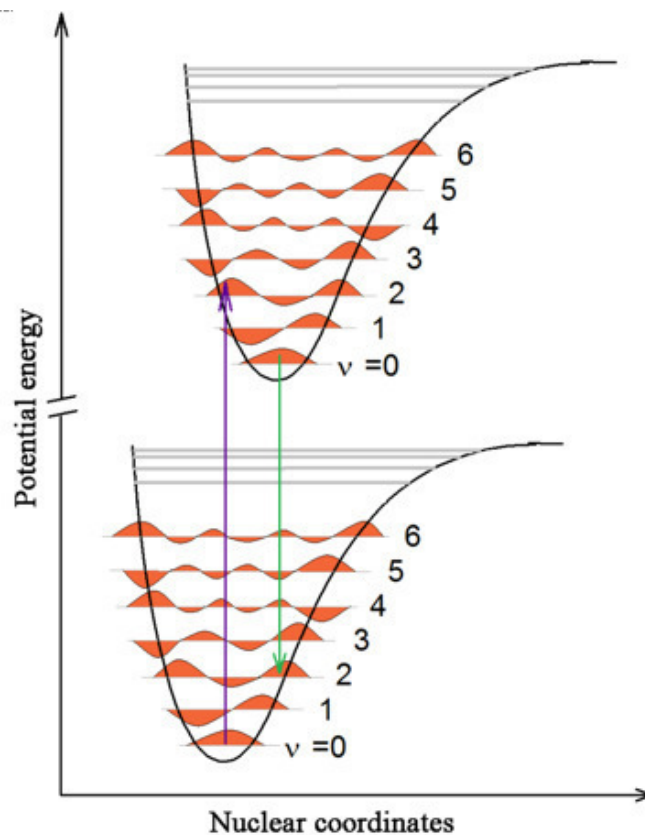


**Figure 1.3: Frank-Condon energy diagram [web ref 3]**

In Frank-Condon energy diagram, the most probable transition is represented as a straight vertical line arising from the lower potential curve running parallel to the potential energy axis and finally meets the upper excited state curve. According to Franck Condon principle “The time scale for electronic transitions are very short ( $10^{-15}$  s) when compared to the nuclear motion ( $10^{-13}$  s) and thus immediately after the electronic transition, the nuclei possess nearly the same relative position and momentum as earlier (Figure 1.3).

The electronic transitions are governed by following selection rules.

- i) no restriction on changes in  $n$ ;  $\Delta n = \text{any value}$ .
- ii) S can combine with its own value;  $\Delta S = 0$
- iii) L can vary by 0 or  $\pm 1$  unit;  $\Delta L = 0, \pm 1$
- iv) Laporte rule: J can vary by 0 or  $\pm 1$  except that  $J = 0$  to  $J = 0$  transition is not allowed;  $\Delta J = 0, \pm 1$

An excited electron has multiple ways to dissipate its excited energy. The energy dissipation can occur either in a non-radiative way or in a radiative way. Figure 1.4 represents the possible electronic transitions.

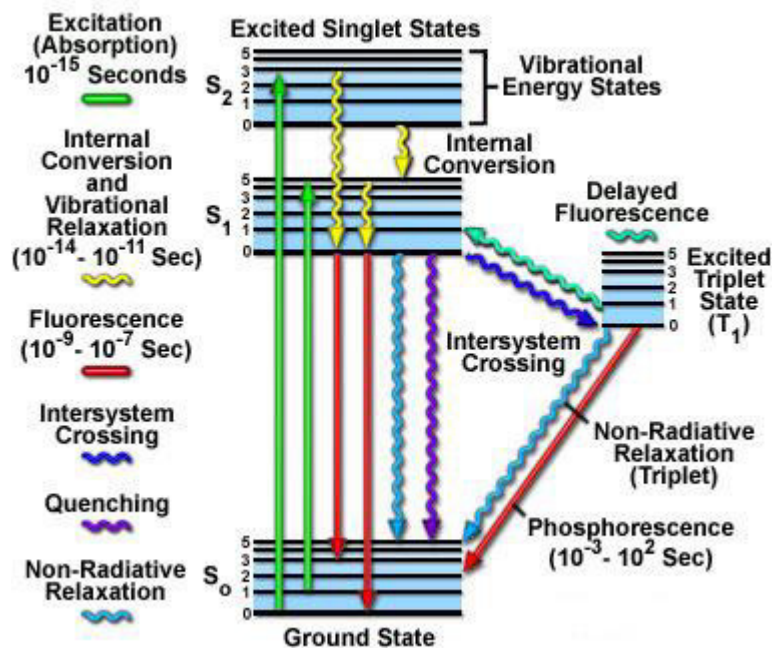


Figure 1.4: A schematic Jablonski diagram presenting possible electronic transitions

[web ref 4]

## 1.2.2 Non-radiative forms of energy dissipation:

### 1.2.2.1 Vibrational relaxation:

It is a non-radiative process. The curved arrow between vibrational levels in fig.1.4 shows vibrational relaxation. Here the excited energy associated to the electron is dissipated away to various nearby vibrational modes as kinetic energy. This kinetic energy again can be dissipated to nearby molecule. This process happens in the order of  $10^{-14}$  to  $10^{-11}$  seconds. Being a very fast transition, vibrational relaxation mostly occurs immediately after the absorbance. Vibrational relaxation shows limitations and its occurrence is within the vibrational levels.

#### **1.2.2.2 Internal conversion:**

Transition of an excited electron from a higher vibration level in one of the higher electronic state to another vibration level placed in a lower electronic state is termed as internal conversion. The reason is vibrational energy levels show strong overlap with electronic energy levels and thus the excited electron makes the transition. The internal conversion process is almost mechanistically similar to vibrational relaxation. In figure 1.4 shows internal conversion by curved arrow lines showing transition between two vibrational levels placed in different electronic states. With increase in energy level, the manifold of vibrational and electronic eigenstates becomes closer.

At higher energy levels, the manifold of vibrational energy levels and electronic levels shows very good overlapping. This energy overlap leads to an easy path way for electron transition between vibrational levels and finally it falls in to a lower electronic state. The time frame for both internal conversion and vibrational relaxation are almost same and that

is why it is very likely for molecules to lose energy from light perturbation. The large energy difference between ground state energy level and the first excited state energy level does not allow overlapping of corresponding vibrational levels and thus internal conversion is not favorable. Electron transitions are always associated with both vibrational relaxation as well as internal conversion.

### **1.2.2.3 Intersystem crossing:**

An excited electron may follow intersystem crossing for the dissipation of excited. Here interestingly within the time frame of  $10^{-8}$  to  $10^{-3}$ S the electron changes its spin multiplicity from an excited singlet state to an excited triplet state. In Fig. 1.4 intersystem crossing is shown. This is the slowest electronic transition process. As per to electronic selection rules this transition is a forbidden one as it does not follow spin conservation rules but the spin orbit coupling relaxes the rule and thus inter system crossing is partially allowed transition. This is also a competitive process with respect to fluorescence. There are also various other non-radiative transitions which lead to many of the molecules not exhibiting fluorescence or phosphorescence. The molecular collision, quenching, energy transfer between molecules, and self-absorption are some of the above process. The overlap in absorption and fluorescence spectrums of a molecule or between two different molecules facilitates energy transfer process. These non-emitting processes takes away the excited energy in a non-radiative way and thus fluorescence gets affected or quenched.

### **1.2.3 Radiative form of transitions:**

#### **1.2.3.1 Fluorescence:**

The radiative pathway deals with emission of photon upon absorption of photon. One form of radiative pathway is termed as fluorescence. The straight line in figure 1.4, i.e. going down parallel to the energy axis between several electronic states represent fluorescence. Fluorescence occurs in the time frame of  $10^{-9}$  to  $10^{-7}$  seconds and thus is a slow process. Fluorescence is an allowed transition and it follows the spin multiplicity rule. At higher energy states, non radiative paths like internal conversion and vibrational relaxations are dominating processes for energy dissipation so when an electron reaches in the first excited electron state, the most probable transition is to the ground electron state and this is known as fluorescence. There is an energy difference between exciting photon and emitted photon in fluorescence process and it is obvious as this difference arises as some of the excited electron undergoes several no-radiative process like internal conversions, vibrational relaxations before coming to the first excited state.

#### **1.2.3.2 Phosphorescence:**

Phosphorescence is also a radiative transition process. Here excited electron placed at excited triplet state make a slow transition to the singlet ground state with a time scale of  $10^{-4}$  to  $10^{-1}$ S. As the spin multiplicity changes during the transition, so this process also a forbidden one. In addition to this, the one more radiative transition is delayed fluorescence.

Here, following the intersystem crossing from a singlet to a triplet state the system again reaches back to the singlet state with support of the thermal energy present in the surrounding leading to fluorescence but with a time lag.

### 1.3 **Luminescent Material** :

A luminescent material, is also known as a phosphor that can convert various types of energy to light energy over and above thermal radiation [40]. These phosphors are mostly solid-state inorganic materials but some organic materials are also known for it. The scientific research on phosphors has a long history of more than 100 years. The world has profited immensely with the advent of phosphor technology that provided emissive devices with high light output at reduced cost. Over the past few years, intensive research has been devoted to realize efficient luminescent materials for their applications in emissive displays and energy saving fluorescent lamps. Recently the appearance of new types of displays and light emitting devices (plasma displays, fluorescent lamp without mercury, white light emitting diodes, and non-radioactive phosphorescent materials) induced an increase in the research activities for phosphors with better luminous efficiency [41-47]. A phosphor consists of a host lattice and a luminescent center, often called as an activator or dopant. The role of the host lattice is to provide a favorable environment for the activator to emit efficiently though presence of the activators is not indispensable to observe the luminescence. Phosphors like  $\text{CaWO}_4$  are known to exhibit strong luminescence without any activator [48]. The role of activators is to activate the host by creating efficient luminescent centers within the forbidden gap of host material. In the process of



and blue emission [51, 52].  $S^2$  metal ion (activator) based phosphors such as NaI:  $Tl^+$ , CsI:  $Tl^+$ ,  $BiGe_3O_{12}:Bi^{3+}$  are well known for their application in X/ $\gamma$  detectors [53-56]. Present day scenario have shown much fascination towards rare-earth ion based phosphors.  $Tb^{3+}$  activator ion is well known for its green luminescence.  $Tb^{3+}$  ion doped in different host matrices like  $LaPO_4$ ,  $CeMgAl_{11}O_{19}$ , (Gd, Ce)  $MgB_5O_{10}$  are commercially useful for green emission and used in FLs whereas  $Pr^{3+}$  emission wavelength is dependent of host matrix [57-60]. The green emitter  $Gd_2O_2S:Pr^{3+}$  is used in CT scanner whereas red emitter  $CaTiO_3: Pr^{3+}$  is used in field emission displays (FEDs) [61-63].  $Y_2O_3: Eu^{3+}$ ,  $YVO_4: Eu^{3+}$  phosphors are well known red emitting phosphors whereas  $Eu^{2+}$  doped systems such as  $SrB_4O_7: Eu^{2+}$ ,  $Sr_4Al_{14}O_{25}: Eu^{2+}$ ,  $BaMgAl_{10}O_{17}: Eu^{2+}$  are good blue emitting phosphors with application in FLs [66-68].  $Y_3Al_5O_{12}: Sm^{3+}$  has been used in laser application [69].  $Ce^{3+}$  based phosphors such as  $LaPO_4: Ce^{3+}$ ,  $Y_3Al_5O_{12}: Ce^{3+}$ ,  $YPO_4: Ce^{3+}$  have found wide application in FLs [70-73]. Some complex anions such as tungstate  $(WO_4)^{2-}$ , vanadate  $(VO_4)^{3-}$ , molybdate  $(MoO_4)^{2-}$  and titanate  $(TiO_4)^{2-}$  are also known to be the better luminescent centers [74]. Interestingly, some lattice defects such as F-centre (an electron trapped in anion vacancy) V-centre (a hole trapped in cation vacancy) also acts as localized luminescence centers.

Luminescence materials has served in many ways and the applications in lighting, imaging and detection is more pronounced. In present thesis, we have approached luminescence studies in solid phosphors from a different perspective.

#### **1.4 Introduction to thesis:**

Fluorescence is a Photophysical process and most of the time it is an intrinsic property of a particular atom/molecule and thus fluorescence behavior acts as a finger print for identification. This particular property has influenced nuclear industry, where identification and detection of actinide elements is an utmost necessary step [75-77]. In order to meet the worldwide energy security and present clean energy demand to avoid global warming, nuclear energy has emerged as an efficient alternative. In this aspect, providing safe, secured and sustainable nuclear energy is a major challenge. The major issues involved here is remediation of old mining and milling sites, control of fissile products throughout the nuclear power production cycle and finally suitable methods for long term disposal of nuclear wastes [78]. Among all the actinide ions, Uranium is a significant soil and water contaminant at sites associated with uranium mining, nuclear fuel production and disposal [79, 80]. Uranium contamination can be found on localities doing carbonate-rich irrigation. Here uranium compounds may get accumulated through leaching or by certain natural geologic processes [81, 82]. The fully oxidized form of uranium i.e. the hexavalent uranyl ion, ( $\text{UO}_2^{2+}$ ) has been investigated in the most detail. The uranyl ion with two tightly bound oxygen atoms are often relatively mobile in the subsurface. Being uranyl, water soluble, it is readily transported through most soil matrices. In contrast, under anoxic conditions U is generally present as U (IV), in the form of sparingly soluble mineral phases such as uraninite ( $\text{UO}_2$ ) and it is relatively immobile [83]. Uranium can form complexes with several ligands such as sulphate, phosphate, carbonate, fluoride and hydroxide depending on pH conditions [84]. In this regard detection and speciation of Uranium and their coordination properties to form complexes in the environment is an important subject to

investigate. Towards this, fluorescence studies involving uranium luminescence is a challenging technique to probe the issues effectively.

### **1.5 Luminescence of Uranium:**

The photo physical behavior of actinide ions differ from their lanthanide ion counter parts. Although in both lanthanides and actinides, f-f transition is the virtue of their luminescence behavior, the actinides photo physical behavior is quite complex compared to that of lanthanides [85]. The complexity is mainly due to the nature of 5f orbital that undergoes easy mixing with ligand fields unlike lanthanide 4f orbitals that are centrally buried orbitals. The f-f transition in 4f orbitals are intra-configurational and it is Laporte forbidden. But in actinide ions f-d orbital mixing as well as spin orbit coupling plays a major role by increasing the oscillator strength and thus relaxes the selection rules also [86]. Figure 1.6 shows the comparison of calculated “free-ion” f-state energies of 3+ lanthanide and actinide ions having the same number of f-electrons [87]. It can be observed that in actinide ions, the energy gap between the observed emitting free ion state and the next lower lying free ion state is smaller compared to its corresponding lanthanide ion. This energy difference are known as energy gaps which are also responsible for non-radiative decay. The strong dependence of the non-radiative decay rate of aquated 3+ lanthanide ions and actinide ions on energy gap results in considerably reduced luminescence from an aquated 5f actinide ion in comparison with some of aquated lanthanide ions. Figure 1.7 shows an energy level

diagram for trivalent actinides, representing the emissive energy states formulated by energy gap law [88].

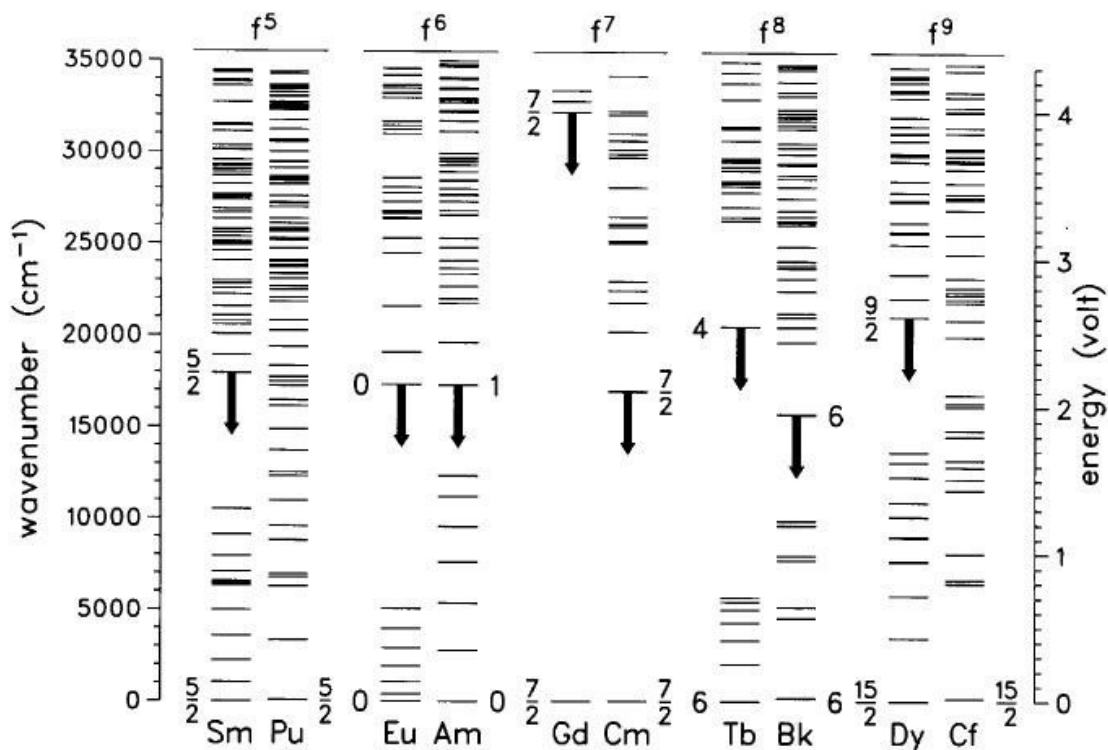


**Figure 1.6: A comparison of f-state energies of 3+ lanthanide and actinide ions having the same number of f-electrons. The J value of the ground and predominant emitting f state is shown [Ref 87].**

The photo physical properties like emission and absorption spectra of actinide ions are more prone to crystal field effects i.e. created by the surrounding ligands. Here the local site symmetry i.e. lower order symmetry or higher order symmetry created by the surrounding atoms also play a major role. More over coupling with vibrational modes of neighboring molecules of the surrounding environment facilitates crystal field splitting and thus actinide

ions have relatively higher transition probabilities. As the electronic transitions in actinides are sensitive to its local environment, it is an advantage to exploit luminescence of actinides to probe its surrounding coordination environment. In this regard uranium luminescence is quite interesting having multiple oxidation states.

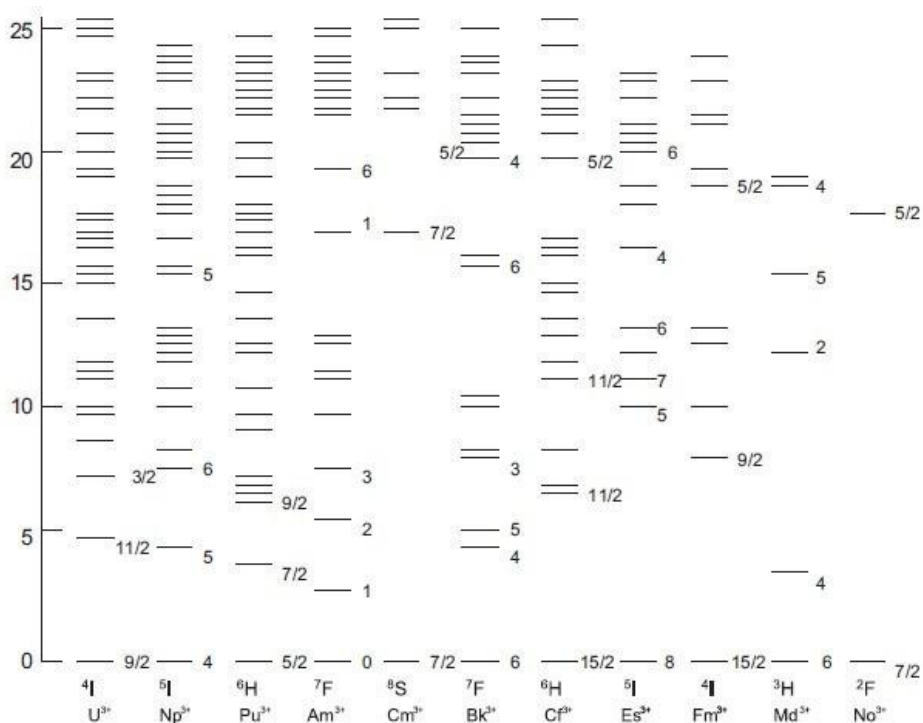


**Figure 1.7: Energy level diagrams for the trivalent actinide ions doped in  $\text{LaCl}_3$ , illustrating the ground state and excited state energy levels. [Ref. 88]**

Uranium shows +3, +4, +5 and +6 oxidation states. Each of this oxidation state exhibits its characteristic luminescence known as its optical fingerprint [89-93]. The luminescence behavior of +6 oxidation state of uranium is slightly different from others as it can be found in various forms such as  $\text{UO}_2^{2+}$ ,  $\text{UO}_4^{2-}$ , or  $\text{UO}_6^{6-}$ . These three different species show

individual emission characteristics. Both uranyl ion ( $\text{UO}_2^{2+}$ ) and octahedral uranate ( $\text{UO}_6^{6-}$ ) shows green luminescence whereas  $\text{UO}_4^{2-}$  shows red luminescence [94-96]. Interestingly stabilization of species like  $\text{UO}_4^{2-}$  and  $\text{UO}_6^{6-}$  is reported only in solid matrices whereas uranyl ion ( $\text{UO}_2^{2+}$ ) is stable both in solids as well as in solutions [97-101].

### **1.5.1 Uranyl luminescence:**

In order to understand the Uranyl luminescence, to know its electronic states and energy levels is very important. In 1961 Mc Glynn and Smith [102] have stated the ground state of uranyl ion as  $(1\sigma_u^+)^2 (1\sigma_g^+)^2 (1\pi_u)^4 (1\pi_g)^4$ . According to them this configuration is a totally symmetric singlet ground state represented as  $^1\Sigma_g^+$  as shown in figure 1.8.

The electronic transition in a uranyl ion from ground state  $^1\Sigma_g^+$  to excited  $3\pi_u$  state leads to splitting of excited state in to 12 sublevels. The—splitting was explained as O-U-O symmetric stretching with point symmetry  $D_{\infty h}$ . A typical uranyl absorption spectra consisted of 12 sub spectrum (revealed by deconvolution) is shown in figure 1.9 [89]. Latter R.G. denning proposed his seminal work on the electronic structure of the closed shell uranyl ion (Figure 1.10). His work reveals that molecular orbitals are more significant in U-O bonding [103]. Uranyl ions possess two primary valence shells, 5f and 6d. Both can form  $\sigma$  and  $\pi$  bonds to oxygen.

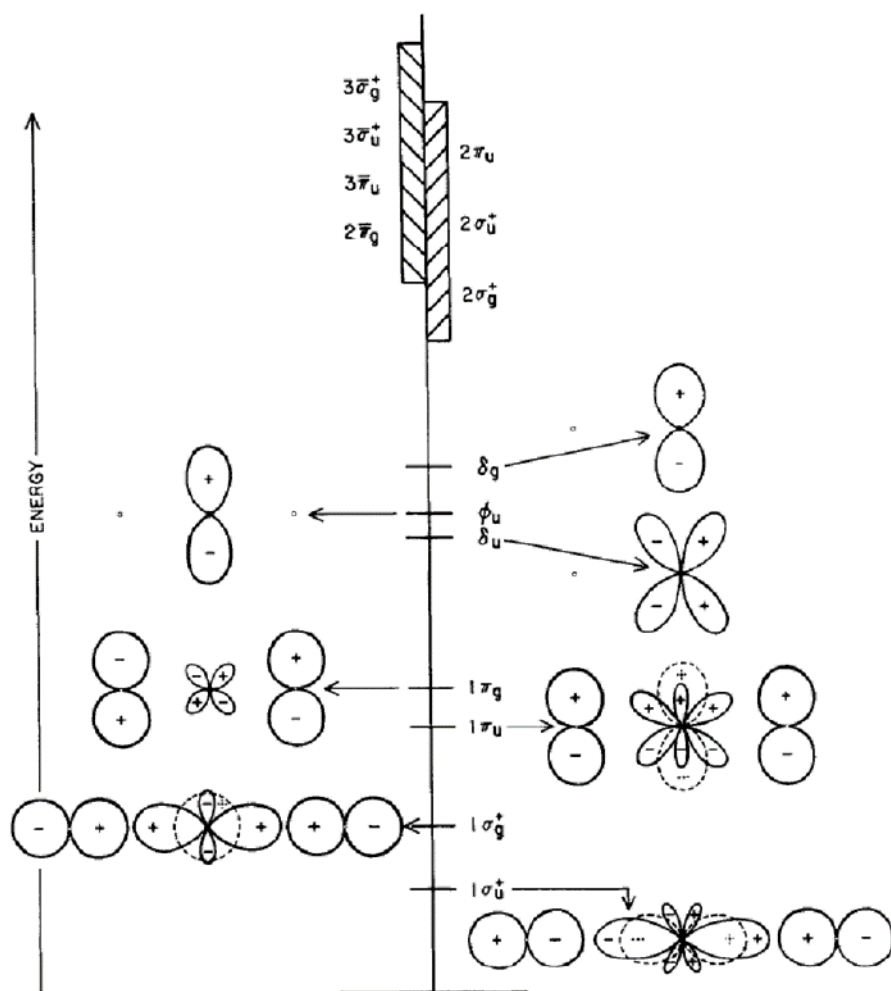
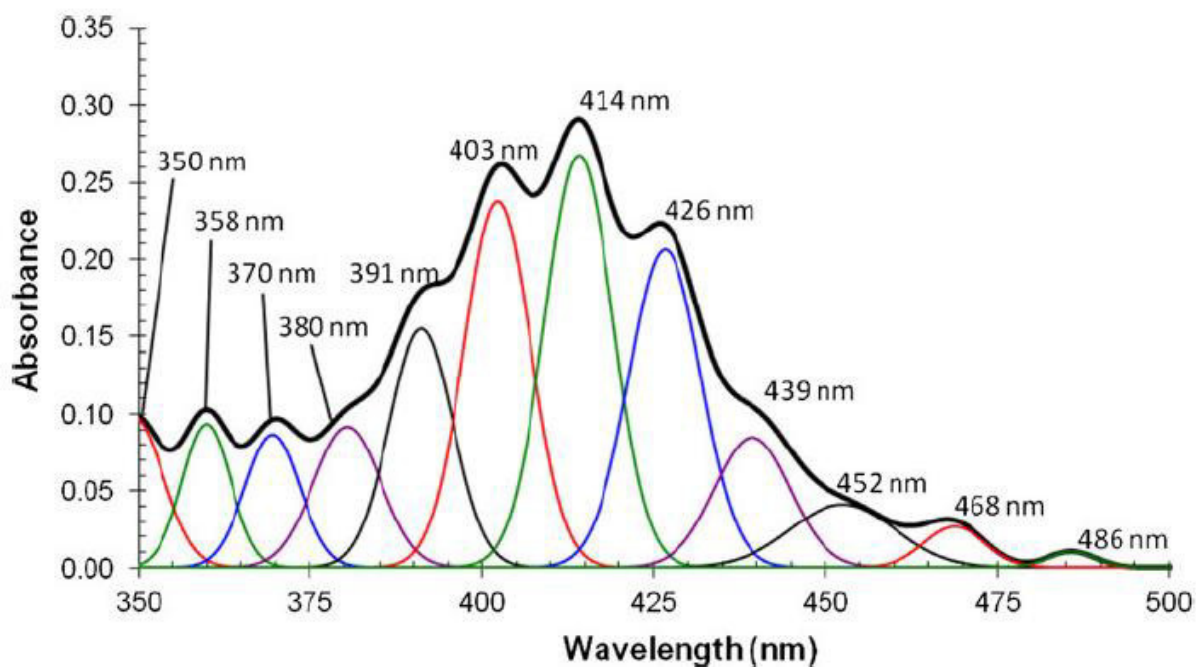


Figure 1.8: One electron MO's of a collinear O-U-O entity. The MO's are shown separated in to their component AO's for reasons of clarity [ref. 102].



**Figure 1.9: Deconvoluted spectra of uranyl absorption, 40.1mmol/L uranyl, 5 mmol/L nitrate ion [ref. 89]**

Figure 1.10. shows that U (5f) and U (6d) overlaps with O (2P). The 6p as well as 6s electrons are considered owing to their larger axial field splitting and radial extension respectively. The consideration of O (2s) orbital is due to its degeneracy as well as interaction with U (6p). In  $\text{UO}_2^{2+}$  the LUMOs are the  $5f_\delta$  and  $5f_\phi$  components of the 5f shell (Fig.4.) as they are excluded by their symmetry from participation in the U-O bond. The four highest filled MOs,  $3\sigma_g$ ,  $3\sigma_u$ ,  $1\pi_g$  and  $2\pi_u$  nominally centered on the oxygen atoms, can be viewed as bonding and thus suggest a notional U-O bond order of three. Denning explained the first excited states of the uranyl ion as an excitation from  $\sigma_u$  orbital to  $5f_\delta$  and  $5f_\phi$  orbitals (Figure 1.10). With his experimental and computational work it was understood

that in uranyl ion, oxygen to uranium charge-transfer i.e. excitation from the bonding orbitals of  $\text{UO}_2^{2+}$  to the nonbonding uranium  $5f_{\delta/\phi}$  redistributes charge in the excited state in such a way as to lower the energies of all oxygen based MOs and raise those on uranium.

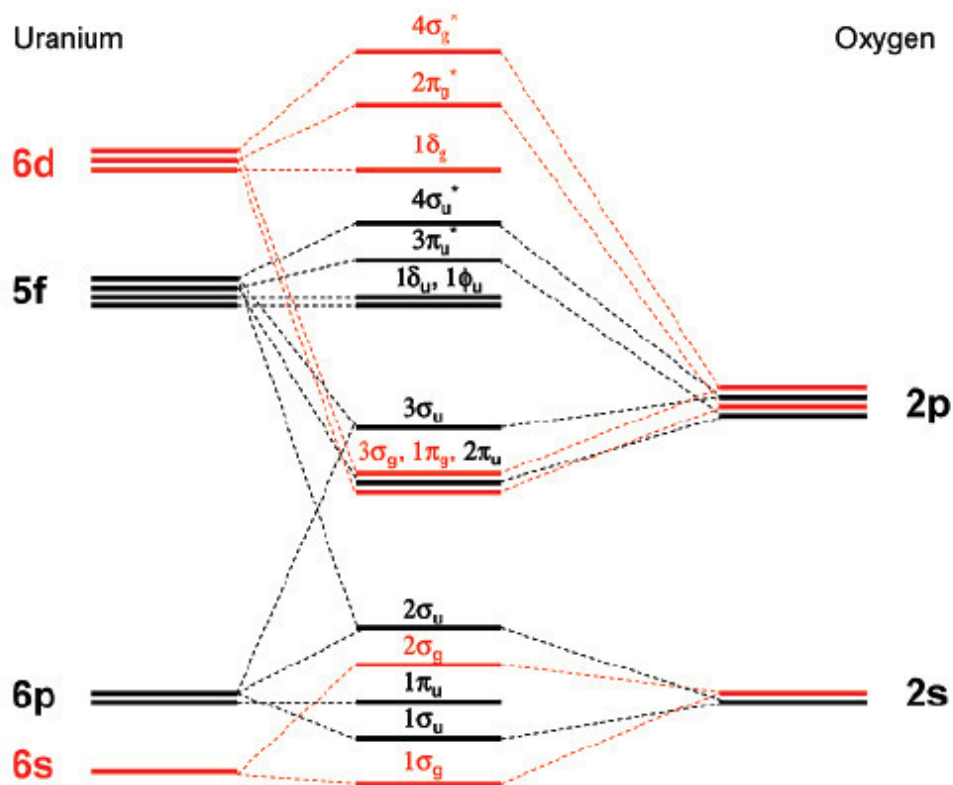


**Figure 1.10: Schematic energies of Uranyl valence orbitals [ref.103].**

In Denning's model different parameters such as spin-orbit coupling, coulomb interactions etc. were used to calculate the energy levels. Although the model was efficient to explain energy levels of the excited states with lower energy quantitatively it could not arrange the excited states in consistent ordering. Further in 2011, G.K. Liu explained Uranyl electronic transitions more appropriately by molecular orbital theory [104]. The speciality of his

model was application of crystal-field Hamiltonian. This Hamiltonian was used to study the effect of axial field of the O=U=O ion. This model states possible ligand-to-metal charge transfer (LMCT) transitions in uranyl, which was earlier known as optical excitation. Here the HOMO is consisted of  $3\sigma_u$ ,  $3\sigma_g$ ,  $2\pi_u$  and  $1\pi_g$  originated from the atomic orbitals of O ( $2s2p$ ) combined with atomic orbitals of U ( $6s6p5f6d7s$ ). The optical absorption takes place from  $3\sigma_u$  the doubly occupied molecular orbital and fluorescence excitation takes place to the lowest excited states i.e.  $5f(\delta_u)$  and  $5f(\varphi_u)$  which are formed by hybridization of nonbonding  $5f(\delta_u)$  and  $5f(\varphi_u)$  orbitals. Here the  $5f(\pi_u)$  and  $5f(\sigma_u)$  orbitals are also bonded with O  $2p(\sigma_u, \pi_u)$  orbitals but comparatively at very higher energies. But when uranyl ion is coupled to ligand clusters then the scenario of energy levels get affected strongly and there the role of an effective Hamiltonian operator is inevitable.

As earlier discussed, absorption in uranyl ion is a LMCT phenomenon which is an ligand to metal charge transfer process. LMCT becomes a forbidden transition in case the ground state shows centre of symmetry. It is well known from various reports that electronic transitions of uranyl ion is best possible by non-centrosymmetric type of coordination i.e. coordination with  $D_{nh}$  symmetry, where  $n=3$  or  $5$  shows greater optical transition intensity [85, 105]. The local coordination environment offers vibrational modes as well as certain crystal symmetry defects and these together favors relaxation of the Laporte selection rule.

The emission spectra of Uranyl is quite interesting with respect to its five finger like structure [106]. The emission spectra centred at 520 nm falls in green region. In both solids and solution uranyl shows its typical finger print type emission characteristics [107,101]. Uranyl being a triatomic linear molecule shows intra-molecular vibrations i.e. two stretching mode ( $\nu_1$  and  $\nu_3$ ) and one doubly degenerate bending ( $\nu_2$ ) mode. Therefore the emission spectra is treated as vibronic progressions. In the ground state of  $O=U=O$ , Raman active symmetric vibrational modes ( $\nu_1$ ) are present. When these vibrational modes get coupled with  $3\pi_u$  electronic triplet excited state, vibrational progressions resulted. Figure 1.11 shows a typical absorption as well as emission spectrum of free uranyl ion in 0.1M  $NaClO_4$  at 25°C [108]. Interestingly absorption and emission spectrum shows common bands like 488 nm (emission)/ 485 nm (absorption) and 473 nm (emission)/ 467 nm (absorption). The absorption band at 488 nm corresponds to the low energy transition i.e. to the lowest lying vibronic state of the first excited electronic state, while the emission band at 473 nm is a transition from an excited vibronic state to the electronic ground state.

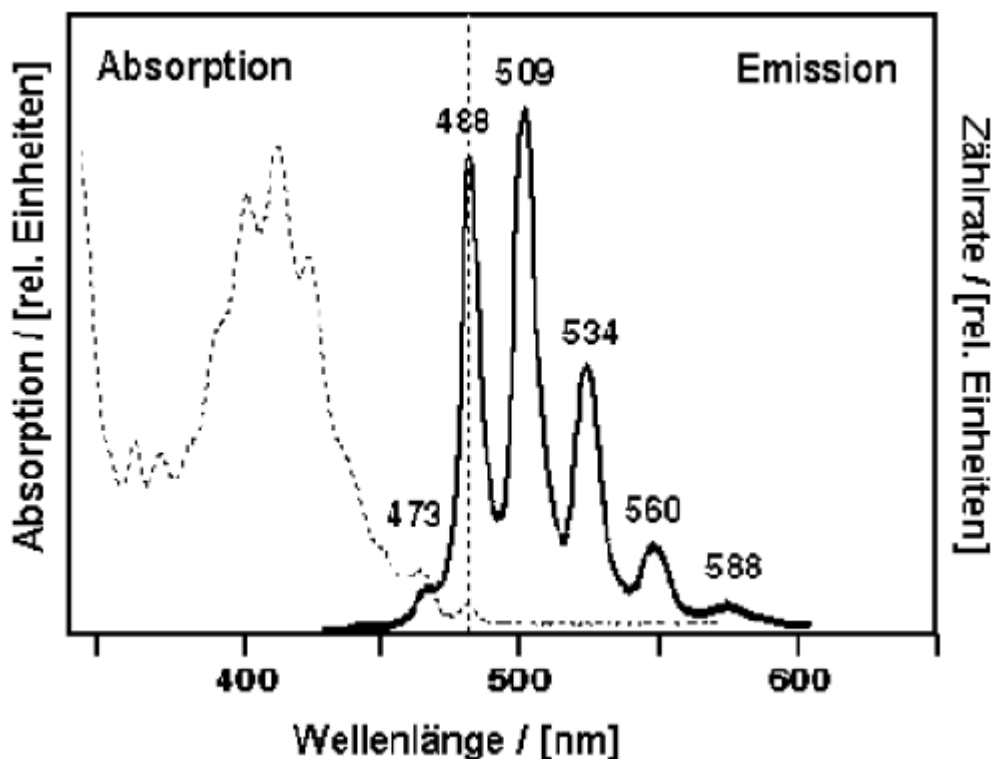


**Figure 1.11: Emission (solid line) and absorption (dashed line) spectrum of Uranyl ion in 0.1M NaClO<sub>4</sub> at 25 °C. Wavelengths given in nm [ref. 108].**

### **1.5.2 Luminescence of octahedral uranate:**

First of all luminescence from octahedral uranate is specific to only solid state luminescence i.e. uranium doped in solid matrices may get stabilized as uranate ( $\text{UO}_6^{6-}$ ) and acts as an optical centre emitting green luminescence. Being a large molecular moiety, luminescence as well as stabilization of  $\text{UO}_6^{6-}$  has been paid much interest. In 1955 Runciman has ascribed for the first time green luminescence to the presence of  $\text{UO}_6^{6-}$  groups [109]. The luminescence of the octahedral uranate group is more influenced by the chemical constitution of its surroundings [110]. In an  $\text{UO}_6^{6-}$  unit the immediate equatorial coordination number is more likely 4 in addition to two axial O atoms. Although two axial

O atoms are present but the emission profile differs from that of a uranyl. Here the emission transition is of electronic origin rather than of vibronic origin as in centrosymmetric uranyl compounds. According to Tanner and et al. during electronic transition in uranate molecule, first a weakening of U-O bond takes place i.e. the triple-bonded uranyl moiety and it occurs as the bonding electrons get delocalized in to neighboring oxygens [111]. When the uranyl ions does not get fitted in to a regular lattice sites it may get affected by various coordination environments. Figure 1.12 shows a typical emission spectrum of uranate from a  $\text{SrB}_4\text{O}_7:\text{U}$  system [112].

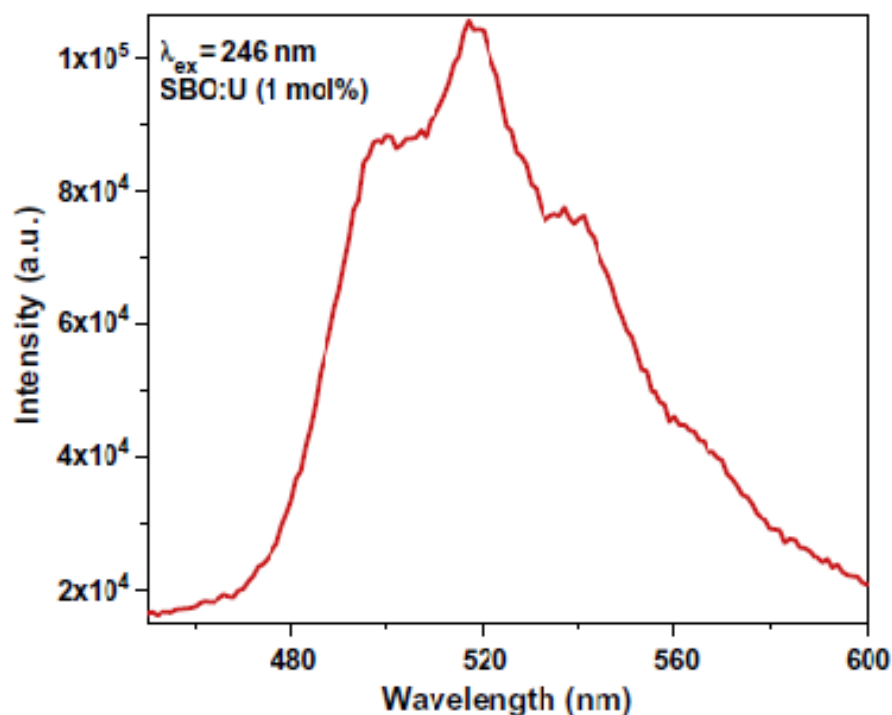


**Figure 1.12: Emission spectrum of  $\text{SrB}_4\text{O}_7:\text{U}$ , at  $\lambda_{\text{excitation}} = 246 \text{ nm}$ : representing  $\text{UO}_6^{6-}$  emission profile [ref. 112].**

The broad emission spectrum is devoid of prominent vibronic structures. Here the emission is a parity forbidden charge transfer transition. The excitation transition for uranate is generally a charge transfer transition that corresponds to the transition from orbitals derived primarily from oxygen (2p) to uranium (6d) orbitals. The transitions are thus partly allowed but not necessarily electric dipole allowed. Figure 1.13. shows a typical excitation spectrum of uranate [113].

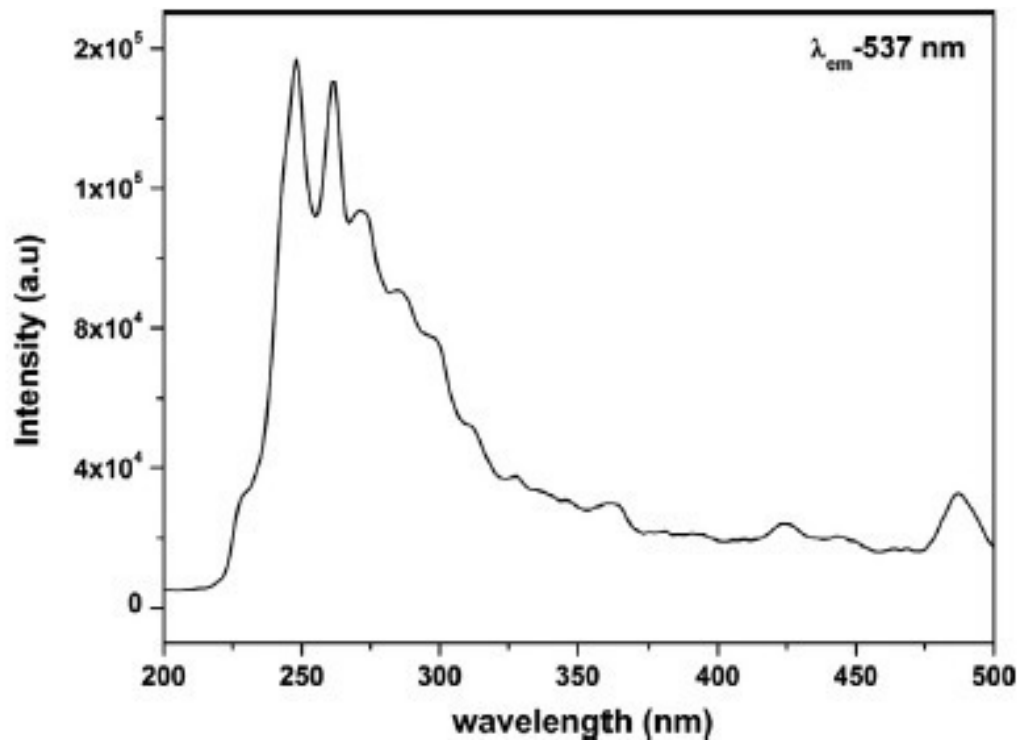


**Figure 1.13: Room temperature excitation spectrum of SrZrO<sub>3</sub>: U under  $\lambda_{em}$  of 537 nm; representing excitation profile of UO<sub>6</sub><sup>6-</sup> [Ref. 113].**

### **1.5.3 Uranium luminescence in solids:**

As discussed earlier study of uranium luminescence in different solid matrices may have different point of view. In many cases detection of uranium is the prime objective. Uranium shows a very long half-life in the order of  $10^5$ - $10^9$  years, so remote detection of uranium in trace level by use of radioactive counting techniques (alpha detectors) are difficult. Here detection of uranium by fluorescence technique is very useful. Besides this, luminescence study of Uranium doped solid matrices are mainly intended to bring out various information about the matrices as well as uranium itself. This optical information can reveal structural ambiguity of the matrix, presence of defect centres, inversion centres, form of stabilization of uranium, solubility of uranium, etc. In earlier times Kroger and Weyl have initiated studies of fundamental aspects of Uranium fluorescence in solids [114, 115]. Latter Blasse investigated emission characteristics of many uranium –activated phosphors. He has studied uranium luminescence in several oxides with perovskite structure like  $\text{Ba}_2\text{CaWO}_6$ ,  $\text{Ba}_2\text{CdWO}_6$ ,  $\text{Ba}_3\text{WO}_6$ ,  $\text{SrLaNaTeO}_6$  etc. [110]. Pervoskites show high symmetry thus allowing an extensive cation substitution [116]. Solid matrices like  $\text{Y}_3\text{Li}_3\text{Te}_2\text{O}_{12}$ ,  $\text{Li}_6\text{WO}_6$ ,  $\text{Mg}_3\text{TeO}_6$  poses isolated tungstate / tellurate octahedra and thus stabilization of isolated  $\text{UO}_6^{6-}$  octahedra was reported [117-119]. Here the green emission was attributed to  $\text{U}^{6+}$  in octahedral positions i.e. octahedral uranate group, occupying a normal octahedral site. Interestingly an orange emission was also reported from  $\text{U}^{6+}$ - activated  $\text{Ba}_2\text{TeO}_5$  [120]. His work proposed both green and red luminescence from uranium and it was observed that the emission spectra is influenced by the chemical constitution of its surroundings as well as quenching temperature. Another source of green emission was reported to be the uranyl

group by Dieke and Duncan [121]. Latter Rabinowitch and Belford explored solids such as nitrates, chlorides, sulphates, phosphates and acetates to study uranyl luminescence [122]. Hoffman reported uranyl luminescence in  $\text{SrZnP}_2\text{O}_7$  and it was suggested that due to stabilization of uranium, the orthorhombic  $\text{SrZnP}_2\text{O}_7$  got distorted to a monoclinic structure [123]. Lattices like  $\text{Ba}_2\text{ZnTeO}_6$  with two different crystallographic sites were also studied and possibility of U to occupy two different sites was proposed [110]. A number of different luminescent uranate centres was reported by Krol in NaF: U system [124]. Besides +6 oxidation state of U, luminescence studies were also reported for uranium with its lower oxidation state like +3, +4 and +5. P.A. Tanner have reported stabilization of U in its +3 oxidation state (in the form of  $\text{UCl}_6^{3-}$ ) in  $\text{Cs}_2\text{NaYCl}_6$ : U single crystal system [125]. Whereas Hessler has reported luminescence behavior of the M-level of  $\text{U}^{3+}$  in  $\text{LaBr}_3$  [126]. Godbole et al. has investigated luminescence of  $\text{U}^{4+}$  in  $\text{LiYF}_4$ : U single crystal system [127]. Stabilization of U in its +5 oxidation in  $\text{CaF}_2$ : U crystal and its luminescence behavior was reported by Lupei [128]. It was also observed that under gamma irradiation  $\text{LiF}$ -  $\text{U}_3\text{O}_8$  crystal shows stabilization of  $\text{U}^{+5}$  as well as its characteristic optical behavior [129]. The important point is that stabilization of Uranium in lower oxidation states is crucial and it needs anoxic environment, thus systems or solid matrices accompanied with oxygen favors uranium to be in +6 oxidation state. The prolonged studies and literature reports by various experts suggest that luminescence of uranium in solid matrices is although an optical phenomena but it is mainly influenced and guided by chemical as well as physical environment of host lattice. Solid host matrices like silicates, borates, tungstates, molybdates, zirconates, phosphates etc. are found to be ideal host matrices for uranium.

## **1.6 Motivation for the present study:**

Recently the concept of immobilization of radioactive waste in ceramic matrix has emerged and also gained much attention as certain fission products are more likely to reside in crystalline phases instead of conventional alkali borosilicate based glass matrices [113]. Glass as a immobilizing material shows some limitations for volatile radionuclides. Volatile radio nuclides like Tc, I, Cs etc. shows difficulties at glass melting temperature. Some of the actinides, with long half-life also face solubility problem in glass matrix. Another limitation is the phase separation at microscopic level i.e. formation of alkaline borate, a second phase that tends to leach out thus affecting the chemical durability of the system. Vitrification process allows substantial reduction of waste volume, it works successfully towards waste safety but at the same time it is also a complex process [130]. In this context geochemically stable materials are explored with an approach to investigate its efficiency towards safe and durable nuclear waste management. Thermodynamically stable minerals poses high isomorphic capacity and thus may retain radionuclides in their structures. Crystalline ceramic materials show higher waste loading capacity and also their analogous to mineral form offer long-term disposal for nuclear wastes as a geological constraint [131]. Ceramic structures are of complex composition and thus able to accommodate radionuclide with different coordination types and can do charge balance. It has been observed that zirconite, monazite, apatite are suitable single-phase ceramics. They can accommodate nearly all of the radionuclides and can form a single structure. Several researchers have investigated the use of Ceramic materials have been in research from a long time especially for waste immobilization studies [132-134]. The best examples are

titanate-based hollandite, perovskite or zirconolite ceramics [135-136]. Synthetic rock materials i.e. synrocks concept has been emerged with very good dissolution rate. These materials like (Ce, Y, La, Th) PO<sub>4</sub>, apatite (Ca<sub>5</sub>PO<sub>4</sub>)<sub>3</sub>(F, Cl, OH) etc. were designed for disposal of high level nuclear waste [137]. Recently the focus is towards phosphate ceramics which are i) chemically stable, ii) can incorporate substantial quantities of actinides in their structure, and iii) are resistant to radiation damage. Although phosphates are not currently part of the high-level waste storage strategy, significant efforts have been made by the scientific community to determine if phosphate based matrices could provide an alternative to the currently planned methods for radioactive waste disposal [138]. In this regard incorporation of actinides in to phosphate matrix is a challenging subject to study but owing to its high radioactivity the scope is very limited, whereas uranium with long half-lives (10<sup>5</sup>-10<sup>9</sup> years) and mostly being an alpha emitter is vastly investigated. Towards this investigation luminescence studies contribute in an effective way to elucidate various information. Information regarding oxidation state of uranium in a particular matrix is very much useful and similarly the form of stabilization of uranium is also very important. During incorporation of uranium the behavior of surrounding host, the neighboring crystal field as well as co-ordination environment of uranium plays a crucial role in order to find out the suitability of the host material. Being a heavy element stabilization of uranium may invite perturbation to the host environment is also a matter of concern. Thus it is interesting as well as challenging to carry out luminescence studies on uranium doped solid matrices.

### **1.7 Scope of the thesis:**

In present study we have mainly focussed on uranium luminescence in phosphate and borate matrices, as it shows very long half-lives ( $10^5$ - $10^9$  years), phosphate/borate based ceramic matrices can be better candidates for long term storage purpose. The prime objective here is to investigate photo luminescence behaviour of uranium in solid matrices like phosphates and borates. In particular we have investigated uranium doped borophosphate solid matrices such as  $\text{CaBPO}_5$ ,  $\text{SrBPO}_5$ , and  $\text{BaBPO}_5$  and also uranium doped borate matrices such as  $\text{BaB}_2\text{O}_4$  and  $\text{BaAl}_2\text{B}_2\text{O}_7$ . Here the synthesis route as well as standardization of synthesis parameters for all above uranium doped and un-doped samples are one of the important part to investigate. The detailed investigation involves characterization of the synthesized samples in order to observe the phase purity as well as morphology studies. Solubility of uranium in a solid host matrix and its concentration limitation is a determining step to avoid formation of any second phase. Optimization of annealing temperature were done with lot of care as it contributes to formation of exact phase, controls the defect concentration and migration and finally it also affects the photo luminescence properties.

The photo luminescence studies were carried out with an aim to observe the photo luminescence (PL) characteristics of dopant ion (uranium) such as excitation, emission and decay time values that indirectly informs about the feasibility of photo luminescence process in that particular matrix as PL process is associated with both radiative as well as non-radiative decay processes, here the host matrix as well as positioning of dopant ion in that particular matrix are responsible for a good PL characteristics. The life time decay

values of uranium ion were studied carefully in order to probe the effect of surrounding lattice as well as defects. All these PL properties were found to be an important clue to optimize the synthesis process which is a crucial step needed to prepare ideal phosphors. Besides this, the uranium PL emission spectra have gained much importance throughout our work, as the emission profile represents the form of stabilization of uranium in the host matrix. The form of stabilization can be octahedral/tetrahedral uranates or uranyl ion. Thus we have tried to probe the presence of dopant ion and its effect on surrounding environment. As it is always being a curious topic to discuss the stabilization of uranyl ion in any solid matrix, considering its size and  $180^\circ$  geometry, we have attempted to address this issue by correlating both luminescence studies along with EXAFS studies. Our work has revealed the importance of host matrix in determining the form of stabilization of uranium. We have reported the uranyl form of stabilization of uranium in  $\text{CaBPO}_5$  and  $\text{SrBPO}_5$  whereas in  $\text{BaBPO}_5$  the form of stabilization is preferred to be uranate. This study have shown the potential of EXAFS in order to probe the crystal lattice surrounding the dopant uranium ion. We have also addressed the stabilization of uranium in  $\text{BaAl}_2\text{B}_2\text{O}_7$  with EXAFS studies, where two competitive Ba and Al sites are present for uranium stabilization.

In our study the interaction of uranium with other co-dopants (Eu, Sm) were also studied. In quality control process, detection as well as estimation of impurity elements is the major work. In nuclear industry depending on the requirement like fuel fabrication, fuel reprocessing, waste management, academic research interest etc. detection of lanthanides like Eu, Sm, Gd, Dy, Tb etc. as an impurity present in uranium is a crucial step owing to its very low concentration. At this point fluorescence spectroscopy has been proven its

potential and towards this end ligand sensitized fluorescence (LSF) has gained much appreciation [99-101]. Here in our study although we have not discussed LSF, which is a solution state bound process but we have focused on energy transfer process occurring from uranium to lanthanides in a solid boro phosphate matrix. As dopant uranium extends its energy towards a co-dopant ion (Eu, Sm), the co-dopant ions PL gets enhanced and it gets detected easily by PL techniques. Our work has studied energy transfer process, mechanism as well as the extent of energy transfer process in details.

### **1.8 References:**

1. R. A. Sheth, J. M. Tam, M. A. Maricevich, L. Josephson, U. Mahmood, *Radiology*, 251 (2009), 813-821.
2. H. N. Kim, M. H. Lee, H. J. Kim, J. S. Kim, J. Yoon, *Chem. Soc. Rev.*, 37 (2008), 1465-1472.
3. R. Weissleder, *Nat. Biotechnol.*, 19 (2001), 316-317.
4. D. T. Quang, J. S. Kim, *Chem. Rev.*, 110 (2010), 6280-6301.
5. M. Ogawa, N. Kosaka, P. L. Choyke, H. Kobayashi, *Cancer Res.*, 69 (4) (2009), 1268-1272.
6. M. Beija, C. A. M. Afonso, J. M. G. Martinho, *Chem. Soc. Rev.*, 38 (8) (2009), 2410-2433.
7. R. M. Clegg, *Curr. Opin. Biotech.*, 6 (1995), 103-110.
8. L. Trón L, J. Szöllösi, S. Damjanovich, *Immunol Lett.*, 16 (1987), 1-9.
9. R. M. Clegg, *Fluorescence Resonance Energy Transfer (FRET). Fluorescence*

- Spectroscopy and Microscopy. X. F. Wang, B. Hermann (eds). J. Wiley and Sons Inc., New York, 1996. Chemical Analysis Series, 137 (1996), 179–252.
10. L. L. Gompels, L. Madden, N. H. Lim, J. J. Inglis, E. McConnell, T. L. Vincent, D. O. Haskard, E. M. Paleolog, *Arthritis Rheum.*, 63 (1) (2011), 107-117.
  11. X. Chen, T. Pradhan, F. Wang, J. S. Kim, J. Yoon, *Chem. Rev.* 112 (3) (2012), 1910-1956.
  12. J. Ju, I. Kheterpal, J.R. Scherer, C. Ruan, C.W. Fuller, A. N. Glazer, R. A. Mathies, *Anal. Biochem.*, 231 (1995), 131-140.
  13. W. Ansorge, B. Sproat, J. Stegemann, C. Schwager, M. Zenke, *Nucleic Acids Res.*, 15(11) (1987), 4593-4602.
  14. Y. Matsuda, V. M. Chapman, *Electrophoresis*, 16 (1995), 261-272.
  15. R. V. Lebo, E. D. Lynch, T. D. Bird, M. S. Golbus, D. F. Barker, P. O'Connell, P. F. Chance, *Am. J. Hum. Genet.*, 50 (1992), 42-55.
  16. B. J. Trask, D. Pinkel, G. van den Engh, *Genomics*, 5 (1989), 710-717.
  17. B. Brandriff, L. Gordon, B. Trask, *Genomics*, 10 (1991), 75-82.
  18. D. Pinkel, T. Straume, J. W. Gray, *Proc. Natl. Acad. Sci. USA*, 83 (1986) 2934-2938.
  19. R. Slim, J. Weissenbach, V. C. Nguyen, G. Danglot, A. Bernheim, *Hum. Genet.*, 88 (1991), 21-26.
  20. R. M. Clegg, *Curr. Opin. Biotech.* 6 (1995), 103–110.
  21. R. H. Fairclough, C. R. Cantor, *Methods Enzymol*, 48 (1978), 347–379.
  22. S. Damjanovich, R. Ga'spa' r, C. Pieri, *Q. Rev. Biophys.*, 30 (1997), 67–106.
  23. L. Ma'tyus L, *J. Photochem. Photobiol. B*, 19 (1992), 67–73.

24. L. Trón: Experimental Methods to Measure Fluorescence Resonance Energy Transfer.  
In: Mobility and Proximity in Biological Membranes, Damjanovich S, Szöllösi J, Trón L, Edidin M (eds). CRC Press, Boca Raton, 1994, 1–47.
25. P. Wu, L. Brand, Anal. Biochem., 218 (1994), 1–13.
26. M. Teichmuller, Org. Geochem., 10 (1986), 581-599.
27. R M. Bustin, M. Orchard, M. Mastalerz, Int. J. Coal Geol., 21 (1992), 261-282.
28. Y. Narukawa, M. Ichikawa, D. Sanga, M. Sano, T. Mukai, J. Phys. D: Appl. Phys., 43 (2010), 354002.
29. C. Shen, Y. Yang, S. Jiu, J. Ming, H. Feng, Z. Xu, Optik, 121 (2010), 1487-1491.
30. H. Y. Lin, C. W. Sher, C. H. Lin, H. H. Tu, X. Y. Chen et al., ACS Appl. Mater. Interfaces, 9(40) (2017), 35279-35286.
31. J.K. Park, J.T. Park, S.Y. Choi, M.A. Lim, C.H. Kim, H.D. Park, Appl. Phys. Lett., 82 (2003), 683-685.
32. S.A. Khan, H. Zhong, W. Ji, L.Y. Hao, H. Abadikhah, X. Xu, N.Z. Khan, S. Agathopoulos, ACS omega, 2 (2017), 6270-6277.
33. L. Chen, C. C. Lin, C. W. Yeh, R. S. Lin, Materials, 3 (2010), 2172-2195.
34. H. Liu, L. Liao, M.S. Molokeyev, Q. Guo, Y. Zhang, L. Mei, RSC Adv., 6 (2016), 24577-24583.
35. H. Daicho, T. Iwasaki, K. Enomoto, Y. Saskai, Nat. Commun, 3 (2012), 1132.
36. S. Ye, F. Xiao, Y. X. Pan, Y.Y. Ma, Q.Y. Zhang, Mater. Sci. Eng., R, 71 (2010), 1-34.
37. S. Shionoya, Phosphor Hand Book, CRC Press, New York 4 (1998).
38. E. I. Rashba, J. Lumin., 100 (2002), 57-64.

39. A. Jablonski, Nature 131 (1933), 839.
40. G. Blasse, B.C. Grabmaier, Luminescent Materials, Springer-Verlag Berlin Heidelberg New York, 1994, ISBN 3-540-58019-0.
41. W. L. Nighan, C.M. Ferrar, Appl. Phys. Lett. 40 (1982), 223-224.
42. J.P. Boeuf, J. Phys. D: Appl. Phys., 36 (6) (2003), R53-R79.
43. Z. Wei, L. Sun, C. Liao, C. Yan, Appl. Phys. Lett., 80 (2002), 1447-1449.
44. J.H. Kim, J.H. Lee, K.W. Whang, J. Appl. Phys., 89 (2001), 2539-2542.
45. S. Mukherjee, P. Tilagar, Chem. Commun., 51 (2015), 10988-11003.
46. J. Kavitha, S.Y. Chan, Y. Chi et al. Adv. Funct. Mater. 15(2) 2005, 223-229.
47. K. Man-C. Wong, X. Zhu, Ling-L. Hung, N. Zhu, V. Wing-W. Yam, et al. Chem. Commun., 2005, 2906-2908.
48. G. Blasse, Luminescent Materials, Springer, Berlin (1994), 77-78.
49. C. R. Ronda, T. Jüstel and H. Nikol., J. Alloys Compd., 669 (1998), 275-277.
50. H. Yau, J. zhang, G. Hong, H. Zhang, J. Phys. Chem. C, 111 (2007), 10657-10661.
51. T.R.N. Kutty, M. Nayak, Mater. Res. Bull., 34(2) (1999), 249-262.
52. T. hase, T. kano, E. Nakazawa, H. Yamamoto, Advances in Electronics and Electron Physics, 79 (1990), 271-373.
53. M. Ishikane, M. Kawanishi, Japanese Journal of Applied Physics, 14 (1) 1975, 64-69.
54. R.G. Lagu, B.V. Thosar, Indian Acad. Sci., 53 (1961), 219-226.
55. Y. Wu, G. Reu, M. Nikl, X. Chen et al., Cryst Eng Comm., 16 (2014), 3312-3317.
56. M.J. Weber, J. Lumin., 100 (2002), 35-45.
57. N. Wang, S. Zhang, X. Zhang, Y. Wei, Ceramics International, Part B, 40 (10) (2014),

- 16253-16258.
58. B. M. Smets, *J. Mater. Chem. Phys.*, 16 (1987), 283-289.
59. J. Zhang, Z. Zhang, Z. Tang, Y. Lin, *Mater. Chem. Phys.*, 72 (2001), 81-84.
60. W. Vanschaik, S.H.M. poort, J.J.H. Schlotter, E. Dorrestijn, G. Blasse, *J. Electrochem. Soc.*, 141(8) 1994, 2201-2207.
61. A. Bagheri, K.R. E. Saraee, H. R. Shakur et al., *Appl. Phys. A*, 122 (2016), 553.
62. P.T. Diallo, K. Jeanlouis, P. Boutinaud, R. Mahiou, J.C. Cousseins, *J. Alloys Compd.*, 323–324 (2001), 218-222.
63. P. Boutinaud, E. Pinel, M. Dubois, A.P. Vink, R. Mahiou, *J. Lumin.*, 111 (1-2) (2005), 69- 80
64. C.R. Ronda, *J. Lumin.*, 49 (1997), 72-74.
65. A. Huignard, V. Buissette, A.-C. Franville, T. Gacoin, and J.-P. Boilot, *J. Phys. Chem. B*, 107 (28) (2003), 6754-6759.
66. R. Stefani, A. des. Maia, C.A. Kodaira et al., *Opt. Mater.*, 29 (12) 2007, 1852-1855.
67. Z. Wu, J. Shi, J. Wang et al., *J Mater Sci: Mater Electron*, 19 (2008), 339-342.
68. K.B. Kim, Y. Kim, H. G. Chun et al., *Chem. Mater.*, 14 (12) (2002), 5045-5052.
69. R. Krsmanović, Ž. Antić, I. Zeković, B. Bártoová, M. D. Dramićanin, *Radiat. Meas.*, 45 (2010), 438-440.
70. X. Ji, F. J. Zhu, H. L. Zhai et al., *Front. Mater. Sci. China*, 4 (2010), 382-386.
71. Y.X. Pan, M.M. Wu, Q. Su, *Mater. Sci. Eng. B*, 106 (2004), 251-256.
72. H.J. Byun, W.S. Song, Y.S. Kim, H. Yang, *J Phys D: Appl Phys*, 43 (2010), 1-6.
73. H. Lai, A. Bao, Y. Yang, Y. Tao et al. *J. Phys.. Chem. C*, 112 (1) (2008), 282-286.

74. S.Shionaya, Phosphor Handbook, CRC Press, New York (1998), 202-206.
75. R. J. Baker, A. Walshe, Chem. Commun., 48 (2012), 985-987.
76. N.J. Curro, T. Caldwell, E.D. Bauer, L.A. Morales, M.J. Graf, Y. Bang, A.V. Balatsky, J.D. Thompson, J.L. Sarrao, Nature, 434 (2005), 622-625.
77. L. Natrajan, M. Mazzanti, J.-P. Bezombes, J. Pecaut, Inorg. Chem., 44 (17) (2005), 6115- 6121.
78. ‘Meeting the Energy Challenge, A White Paper on Energy’, Department of Trade and Industry (May 2007) Crown Copyright, 2007. ; ‘Meeting the Energy Challenge, A White Paper on Energy’, Department of Trade and Industry (January 2008) Crown Copyright, 2008.
79. R.G. Riley, J.M. Zachara, F.J. Wobber, Chemical contaminants on DOE lands and selection of contaminant mixtures for subsurface science research, Pacific Northwest Lab, DOE/ER-0547T, Richland, WA, 1992.
80. J.L. de Lemos, B.C. Bostick, A.N. Quicksall, J.D. Landis, C.C. George, N.L. Slagowski, T. Rock, D. Brugge, J. Lewis, J.L. Durant, Environ. Sci. Technol., 42 (2008), 3951–3957.
81. M.C. Duff, D.E. Morris, D.B. Hunter, P.M. Bertsch, Geochim. Cosmochim. Acta, 64 (2000), 1535–1550.
82. A.P. Meshik, C.M. Hohenberg, O.V. Pravdivtseva, Phys. Rev. Lett., 93 (2004), 182302.
83. D. Langmuir, Geochim. Cosmochim. Acta, 42 (1978), 547–569.
84. S. D. Ebbs, D.J. Brady, L.V. Kochian, J. Exp. Bot., 49 (1998), 1183e1190.
85. Rao Linfeng, G. Tian, Symmetry, 2 (1) (2010), 1-14.

86. G.V. Inova, G.A. Gerasimova, *Russ. Chem. Rev.*, 61 (1992), 907-924.
87. J. V. Beitz, *J. Alloys Compd.*, 207-208 (1994), 41-50.
88. N. Edelstein, *Lanthanide and Actinide Chemistry and Spectroscopy*, ACS Symposium Series, American Chemical Society, Washington DC, 1980.
89. N.A. Smith, G.S. Cerefice, K.R. Czerwinski, *J. Radioanal Nucl Chem.*, (2013), 1553-1560.
90. A. Kirishima, T. Rimura, O. Tochiyama, Z. Yoshida, *Chem. Commun.*, (2003), 910-911.
91. R. Steudtner, T. Arnold, K. Großmann, G. Geipel, V. Brendler, *Inorg Chem Commun*, 9 (2006), 939-941.
92. A. Kirishima, T. Kimura, R. Nagaishi, O. Tochiyama, *Radiochim Acta*, 92 (9-11) (2004), 705-710.
93. J.T. Bell, R.E. Biggers *J. Mol. Spectrosc.*, 25 (1968), 312-329.
94. H. Gobrecht, W. Weiss, *Z. Phys.*, 140 (2) (1955), 139-149.
95. G. Blasse, *J. Electrochem. Soc.* 115 (7) (1968), 738-742.
96. M. Mohapatra, V. Natarajan, *J. Radioanal. Nucl. Chem.*, 302 (3) (2014), 1327-1332.
97. D. R. Taikar, C.P. Joshi and S.V. Moharil, *J. Lumin.*, 153 (2014), 304-306.
98. M. Kumar, M. Mohapatra, V. Natarajan, *Mater. Res. Bull.*, 60 (2014), 858-863.
99. S. Maji, S. Kumar, K. Sankaran, *J. Radioanal. Nucl. Chem.*, 302 (3) (2014), 1277-1281.
100. S. Maji, K.S. Viswanathan, *J. Lumin.*, 129 (11) (2009), 1242-1248.
101. S. Maji, K.S. Viswanathan, *J. Lumin.*, 131 (9) (2011), 1848-1852.
102. S.P. McGlynn, J.K. Smith, *J. Mol. Spectrosc.*, 6 (1961), 164-187.

103. R. G. denning *J. Phys. Chem. A*, 111 (2007), 4215-4143.
104. G.K. Liu, *J. phys. Chem. A*, 115 (2011), 2419-12425.
105. G. Tian, J. Xu, L. Rao, *Angew. Chem. Int. Ed.*, 44 (2005) 6200.
106. M. Mohapatra, A.K. Yadav, S.N. Jha et al., *Chem. Phys. Lett.*, 601 (2014), 81-86.
107. D.H. Metcalf, S. Dai, G.D. Del Cul et al., *Inorg. Chem.*, 34 (1995), 5573-5577.
108. G. Meinrath, *Freiberg On-line geoscience*, ISSN- 1434-7512, 1 (1998), 20.
109. W.A. Runciman, *Brit. J. Appl. Phys.*, Suppl. no. 4 (1955), S78.
110. J. Th. W. De Hair, G. Blasse, *J. Solid state Chem.*, 19 (1976), 263-270.
111. P. A. Tanner, P. Zhi-Wu, L. Jun, L. Yulong, Su Qiang, *J. Phys. Chem. Solids*, 58 (1997), 1143-1146.
112. M. Mohapatra, B. Rajeswari, R.M. Kadam, M. Kumar, T.K. Seshagiri, N.K. Porwal, S.V. Godbole, V. Natarajan, *J. Alloys Compd.*, 611 (2014), 74–81.
113. S.K. Gupta, N. Pathak, R. Gupta, S.K. Thulasidas, V. Natarajan, *J. Mol. Struct.*, 1068 (2014), 204-209.
114. W. A. Weyl, "Coloured Glasses," Dawson's of Pall Mall, London (1959).
115. F. A. Kroger, "Some Aspects of the Luminescence of Solids," Chap. IV, Elsevier Publishing Co. New York (1948).
116. J. B. Goodenough, J. M. Longo, *Landolt Bornstein* (K. H. Hellwege, Ed.), Group III, Springer-Verlag, Berlin, Vol. 4a, (1970), 275
117. R. H. Alberda, G. Blasse, *J. Lumin.*, (12/ 13) 1976, 687-692.
118. G. Blasse, *J. Electrochem. Soc.*, 124 (1977), 1280-1285.
119. G. Blasse, *Chem. Phys. Lett.*, 41 (1976), 210-212.

120. G. Blasse, G.P.M. van den heuvel, *J. Lumin.*, 8 (1974), 406-414.
121. G.H. dieke, A. B. F. Duncan, "Spectroscopic Properties of Uranium Compounds," McGraw-Hill Publishing Co., New York (1949).
122. E. Rabinowitch, R. L. Belford, "Spectroscopy and Photochemistry of Uranyl Compounds," MacMillan Co. (1964).
123. M. V. Hoffman, *J. Electrochem. Soc.: Solid Stae Science*, 117 (2) (1970), 227-232.
124. G. Blasse, K. C. Bleijenberg, D. M. Krol, *J. Lumin.*, 18/19 (1979), 57-62.
125. P. A. Tanner, *J. Mol. Struct.*, 355 (1995), 299-302.
126. J. Hessler, J. Hegarty, C.G. Levey et al. *J. Lumin.*, 18/19 (1979), 73-75.
127. S.V. Godbole, Chung-Hsin Lu, A.G. Page, *Radiat. Mes.*, 37 (2003), 621-626.
128. A. Lupei, V. Lupei, *J. Phys. C: Solid State Phys.*, 12 (1979), 1123-1130.
129. R. parrot, C. Nand, *Phys. Rev. B*, 15 (1) (1977), 137-145.
130. C. Erdogan, M. Bengisu, S. A. Erenturk, *J. Nucl. Mater.*, 445 (2014), 154-164.
131. M. I. Ojovan, W. E. Lee, "An Introduction to Nuclear Waste Immobilisation", 2<sup>nd</sup> Edition, Elsevier, 2014.
132. E. Du Fou de Kerdaniel, N. Clavier, N. Dacheux, O. terra, R. Podor, *J. Nucl. Mater.*, 362 (2007), 451-458.
133. S. Nakayama, K. Itoh, *J. Eur. Ceram. Soc.*, 23 (2003), 1047-1052.
134. O. Terra, N. dacheux, F. Audubert, R. Podor, *J. Nucl. Mater.*, 352 (2006), 224-232.
135. M.L. carter, H. li, Y. Zhang, E.R. Vance, D.R.G. Mitchell, *J. Nucl. Mater.*, 384 (2009), 322-326.
136. Y. Zhang, M.W.A. Stewart, H. Li, M. L. carter, E. R. Vance, S. Moricca, *J. Nucl.*

Mater., 395 (2009), 69-74.

137. L. Bois, M. J. Guittet, F. Carrot, P. Trocellier, M. G-Soyer, J. Nucl. Mater., 297 (2001), 129-137.

138. E.H. Oelkers, J-M. Montel, Elements, 4 (2008), 113-116.

### **1.9 Web references:**

1. <https://www.med.unc.edu/microscopy/files/2018/06/jablonski-diagram.pdf>

2. [https://dynamic.libretexts.org/print/url=https://chem.libretexts.org/Textbook\\_Maps/Physical\\_and\\_Theoretical\\_Chemistry\\_Textbook\\_Maps/Supplemental\\_Modules\\_\(Physical\\_and\\_Theoretical\\_Chemistry\)/Spectroscopy/Electronic\\_Spectroscopy/Jablonski\\_diagram.pdf](https://dynamic.libretexts.org/print/url=https://chem.libretexts.org/Textbook_Maps/Physical_and_Theoretical_Chemistry_Textbook_Maps/Supplemental_Modules_(Physical_and_Theoretical_Chemistry)/Spectroscopy/Electronic_Spectroscopy/Jablonski_diagram.pdf)

3. [https://en.wikipedia.org/wiki/Franck%E2%80%93Condon\\_principle](https://en.wikipedia.org/wiki/Franck%E2%80%93Condon_principle)

4. <https://www.olympus-lifescience.com/pt/microscope-resource/primer/java/jablonski/jabintro/>

5. [https://www.fh-muenster.de/ciw/downloads/personal/juestel/juestel/7-InkohaerenteLichtquellen-Leuchtstoffe\\_english\\_.pdf](https://www.fh-muenster.de/ciw/downloads/personal/juestel/juestel/7-InkohaerenteLichtquellen-Leuchtstoffe_english_.pdf)



## **Chapter 2**

# **General Experimental Procedures and Technical Details**



## **2.1 Introduction:**

This chapter describes the experimental procedures of synthesis of phosphors through different routes and the analytical techniques used to characterize and study the luminescence properties of the phosphors. The conventional solid-state reaction was adopted in the present work for synthesis of phosphate based solid samples whereas co-precipitation as well as combustion synthesis route were followed for barium borate and barium aluminum borate samples. The synthesized phosphor samples were analyzed by XRD diffraction technique for their phase identification. SEM studies were also carried out for morphology study. Photoluminescence studies were conducted using a spectrofluorimeter. EXAFS (Extended X-ray Absorption Fine Structure) studies were performed at BL-9, RRCAT, Indore.

## **2.2 Phosphor synthesis by solid-state reaction:**

$\text{CaBPO}_5$ ,  $\text{SrBPO}_5$  and  $\text{BaBPO}_5$  samples were synthesized by conventional solid state reaction. Here carbonate form of divalent alkaline earth metals ( $\text{Ca}^{2+}$ ,  $\text{Sr}^{2+}$ ,  $\text{Ba}^{2+}$ ), Boric acid ( $\text{H}_3\text{BO}_3$ ) and Di-Ammonium hydrogen Phosphate ( $(\text{NH}_4)_2\text{HPO}_4$ ) were used as starting material. In uranium doped samples Uranyl nitrate hexa hydrate was used ( $\text{UO}_2(\text{NO}_3)_2 \cdot 6\text{H}_2\text{O}$ ). Europium nitrate [ $\text{Eu}(\text{NO}_3)_3 \cdot 5\text{H}_2\text{O}$ ] and Samarium nitrate [ $\text{Sm}(\text{NO}_3)_3 \cdot 5\text{H}_2\text{O}$ ] were used to dope europium or dysprosium in the host. All the reagents were of analytical grade (99.9%) reagent. During synthesis the stoichiometric ratio of the reactants were maintained carefully. In the synthesis process the 1<sup>st</sup> step followed was grinding of all the reactants in an agate mortar for 20 minutes to ensure homogenous mixing of the reactants. The mixture of reactants were pelletized and placed in an array in the

alumina boats and kept inside the tubular furnace. All the samples were given two-stage firing. Prefiring was done at 600°C for 3 hours because at this temperature the precursors completely decompose to yield the reactive starting materials (e.g.  $\text{MCO}_3(\text{s}) \rightarrow \text{MO}(\text{s}) + \text{CO}_2(\text{g})$ ). Later, pellets were cooled, ground and re-pelletized before the next firing. At the second stage, the reaction was carried out at 900°C for 3 h. During annealing, in order to monitor the accurate temperature profile in the tubular furnace thermocouple was used. Different annealing temperature as well as different annealing time were also applied to get study the effect of annealing temperature and time on the structure as well as luminescence property of the samples.

### **2.3 Phosphor synthesis by co-precipitation:**

Doped and undoped  $\text{BaB}_2\text{O}_4$  samples were prepared via co-precipitation route. The starting reactants were barium nitrate ( $\text{Ba}(\text{NO}_3)_2$ ) and boric acid ( $\text{H}_3\text{BO}_3$ ). The required dopants such as uranium and europium were taken in their nitrate form. Initially required amount of  $\text{Ba}(\text{NO}_3)_2$  and  $\text{H}_3\text{BO}_3$  were dissolved in de-ionized water separately. Then required amount of dopant ion (U/Eu) solution (nitrate form) was added into the  $\text{Ba}(\text{NO}_3)_2$  solution and mixed thoroughly with continuous stirring. Then, the mixture was dropped in to the  $\text{H}_3\text{BO}_3$  solution at 50°C under magnetic stirring. At each step the stoichiometry of all the reactants were maintained accurately. After certain period of stirring, precipitate was formed and it was collected by careful filtration. The collected precipitate was washed thoroughly with de-ionized water and dried in an oven at 100°C for 24 h. After this the samples were annealed at 800°C for 2 hrs. The annealed samples were taken for pl as well as physical characterization measurements.

#### **2.4 Phosphor synthesis by combustion synthesis:**

The powder samples of uranium doped  $\text{BaAl}_2\text{B}_2\text{O}_7$  were prepared by a solution combustion technique. The high purity starting materials,  $\text{Ba}(\text{NO}_3)_2$ ,  $\text{Al}(\text{NO}_3)_3 \cdot 9\text{H}_2\text{O}$ , Uranyl nitrate,  $\text{H}_3\text{BO}_3$ ,  $\text{CO}(\text{NH}_2)_2$  have been used for phosphor preparation. All the reagents are of A.R. grade. The stoichiometric amounts of the ingredients were thoroughly mixed in an Agate Mortar, adding little amount of double distilled water to obtain an aqueous homogeneous solution. The aqueous solution was then transferred into a china basin and slowly heated at lower temperature of  $70^\circ\text{C}$  in order to remove the excess water. The solution was then introduced into a preheated muffle furnace maintained at  $500^\circ\text{C}$ . The solution boils. Then foams came out and immediately it ignites to burn with flame; thus a voluminous, foamy powder was obtained (Figure 2.1). The entire combustion process was over in about 5 min. Following the combustion, the resulting fine powders were annealed at a temperature of  $800^\circ\text{C}$  for about 3 hrs. and subsequently quenched to room temperature.



**Figure 2.1: Combustion flame generated during combustion synthesis**

### **2.5 Pelletizer:**

Powder samples after homogenous mixing in mortar and pestle were converted into pellets before loading into furnace. A hydraulic press was used for making pellets from the powder samples. Required amount of powder was initially added into the die and plugged with plunger. About 2- 4 tonnes of pressure (depending on the phosphor powder) was applied to obtain stable pellets of 10 mm size weighing around 150-200 mg. The purpose of pelletization was to achieve better diffusion and to anneal more samples in a single batch. For weighing the reactants a high precision electronic balance (make:Adair Dutt) with an accuracy of  $\pm 0.01\text{mg}$  was used.

### **2.6 Tubular furnace:**

A horizontal tubular furnace (50 mm dia X 1500 mm length) as shown in figure 2.2, was used for the synthesis of phosphors. The tube was made of refractory alumina (m.p 1950°C). The heating elements consist of silicon carbide (SiC) rods that generate heat by resistive heating method. The furnace was having a heating rate of 4.5 kw/m and powered by 230 V AC. The length of the hot zone is 150 mm within which the alumina boats containing samples are normally placed. By design, this furnace did not have the provision for heating the samples at desired gas atmosphere. Hence, we modified the furnace by providing two end plugs which contain inlet and outlet provisions. Using these end plugs, the required atmosphere can be easily maintained. The outlet was safely vented out to environment. This furnace is designed for attaining maximum temperature of  $1400^{\circ}\text{C}\pm 5^{\circ}\text{C}$ . A microprocessor based programmable controller was connected to the furnace to vary the synthesis parameters. With the help of this, the ramping temperature and soaking temperature were fixed. The heating rate was set at  $4^{\circ}\text{C}/\text{min}$  and the samples were natural cooled.



**Figure 2.2: Schematic sketch of modified tubular furnace**

### **2.7 Characterization of phosphors by XRD and SEM:**

Powder X-ray diffraction measurements were recorded in reflection mode at room temperature using a Phillips PW 1800 diffractometer. The copper  $K_{\alpha}$  radiation ( $\lambda = 1.5046\text{\AA}$ ) was used with nickel as  $K_{\beta}$  filter. A silicon wafer with (911) crystallographic plane was used as a sample holder as this has a low X-ray background and no diffraction peaks. A continuous scanning was used to obtain the diffraction spectra from  $10^{\circ}$  to  $80^{\circ}$  with a minimum scanning step of  $0.05^{\circ}$ . The intensity of the diffracted beam was measured using NaI (Tl) scintillation detector. The X-ray diffraction spectra show the intensities of the diffraction peaks as a function of the detecting angle  $2\theta$ .

The morphology of the samples was recorded by scanning electron microscopy (SEM) model-AIS-2100, Merero Inc, South Korea. This was carried out on an instrument having

both secondary electron detector and solid-state back-scattered electron detector. The micrographs were taken at 20 KeV acceleration voltages.

## **2.8 Spectrofluorimeter and life time decay studies:**



**Figure 2.3: Shimadzu RF 5301pc spectrofluorimeter**

The instrumental requirements for measuring fluorescence are: a light source, a light-dispersing element, and a light detector i.e. 1) xenon lamp, 2) excitation monochromator, 3) emission monochromator and 4) photomultiplier tube respectively. We have used Japan make Shimadzu RF 5301pc spectrofluorimeter (Figure 2.3) for photoluminescence (PL) measurements (both excitation and emission). The excitation source was a 150W CW (continuous wave) xenon lamp. Since the intensity of the lamp is high, a tremendous amount of heat is generated during operation and therefore a fan is provided to cool the lamp housing. In this system the bandwidths for the excitation and emission monochromator can be set at 1.5, 3 or 5 nm. A long-wavelength-pass filter (UV-35, Shimadzu), with a maximum and uniform transmittance (more than 85%) above 350 nm, was placed in front of the emission monochromator in order to reduce the scatter of the incident beam into the emission monochromator. In the RF 5301pc spectrofluorimeter, the

gain of the photometric photomultiplier tube is dynamically adjusted to correct for the changes in the Xe lamp output intensity using a monitoring photomultiplier. The high-throughput optical system in the RF-5301PC employs a blazed holographic grating, photomultiplier and digital circuit to provide best level of S/N ratio. Here a spectrum can be measured in seconds due to high-speed scanning up to 5,500nm/min. The monochromator slewing is adjust to about 20,000nm/min, thus setting of two or more wavelengths can be performed quickly and easily. The sample compartment provided here is of 140mm wide, 170mm deep and 140mm high.



**Figure 2.4: Image of solid sample holder**

Figure 2.4 shows the sample holder used for fluorescence measurement of solid samples. The angle of the holder is designed to limit the reflected excitation beam from the emission monochromator. Standard accessories include a sample holder, quartz plate, powder sample plate, spacers and a sample fixing bar. Cutoff filters are included to reduce further scattering (UV-31, UV-35, UV-39, UV-Y43, UV-Y45, UV-Y47). The PL decay time measurements

were carried out using an Edinburgh FLS-900 time resolved fluorescence spectrometer at room temperature.

## **2.9 EXAFS Analysis:**

The Extended X-ray Absorption fine structure (EXAFS) technique, with synchrotron radiation as the X-ray source, is a powerful tool to study short range order and local structures around any particular element in a material. The basic principle deals with the modulation of an atoms X-ray absorption probability which is a reflection of its chemical and physical state in a particular environment. EXAFS deals with the fine structure oscillations observed in the X-ray absorption spectra of an element from 50 eV to ~700 eV above its absorption edge, gives precise information regarding the short range order and local structure around the particular atomic species in the material [1]. The use of modern bright Synchrotron radiation sources, has made EXAFS a powerful local structure determination technique, which can be applied to a large group of material viz. amorphous, polycrystalline, polymers, surfaces and solutions.

RRCAT, Indore, India has developed a comprehensive facility for carrying out EXAFS measurements with 2.5 GeV, Synchrotron Radiation Source (INDUS-2) [1]. The facility consists of two operational beam lines viz., the Energy Dispersive EXAFS beam line (BL-8) and the Energy Scanning EXAFS beam line (BL-9) [2]. In our experiment, we have used Scanning EXAFS Beam line (BL-9). The Energy Scanning EXAFS beam line (BL-9), can be operated both in transmission as well as fluorescence modes within the energy range of 4-25 keV. The beam line optics consists of an Rh-Pt coated cylindrical collimating mirror, a Double Crystal Monochromator (DCM) with sagittally bent 2nd crystal for horizontal

focusing and a cylindrical post mirror for vertical focusing of the beam [3]. Figure 2.5. shows the optical lay out of BL-9.

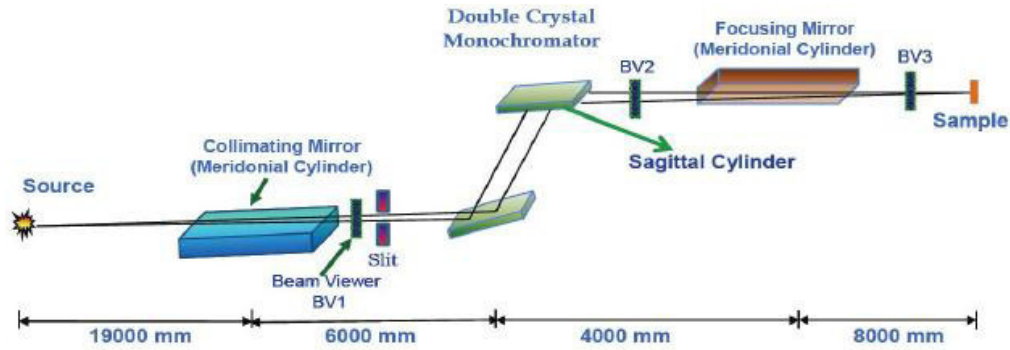


**Figure 2.5: Optical layout of BL-9**

The double crystal monochromator (DCM) works in the photon energy range of 4-25 KeV with a resolution of  $10^4$  at 10 KeV. A 1.5 m horizontal pre-mirror with meridional cylindrical curvature is used prior to the DCM for collimation of the beam and higher harmonic rejection. The second crystal of the DCM is a sagittal cylinder with radius of curvature in the range 1.28-12.91 meters which provides horizontal focusing to the beam. For measurements in the fluorescence mode, the sample is placed at  $45^\circ$  to the incident X-ray beam and the fluorescence signal ( $I_f$ ) is detected using a Si drift detector placed at  $90^\circ$  to the incident X-ray beam. An ionization chamber detector is used prior to the sample to measure the incident X ray flux ( $I_0$ ) and the absorbance of the sample ( $\mu = \frac{I_f}{I_0}$ ) is obtained as a function of energy by scanning the monochromator over the specified energy range.

The experimental EXAFS data is analysed using EXAFS data analysis program offered by IFEFFIT software package [4].

### **2.10 References:**

1. M.J. Fay, A. Proctor, D. P. Hoffman, D. M. Hercules, *Anal. Chem.*, 60 (21) (1998), 1225A- 1243A.
2. S. Basu et al, *J. Phys.: Conf. Ser.*, 493 (2014), 012032.
3. A. K. Poswal, A. Agrawal, A. K. Yadav, C. Nayak, S. Basu *et al.*, “Commissioning and First Results of Scanning Type EXAFS Beamline (BL-09) at INDUS-2 Synchrotron Source,” *AIP Conf. Proc.*, 1591 (2014), 649-651.
4. M. Newville, B.Ravel, D. Haskel, J.J. Rehr, E.A. Stern, and Y. Yacoby, “Analysis of Multiple- scattering XAFS Data Using Theoretical Standards,” *Physica B*, 2008 (1995) ,154-156



## **Chapter 3**

### **Photoluminescence properties of U in SrBPO<sub>5</sub> host: Effect of concentration and annealing temperature**



### **3.1 Introduction:**

Actinide ions with their partly filled 5f orbitals exhibit interesting photo luminescence properties which can throw light on the electronic structure and nature of metal-ligand bonding for the ions [1]. The later actinides with their closely spaced energy levels do not show efficient PL and decay via non-radiative mode. However, amongst the first half of the actinide series, U, Am and Cm are known to have good PL yield, when excited by a suitable wavelength [2]. Unlike their 4f series counter parts, the early actinide series members show variable valence states which make them as an interesting class of compounds. In case of most of the actinide ions, electronic transitions within the 5f<sup>n</sup> levels occur in visible and near UV region that are Laporte forbidden thereby making them very less intense. The forbiddenness of the Laporte selection rule can be made less rigorous by stabilising the actinide ions in different crystalline matrices [3-4]. Many efforts have been made to explore suitable matrices, in order to achieve better luminescence from actinide elements. Among the actinide elements photo luminescence studies of uranium activated solid matrices have gained much attention owing to its application in the nuclear industries, as the requirement of inert solid matrix for incorporation of nuclear waste is a challenging area of investigation [5]. Uranium activated matrices are well known and promising catalyst for thermal degradation of pollutant molecules [6]. Moreover many uranium doped solid matrices are known to be efficient green light emitting phosphor [7]. Uranium being a strategic element for nuclear industry (fissile element) has got limited scope of investigation, as it is associated with safety and security concerns. At the same time the

unique photo physical and photo electronic properties of uranium has fascinated and restored the research interest [8].

Plenty of literature reports are available dealing with the PL properties of various oxidation states of U such as U(VI), U(V), U(IV) and U(III) in different matrices [9-12]. Out of these, the most investigated and the most commonly encountered species is the hexavalent uranium ion in uranyl form ( $\text{UO}_2^{2+}$ ). The PL emission spectra of these species gives unique vibrationally resolved ligand to-metal charge transfer (LMCT) emission in green region [13]. Unlike lanthanides, the 5f electrons (in  $5f^{n-1} 6d$  configuration) of uranium show high oscillator strength and more sensitivity towards ligand and crystal field effects. Consequently, the PL properties like excitation, emission and life time data are greatly influenced by the symmetry and coupling to external vibrational modes of closely lying ligands and crystal fields that in turn makes it an useful probe for investigating the coordination environment [14]. In solids the crystal structure of host matrix and synthesis conditions are responsible factors for stabilization of Uranium in different forms such as octahedral/tetrahedral uranium groups ( $\text{UO}_6^{6-}$ ,  $\text{UO}_4^{2-}$  and  $\text{U}^{6+}$ ) other than the usual uranyl species [15]. Thus stabilization of uranium indirectly gives information about the lattice chemistry as well as the crystal field experienced in that particular matrix. The  $\text{UO}_2^{2+}$ ,  $\text{UO}_6^{6-}$ , and  $\text{U}^{6+}$  centres are well documented for green emission where as  $\text{UO}_4^{2-}$  centre is known for red emission [16]. Among the above forms of uranium, only uranyl ( $\text{UO}_2^{2+}$ ) is stable both in aqueous solution and in solid state and also different from other species with respect to its characteristic emission consisting of equidistant vibronic progressions. The near linear O-U-O structural geometry with individual U-O bond length of  $\sim 1.8\text{\AA}$  is a constraint

on stabilizing the whole moiety in a crystal lattice. The stabilization of uranyl varies with respect to host crystal lattice. It has been reported that uranium can either form a second phase with the host matrix to stabilize its uranyl form, or in some cases the inversion centre present in the crystal lattice appears to be the stabilization centre [17]. Suitable lattice sites for stabilizing Uranyl ion is a continuing matter of investigation.

The nature of uranium PL can also be influenced by concentration of the dopant ion and synthesis conditions. In this regard, the nature of uranium emission spectra has been studied in many matrices. In the series of matrices, phosphate based host lattices are well investigated and it has been observed that matrices like  $\text{Sr}_3(\text{PO}_4)_2$ ,  $\text{SrP}_2\text{O}_7$  offer the regular  $\text{Sr}^{2+}$  lattice sites to stabilize uranium as U(VI) without affecting the crystal structure [18-19]. Recently Kumar et al have reported the stabilisation of uranium as uranyl in one of the borophosphate based host i.e.  $\text{SrBPO}_5$  (SBP) prepared through solid state reaction route [20]. However, the dopant ion concentration in the work was arbitrarily fixed at 1 mol%. There has not been any effort to explore the luminescence properties of this actinide ion as a function of concentration or annealing temperature. In the present investigation we report an extensive PL study of uranium ion in the borophosphate host and its effect on the dopant ion concentration and annealing temperature. In addition, CIE color coordinates of the system was also evaluated.

### **3.2 Experimental:**

The undoped and uranium doped samples were prepared via solid state reaction route. All the chemicals used here were of Analytical Reagent (AR) grade. Stoichiometric proportions of  $\text{SrCO}_3$ ,  $(\text{NH}_4)_2\text{HPO}_4$ ,  $\text{H}_3\text{BO}_3$  (5 mol% excess), and  $\text{UO}_2(\text{NO}_3)_2 \cdot 6\text{H}_2\text{O}$  were ground

together thoroughly to prepare a homogenised mixture followed by pelletization. In the first phase, all the samples were fired at 600°C in air atmosphere for three hours in a muffle furnace. The samples were cooled to room temperature and thoroughly ground again before pelletization. In the second phase, pre fired samples were annealed at 900°C for 3 hours in air atmosphere and cooled to room temperature. The reactants react with each other by the following equation to form the final product.



To investigate the effect of annealing temperature on the system, the samples were further heated at 1000 and 1100°C. The dopant ion concentration was varied between 1 to 8 mol %. The crystal Structure and phase purity of the prepared powders were examined through powder X-ray diffraction using a Philips diffractometer (model PW 1071) operating with monochromatic  $\text{CuK}_\alpha$  ( $\lambda = 1.5418\text{\AA}$ ) radiation. The diffraction pattern was recorded at a scan rate of 0.05°/s in the scattering angle range ( $2\theta$ ) of 10°-80°. The morphology of the samples was recorded by scanning electron microscopy (SEM) model-AIS-2100, Merero Inc. PL excitation and emission measurements were made using a Shimadzu RF 5301pc spectrofluorimeter. The excitation source was a 150W CW (continuous wave) xenon lamp. The bandwidths for the excitation and emission monochromator were set at 3 nm. A long-wavelength-pass filter (UV-35, Shimadzu), with a maximum and uniform transmittance (more than 85%) above 350 nm, was placed in front of the emission monochromator in order to reduce the scatter of the incident beam into the emission monochromator. In the

RF 5301pc spectrofluorimeter, the gain of the photometric photomultiplier tube is dynamically adjusted to correct for the changes in the Xe lamp output intensity using a monitoring photomultiplier. The PL decay time measurements were carried out using an Edinburgh FLS-900 time resolved fluorescence spectrometer at room temperature.

### **3.3 Results and Discussion:**

#### **3.3.1 Crystal structure and Morphology:**

SrBPO<sub>5</sub> belongs to the stillwellite (LnBSiO<sub>5</sub>) type compound with trigonal system with hexagonal setting [21]. (BO<sub>4</sub>)<sup>3-</sup> and (SiO<sub>4</sub>)<sup>4-</sup> tetrahedra anions are two primary constituents of the borophosphate host. The (SiO<sub>4</sub>)<sup>4-</sup> tetrahedral form edge sharing vertical columns parallel to the c-axis. Each (BO<sub>4</sub>)<sup>3-</sup> tetrahedron is linked to two (SiO<sub>4</sub>)<sup>4-</sup> tetrahedra and has two common edges with the lanthanide polyhedral of adjacent columns resulting in a helical chain like structure [22]. The anionic network forms tortuous vertical channels that surround the lanthanide polyhedral, the lanthanide ion being in a 9-coordinated site with oxygens. However in case of SrBPO<sub>5</sub> crystal structure (that mimics stillwellite (LnBSiO<sub>5</sub>)), the incorporation of Sr<sup>2+</sup> in to a nine-coordinated polyhedron found to be difficult because of its smaller charge to size ratio compared to Ln<sup>3+</sup>. In order to stabilize the system the bond length of the anion network gets in to readjustment with formation of some kind of oxygen defects and finally an eight coordinated Sr<sup>2+</sup> site is formed. It is the internal crystal lattice arrangement of SrBPO<sub>5</sub> that stabilizes different types of dopants (rare earths, transition metals and actinides) in it. A schematic of the crystal structure is shown in figures- 3.1 A and B. Figure-3.2 and 3.3 show the XRD patterns of the SBP: U system as a function of dopant ion concentration and annealing temperature respectively. The observed patterns

indicated that the synthesized samples are single hexagonal phase with a space group of  $P3_221$  matching with ICDD file no 18-1270. There was no detectable impurity peak observed indicating successful synthesis of material in pure and single phase. The Uranyl being a heavy molecule and having higher charge to size ratio, solubility in  $SrBPO_5$  matrix was studied with different Uranium concentration (1 mol%, 4 mol% and 8 mol %) by recording XRD. It can be seen from the figure 3.2 that with dopant ion concentration up to 8 mol%, there was no change in the patterns suggesting no impurity phase formation in the system.

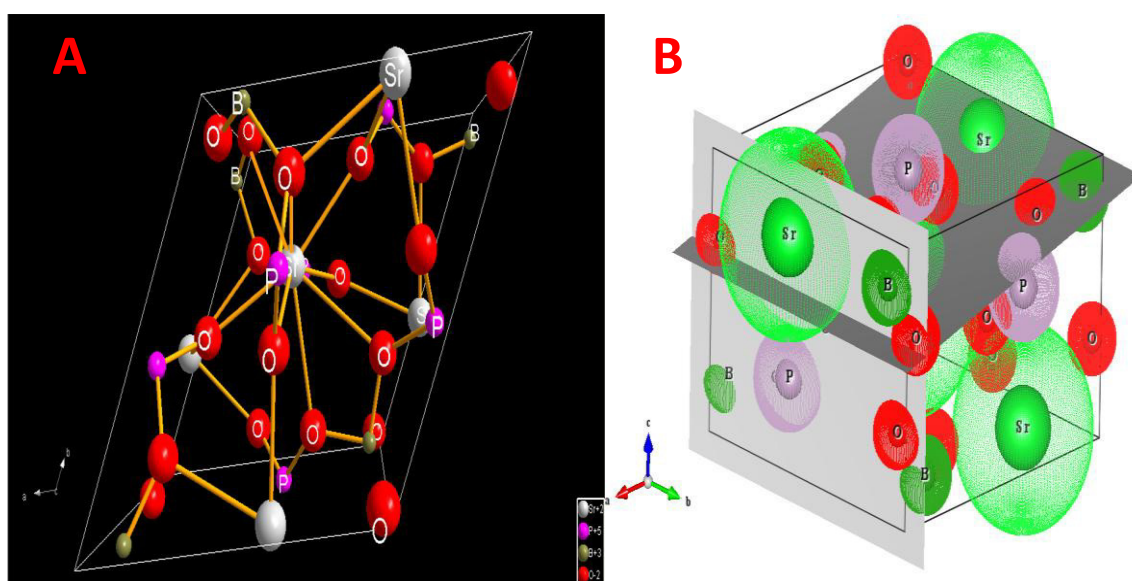


**Figure 3.1: (A) Shows the crystal structure of SrBPO<sub>5</sub> showing the 8 coordinated ‘Sr’ site; The figure 1 (B) shows the crystal structure with the two planes (2 0 0) and (1 0 4) (the shaded region) that show the highest intensity in XRD data.**

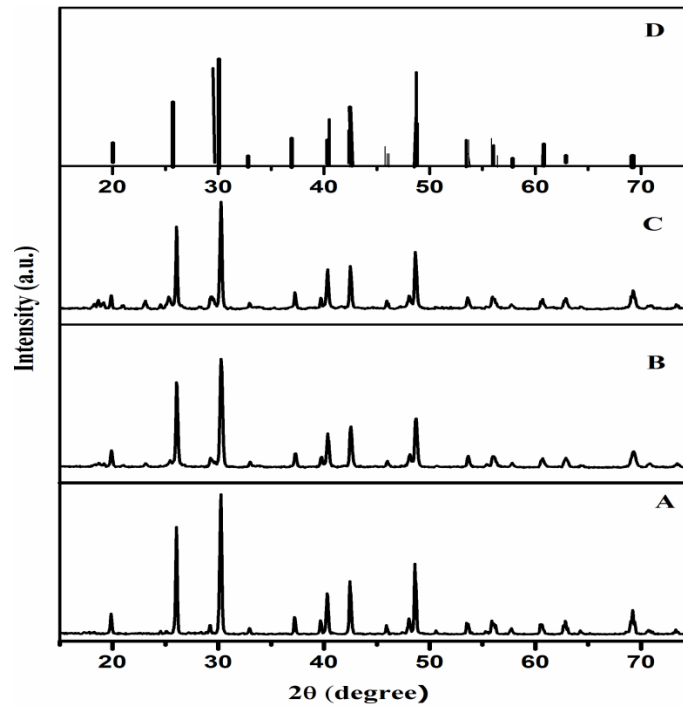


**Figure 3.2: XRD patterns for SrBPO<sub>5</sub> doped with uranium as a function of dopant ion concentration (in mole %) A- 1 mol%, B- 4mol% C- 8 mol%; all samples are synthesized at 900°C annealing temp. The figure D indicates the standard pattern of the ICDD file no- 18-1270.**

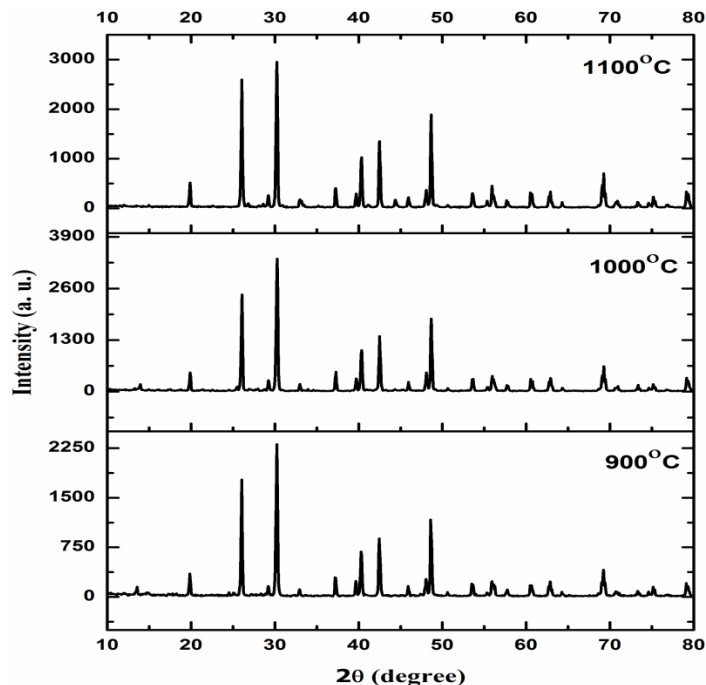


**Figure 3.3: XRD patterns for SrBPO<sub>5</sub> doped with uranium as a function of annealing temperature.**

The detailed XRD data for some of the major peaks of the SBP system are given in table-1. The average cell parameters calculated from the observed ‘d’ values for these samples were  $a = 6.869(2) \text{ \AA}$ ,  $c = 6.7969(7) \text{ \AA}$  which are in close agreement with the reported values. This observation could be due to the fact that the lattice parameters with higher Uranium concentration may be below the detection limit of the XRD technique. Another possibility is that the Uranium ion before reaching the lattice sites got stabilized in the interstitial sites without affecting the cell parameters. Recently it has been strongly emphasized that in strontium pyrophosphate ( $\text{Sr}_2\text{P}_2\text{O}_7$ ) matrix uranium got stabilized at regular  $\text{Sr}^{2+}$  site [19]. In present case uranium may be stabilized in the same manner. As discussed earlier, the present host lattice is a stillwellite type of compound: a trigonal system with hexagonal settings as observed in rare earth borosilicate, LnBO ( $\text{SiO}_4$ ) with three formula units per cell. The

charge to size ratio of Uranium ( $U^{6+}$ ) is greater than the charge to size ratio of  $Sr^{2+}$  and  $Ln^{3+}$ , so unlike  $Sr^{2+}$  it can suitably rest at nine oxygen co-ordinated sites.

From the XRD data of the samples with varying annealing temperature (figure 3.3), it can be noticed that between  $900^{\circ}C$  to  $1100^{\circ}C$  there was no change in the XRD pattern. However, the intensity of the diffraction peaks got enhanced at higher temperatures which are probably due to better crystallinity at higher annealing temperatures indicating a better thermal stability of the material.

Figure 3.4 shows the SEM data for the SBP system as a function of annealing temperature. The figure shows an inhomogeneous size distribution and agglomeration of the particles in the SBP system. From the figure it is clear that, on annealing beyond  $900^{\circ}C$ , the overall roughness of the edges of the samples gets improved owing to the improved crystallinity. The overall particle size for the system was found to be less than  $1\mu m$  based on the statistical analysis from several micrographs. The uneven shape of the particles observed in this case was due to the synthesis procedure.

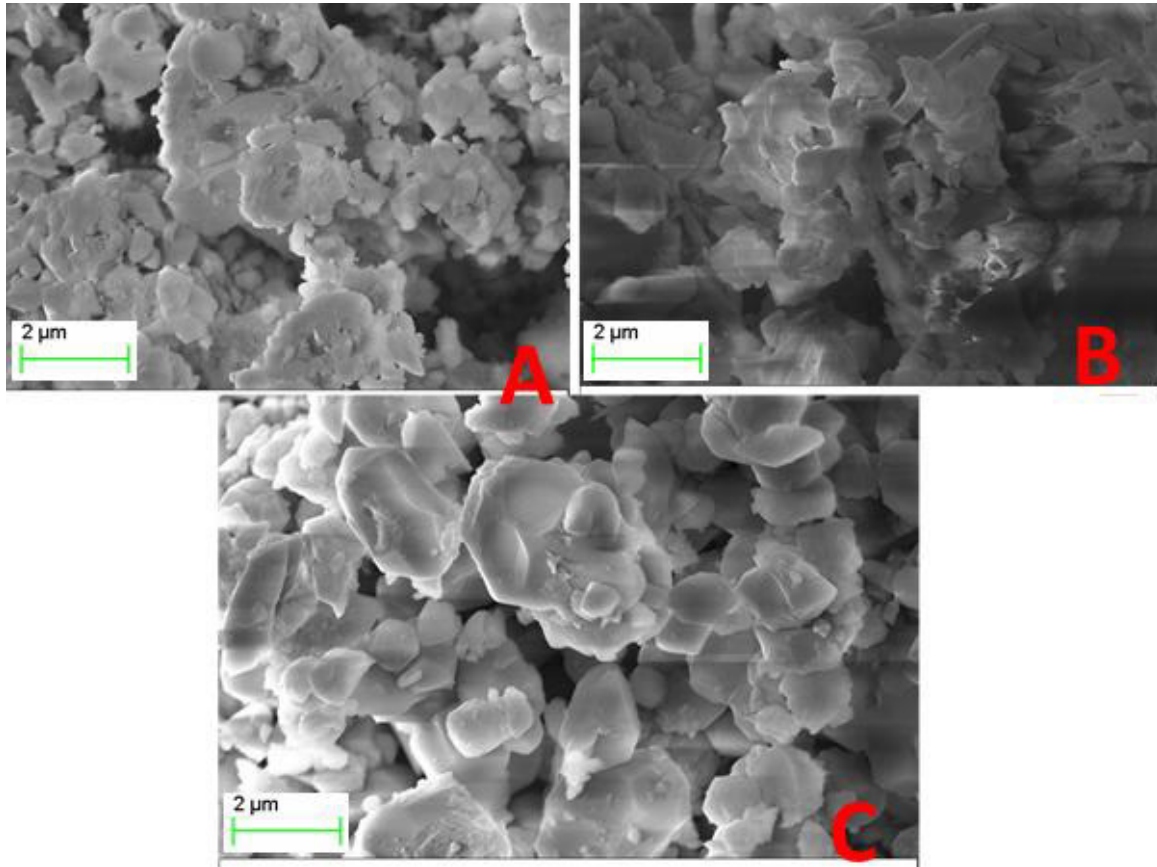


**Figure 3.4: SEM micrographs of the SBP samples as a function of annealing temperature; A-900, B-1000 and C-1100°C.**

### **3.3.2 PL investigations:**

Figure 3.5 shows the emission spectra of SBP: U system as a function of the dopant ion concentration with 434 nm excitation. The spectra is similar to the data reported by Kumar et al [20] that showed a five band structure for the samples with peaks at 481 nm ( $20790\text{ cm}^{-1}$ ), 498 nm ( $20080\text{ cm}^{-1}$ ), 519 nm ( $19268\text{ cm}^{-1}$ ), 539 nm ( $18518\text{ cm}^{-1}$ ) and 560 nm ( $17875\text{ cm}^{-1}$ ). Another weak but prominent hump in the spectra was observable at 595 nm ( $16,806\text{ cm}^{-1}$ ). These bands are known to be associated with Uranyl emissions [23].

**Table 3.1: X-ray diffraction data of SBP: U system**

Sr.No.	d observed ( $\text{\AA}^0$ )	d calculated ( $\text{\AA}^0$ )	<i>hkl</i>	<i>I</i>
1.	4.480	4.476	102	20
2.	3.439	3.426	110	80
3.	2.966	2.967	200	100
4.	2.957	2.956	104	100
5.	2.416	2.416	114	10
6.	2.272	2.273	006	10
7.	2.242	2.243	210	40
8.	2.239	2.238	204	40
9.	2.129	2.129	106	50
10.	1.894	1.894	116	10
11.	1.873	1.874	214	60
12.	1.713	1.713	220	10
13.	1.711	1.711	304	10
14.	1.531	1.531	224	10
15.	1.526	1.526	118	10

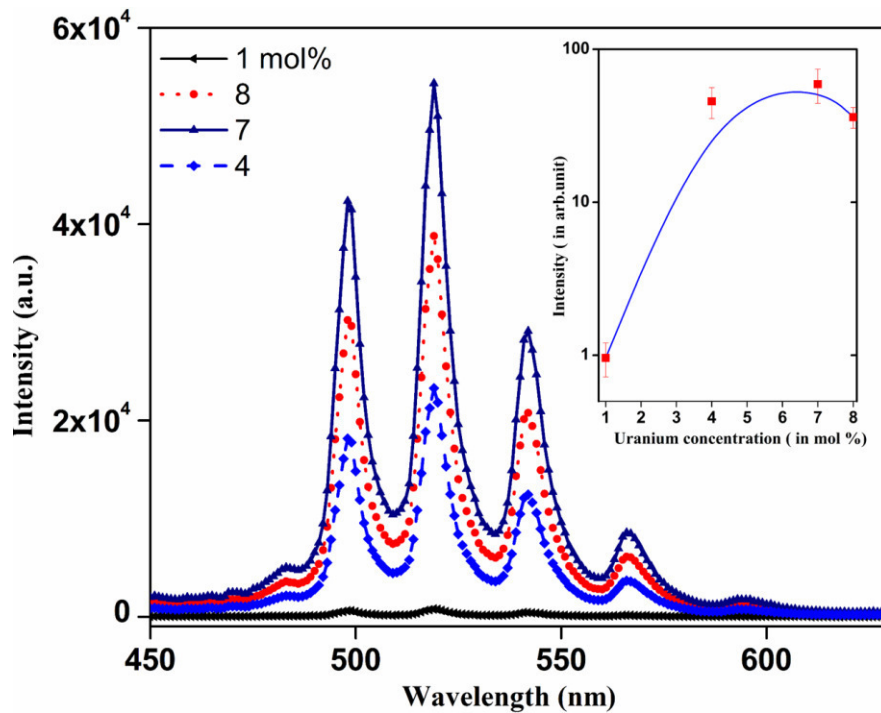


**Figure 3.5: PL emission spectra of the SBP:U system as a function of dopant ion concentration; the inset figure shows the emission intensity values for the 520 nm peak as a function of Uranium concentration.**

Uranyl with  $D_{\infty h}$  symmetry makes the ligand to metal charge transfer (LMCT) process parity forbidden. It is the local co-ordination environment that lowers the symmetry and results in relaxation of parity allowing the transition [24]. One of the significant electronic transitions, the zero phonon (zp) transition is a result of electronic excitation from the  $3\sigma_u$  ground state, a highly hybridized configuration of the O (2s, 2p) and U (5p, 5f, 6d, 7s) atomic orbitals to the  $f_{\delta,\phi}$  orbitals of uranyl. In the present case, the emission band centred at 481 nm is ascribed as the zp line while other bands are assigned as radiative transition from electronic excited state to various higher vibronic levels in ground state [25]. The position of the zp line can vary from 470 to 520 nm depending on the equatorial coordination environment of Uranium in the system. The five emission bands at higher wavelengths are known to be vibration progressions resulting from strong coupling of the ground state Raman active symmetric vibrational ( $\nu_1$ ) mode with the  $^3\Pi_u$  electronic excited state [26]. The average spacing between the five lowest energy bands is  $798\text{ cm}^{-1}$  that corresponds to the vibrational spacing in the ground state indicating a high force constant of the electronic state [27].

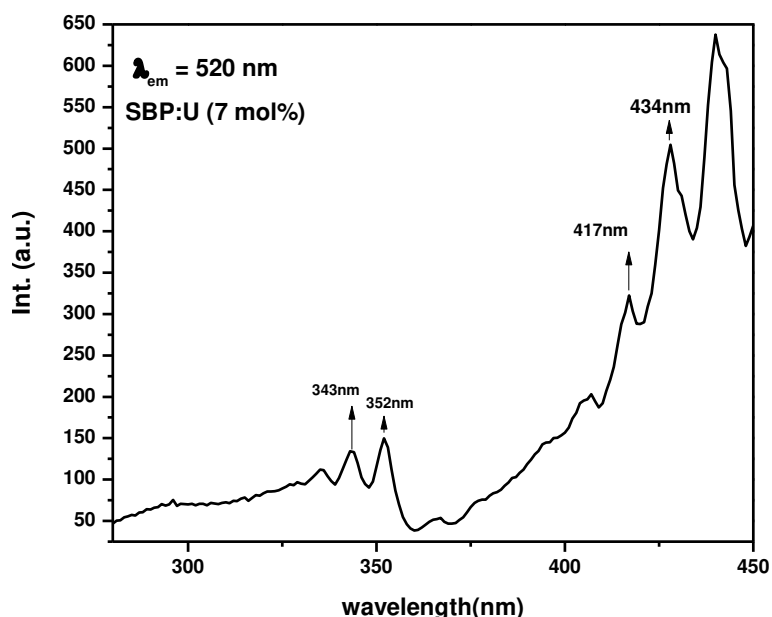
From the figure 3.5, it is clear that, with increase in the dopant ion concentration, the PL emission intensity increases up to 7 mol% of the uranium ion. The decrease in PL intensity beyond 7 mol % could be ascribed to concentration quenching, a cross relaxation between Uranyl ions with loss of excited state energy through a non-radiative path. There are two types of mechanism to investigate the non-radiative transfer of energy. One is Dexter type, a collisional energy transfer and other one is Forster resonance energy transfer (FRET), a multipole – multipole interaction mechanism [28]. Generally the energy transfer depends

on the donor-acceptor spectral overlap (the emission of donor and excitation of the acceptor should have an overlap) and the relative orientation of the dipole moments. In addition to these in case of FRET, the distance ( $L$ ) between the donor and acceptor ion is important as the probability of the energy transfer decreases at a rate of  $1/L^6$ . The typical distance (critical distance,  $L_c$ ) for FRET is maximum  $100\text{\AA}$ . In case of Dexter mechanism the probability of energy transfer decreases as  $(\exp)^{-L}$  and here maximum typical distance is  $\leq 10\text{\AA}$ . In present case an approximate  $L_c$  value was calculated using the following relation [24].

$$L_c = 2(3V/4\pi NX_c)^{1/3} \quad (2)$$

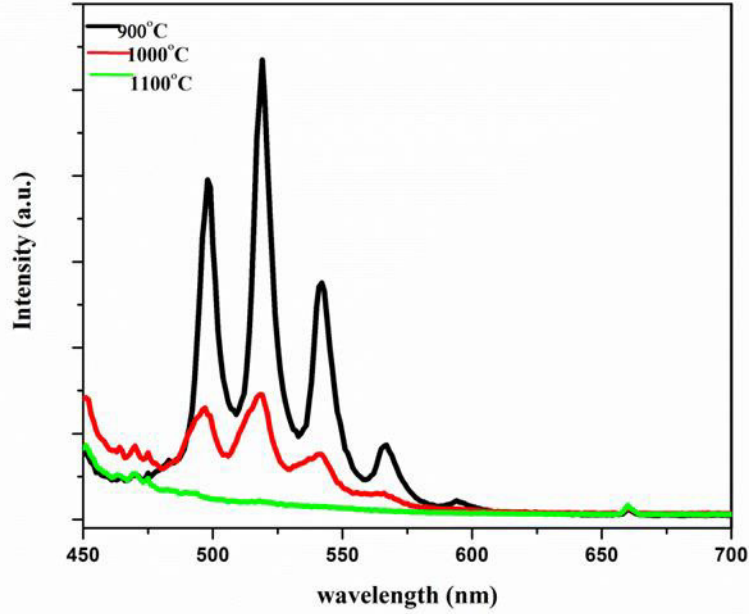
Where  $V$  is the unit cell volume,  $N$  the number of sites and  $X_c$  is the critical concentration. The value of  $N$  and  $V$  are obtained from XRD data. Considering 7 mol% as the critical concentration value,  $L_c$  was calculated to be  $3\text{\AA}$ . This shows that the Dexter type energy transfer process is the reason leading to Uranyl luminescence quenching in the present matrix for  $\text{UO}_2^{2+}$  concentration  $> 7\text{mol}\%$ .

Figure 3.6 shows the corresponding excitation spectra for the 7 mol% uranium doped sample at 520 nm emission wavelength. The sample was annealed at  $900^\circ\text{C}$ . It can be seen from the figure that the broad excitation spectra has peak maxima at 335, 343, 352, 407, 417, 434, and 440nm. For Uranyl, the optical excitation is purely a ligand-to-metal charge transfer (LMCT) process, where an electron transition occurs from a bonding oxygen orbital ( $\sigma_u$ ,  $\sigma_g$ ,  $\pi_u$ ,  $\pi_g$ ) to a non-bonding Uranium 5f orbital.



**Figure 3.6: Excitation spectrum for the 7 mol% uranium doped SBP system annealed at 900°C**

Earlier the XRD studies had indicated a higher thermal structural stability of the annealed samples. Figure 3.7 shows the PL emission data of the 7 mol% U doped SBP samples as a function of annealing temperature. From the figure it can be observed that, with increase in the annealing temperature, the PL yield decreased so much so that at 1100°C, the spectrum is barely visible. As discussed earlier, in this matrix oxygen vacancies can act as defect centres for the charge neutrality purpose. At higher annealed temperatures, defects can arise which can migrate or diffuse and combined to form defects of larger size. These defect centres can enhance the non-radiative energy loss of Uranyl ion and thereby decreasing the PL yield [29].



**Figure 3.7: PL emission spectra for the U: SBP system as a function of annealing temperature**

To further confirm this fact, PL decay time investigations were carried out on the U: SBP samples heated at different temperatures as shown in figure 3.8. The decay time curves were recorded with  $\lambda_{\text{ex}} = 434 \text{ nm}$  and  $\lambda_{\text{em}} = 520 \text{ nm}$ . The decay curves could be fitted in to bi-exponential decay using the following iterative formula. Here,  $A_1$  and  $A_2$  are pre-exponential factors that are scalar quantities, 't' is the time of measurement and  $\tau_1$  and  $\tau_2$  are the decay time values.

$$\mathbf{I(t) = A_1 \exp(-t/\tau_1) + A_2 \exp(-t/\tau_2) + y_0} \quad \mathbf{(3)}$$

The PL decay time values for the 900 °C annealed sample were observed to be  $\tau_1 = 165 \mu\text{s}$  (65%) and  $\tau_2 = 54 \mu\text{s}$  (35 %) with  $\chi^2 = 1.489$ . The data suggests the presence of Uranyl ions at sites with two different types of surrounding environment. The crystal structure of

SrBPO<sub>5</sub> informs the presence of single type of Sr<sup>2+</sup> site and the system is accompanied with oxygen defects. The defect centres are responsible for energy loss through non-radiative decay, thus a luminescent species surrounded by defect centres may lose its energy non-radiatively resulting in a reduced lifetime with respect to the same type of species present at a site where the concentration of defect centres is less. As observed in case of the PL emission data, the decay time values were also decreasing with increasing temperature. Thus corroborating the fact that, on annealing, more and more number of defect centres are agglomerating in the system to form large defect centre volumes which provides a non radiative path there by reducing the PL emission intensity and PL decay time.

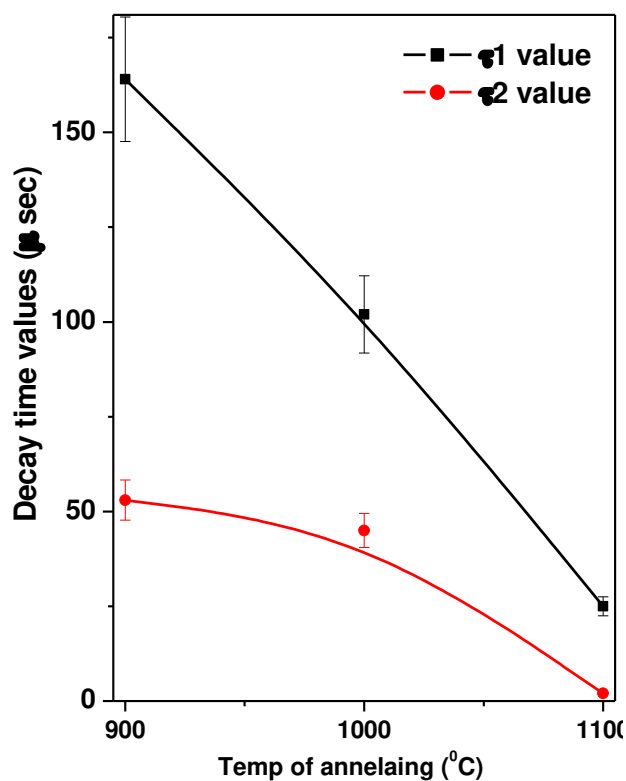


**Figure 3.8: PL decay time data for the U: SBP system as a function of annealing temperature**

### 3.3.3 Evaluation of color coordinates:

Color coordinates for the 900°C annealed and 7 mol% uranium doped sample were evaluated adopting standard procedure [30]. Recently Taikar et al. have reported Uranium doped SrO as a green light emitting phosphor and compared it with another green phosphor namely ZnS: Cu, Al [7]. The CIE (Commission Internationale de l'éclairage) chromaticity coordinates are useful to determine a light emitting materials performance on color luminescent emission. A (x, y) co-ordinate in the color space determines the color of any light source. The spectral power distribution (SPD) of the light source and the CIE color matching functions are the required parameters to determine the (x, y) coordinate. The chromaticity coordinates x, y, z can be obtained from tristimulus value X, Y and Z as follows:

$$x = X/X+Y+Z, y = Y/X+Y+Z \text{ and } z = Z/X+Y+Z \quad (4)$$

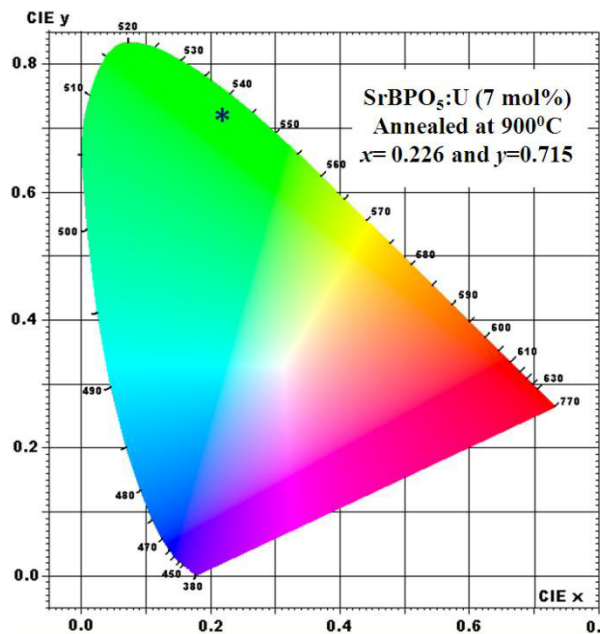


Figure 3.9: CIE chromaticity diagram for the SBP: U (7 mol %) system annealed at 900°C; The coordinates are demarked by an asterisk

The predominating wavelength from a light source is evaluated using CIE chromaticity diagram. This wavelength is an interception point of a straight line drawn from one of the CIE white illuminants, through the (x, y) coordinates up to the extent, where it touches the outer locus of points along the spectral edge of the 1931 CIE chromatic diagram. In SrBPO<sub>5</sub>: UO<sub>2</sub><sup>2+</sup> the calculated values of x and y coordinates were found to be 0.226 and 0.715 respectively indicated as an asterisk mark (\*) in the figure 3.9. The CIE index values show that the present compound can be used as a potential 'Green' emitting phosphor.

### **3.4 Conclusion:**

Uranium doped SrBPO<sub>5</sub> samples were prepared via solid state reaction route in air atmosphere. XRD studies confirmed the formation of single phase and better solubility of uranium at higher concentration. It was observed that up to 8 mol% of the dopant ion there was no phase separation in the system. SEM studies indicated the presence of uneven, agglomerated particles with less than 1 μm individual particle size. PL studies confirmed the stabilisation of uranium as UO<sub>2</sub><sup>2+</sup> in the system. Based on the PL emission data, concentration quenching was observed beyond 7 mol% of the dopant ion. The estimated critical distance (L<sub>c</sub>) of 3A° suggests Dexter type energy transfer mechanism to be the predominant one in the system. The life time decay studies indicated the presence of two different types of environment around Uranyl ion. On annealing at temperatures beyond 900°C the PL emission and decay time values reduced drastically. It was concluded that on annealing at temperatures beyond 900°C, defect centres get agglomerated around the metal ion providing non radiative pathways for the energy to get dissipated thereby reducing the PL emission and decay time. The CIE indices for the 7 mol% uranium doped

sample annealed at 900°C suggested that the material can be used as a potential green emitting phosphor.

### **3.5 References:**

1. (a) W.M.A. Smit, G. Blasse, *J. Lumin.*, 29 (1984), 367-380.  
(b) J.T.W.D. Hair, G. Blasse, *J. Lumin.*, 14 (1976), 307–323.  
(c) R.U.E. ‘t Lam, G. Blasse, *J. Chem. Phys.*, 72 (1980), 1803–1808.
2. (a) L.S. Natrajan, *Co-ordination Chemistry Reviews*, 256 ( 2012), 1583-1603.  
(b) S. Hubert, N.M. Edelstein, *Encyclopaedia of materials: Science and Technology*, Elsevier, 2001, (18-22).  
(c) J.C. Krupa, *Inorg. Chim. Acta*, 139 (1987), 223-241.
3. J.V.Beitz, *J. Alloys Compd.*, 207-208 (1994), 41-50.
4. D. C Harris, M. D. Bertolucci, *Symmetry and Spectroscopy: An Introduction to Vibrational and Electronic Spectroscopy*, New York: Oxford University Press, 1978.
5. A. Singh, J.G. Catalano, K.U. Ulrich, D.E. Giammar, *Environ. Sci. Technol.*, 46 (2012), 6594–6603.
6. S.D. Pollington, A.F. Lee, T.L. Overtone, P.J. Sears, P.B. Wells, S.E. Hawley, I.D. Hudson, D.F. Lee, V. Ruddock, *Chem. Commun.*, (1999), 725–726.
7. D.R. Taikar, C.P.Joshi, S.V.Moharil, *J. Lumin.*, 153 (2014), 304-306.
8. G. Liu, N. P. Deifel, C. L. Cahill, V. V. Zhurov, A. A. Pinkerton , *J. Phys. Chem. A*, 116 (2012), 855–864.
9. M. Sobczyk, J. Drozdzyński, R. Lisiecki, W.R. Romanowski, *Opt. Mater.*, 29 (2007),

- 1029-1034.
10. R. Parrot, C. Naud, C.J. Delbecq, P.H. Yuster, *Phys. Rev. B*, 15 (1976), 137–145.
  11. M. Louis, E. Simoni, S. Hubert, J.Y. Gesland, *Opt. Mater.*, 4 (1995), p. 657–662.
  12. S.V. Godbole, A.G. Page, S.C. Sabharwal, Sangeeta, J.Y. Gesland, M.D. Sastry, *J. Lumin.*, 93 (2001), p. 213–221.
  13. T. K. Seshagiri, M. Mohapatra, T K Gundu Rao, R M Kadam, V Natarajan and S. V. Godbole, *J. Phys.Chem. Solids.*, 70 (2009), 1261-1266.
  14. G. Blasse, K.C. Bleijenberg, D.M. Krol, *J. Lumin.*, 18 (19) (1979) p. 57–62.
  15. G. Blasse, *J. Electrochem. Soc.*, 115 (1968), 738.
  16. M.Mohapatra, V.Natarajan, *J. Radioanal.Nucl. Chem.*, 302 (3) (2014), p. 1327-1332.
  17. (a) G. Blasse, J.P.M. vanden Dungen, *J. Inorg. Nucl. Chem.*, 40 (1978), p. 2037.  
(b) L. Schwarz, E. Brecht, E. Birckner, B.Reimer, *Proc. 2<sup>nd</sup> Int. Meeting on luminescence*, E.M. Amdt Universität, Griefswald, (1989), p. 153.
  18. M.E. Azenha, G. Blasse, *J. Alloys Compd.*, 196, (1993), p. 81-85.
  19. M. Mohapatra, A.K. Yadav, S.N. Jha, D. Bhattacharyya, S.V.Godbole, V. Natarajan, *Chem. Phys. Lett.*, 601 (2014), 81-86.
  20. Mithlesh Kumar, M. Mohapatra, V. Natarajan, *Mater. Res. Bull.* , 60 (2014), 858-863.
  21. A. Karthikeyania, R. Jagannathan, *J. Lumin.*, 86 (2000), 79–85.
  22. Z. Qinghua, K. Nathan, R. Mark, *J. Lumin.* 101 (2003), 167.

23. M. Mohapatra, B. Rajeswari, R. M. Kadam, M. Kumar, T. K. Seshagiri, N. K. Porwal,  
S. V. Godbole, V. Natarajan, *J. Alloys Compd.*, 611 (2014), 74-81.
24. G. Blasse, B. C. Grabmaier, *Luminescent Materials*, Springer-Verlag Berlin, Heidelberg, ISBN: 978-3-540-58019-5, (1994), 91-107.
25. (a) J. Su, Z. Wang, D. Pan, J. Li, *Inorg. Chem.*, 53 (2014), 7340–7350.  
(b) R. G. Denning, *J. Phys. Chem., A* 111 (2007), 125-4143.
26. G. Blasse, *Spectra and Chemical Interactions, Structure and Bonding, The influence of charge-transfer and Rydberg states on the luminescence properties of lanthanides and actinides*, 26 (1976), 43-79.
27. G. Blasse, *J. Electrochem., Soc.* 124 (1977), 1280-1285.
28. Th. Förster, *Discuss. Faraday Soc.*, 27 (1959), 7-17.
29. S.K. Gupta, M. Mohapatra, S. Kaity, V. Natarajan, S.V. Godbole, *J. Lumin.*, 132 (2012), 1329–1338.
30. T Smith, *J Guild, Trans. Opt. Soc.*, 33 (3) (1931–32), 73–134.

**Chapter 4**  
**Uranium speciation and its site occupancy in  
alkaline earth borophosphates**



#### **4.1 Introduction:**

Borates and phosphates have found wide applications as nonlinear optical (NLO) materials. Thereafter, the combination of borate and phosphate i.e. borophosphates (BPOs) drew the attention and more investigations were carried out to reveal its structural chemistry [1, 2]. A systematic study on borophosphate based materials was initiated by Kniep et al. though Bauer has earlier established the synthesis procedure and XRD pattern of MBPO<sub>5</sub> (M= Ca, Sr, and Ba) [3, 4]. These matrices were found to have a broad range of application as advanced materials in various research fields such as nonlinear optical (NLO) material, optical data storage, high density memory devices and phosphors for light emitting diodes. Incorporation of luminescent activator ions in to MBPO<sub>5</sub> (MBP) matrices has drawn research interest for their possible use as luminescent phosphors. The M<sup>2+</sup> (M= Ca, Sr, Ba) site in MBPO<sub>5</sub> system readily accommodates lanthanide ions as luminescent activators. Han et al. has reported SrBPO<sub>5</sub>: R, Na<sup>+</sup> (R = Eu<sup>3+</sup>, Tb<sup>3+</sup>) phosphor as a potential UV convertible phosphor for application in white light emitting diodes (WLED) [5]. Bi<sup>2+</sup> doped MBPO<sub>5</sub> (M= Ca, Sr, Ba) phosphors are also investigated for WLED applications [6]. SrBPO<sub>5</sub>:Eu<sup>2+</sup> is also reported as an possible X-ray as well as neutron storage phosphor [7-9]. The structural frame work of MBPO<sub>5</sub> systems are well suited for different types of guest metal ions starting from transition metals, lanthanides to actinide ions [10-13]. Although the crystal structure of BPO<sub>4</sub> resembles with silica, MBPO<sub>5</sub> systems appeared to follow stillwellite structure type that resembles with rare earth boro silicates i.e. CeBO(SiO)<sub>4</sub> [14-16]. In MBPO<sub>5</sub> compounds, BO<sub>4</sub> and PO<sub>4</sub> tetrahedral units act as the primary building blocks joined at common vertexes to give a complex anionic structure. Single chains of

BO<sub>4</sub> tetrahedral run parallel to [001] direction and get connected to terminal PO<sub>4</sub> units to form a spiral chain screwing along the 3<sub>2</sub> axis. The structural rigidity favours stabilization of activator ions and contributes towards better luminescence properties. It is also reported that rare earth ions like Eu<sup>3+</sup>, Ce<sup>4+</sup> and Sm<sup>3+</sup> get partially reduced to their corresponding lower oxidation states in absence of reducing atmosphere in SrBPO<sub>5</sub> matrix [17-19]. The presence of anionic AO<sub>4</sub> (A= B or P) tetrahedral units as well as aliovalent substitution of rare earths with respect to Sr<sup>2+</sup> ion propose reducing behaviour of SrBPO<sub>5</sub> matrix. There are very few reports in literature about actinide luminescence in MBPO<sub>5</sub> lattice [13, 20]. Some of the actinides with 5f electronic configuration show high oscillator strength unlike lanthanides and thus are more labile towards local structural environment. Therefore, studying luminescence properties of actinides in solid hosts is fascinating as it can probe the crystal lattice environment.

Among the actinides, uranium has gained much attention owing to its potential application in nuclear industry. Uranium is considered as an intermediate-level radioactive waste that along with its isotopes impart long-term dose. Although uranium is an alpha active radio nuclei, its long half-life (10<sup>5</sup>-10<sup>9</sup> years) makes it difficult to detect it through alpha counting techniques. However, fluorescence spectroscopy offers an easy approach to detect uranium in both solid as well as aqueous states [21-24]. Uranium has multiple oxidation states: U (III), U (IV), U (V) and U (VI) but among these the hexavalent state is the most stable state. Hexavalent uranium can get stabilized in solids in different forms like UO<sub>6</sub><sup>6-</sup>, UO<sub>4</sub><sup>2-</sup>, UO<sub>2</sub><sup>2+</sup>, or U<sup>6+</sup> [25]. The parameters like synthesis condition, crystal structure of host lattice and the local structure around the uranium ion contribute towards the stabilization of a particular

uranium species. The important fact is that the fluorescence emission spectroscopy can help in identifying the luminescent species of uranium present in a system. The  $\text{UO}_4^{2-}$  emits in red region where as others emit in green region [26]. The  $\text{UO}_2^{2+}$  (uranyl) emission is unique with respect to its vibronic progressions and zero point line as it's fingerprint unlike the characteristic emission lines of  $\text{UO}_6^{6-}$  as well as  $\text{U}^{6+}$  [27,28]. The speciation of uranium in different solid matrices needs to be addressed in order to investigate its physical, chemical as well as radiological aspects.

Uranium doped solid matrices have found wide range of application. In recent years, ceramic matrices mimicking natural minerals have been explored as an alternative host to conventional alkali borosilicate glasses for radioactive waste storage [29, 30]. Ceramics have great advantages over glass materials as they are thermally stable compounds and highly resistant to corrosion and radiation damage [31, 32]. Phosphate based ceramics were evaluated and found to be an excellent host to stabilize substantial quantities of nuclear waste for a long term purpose [33, 34]. Raicevic et al. have investigated phosphate based solid matrices (apatite) capable of in-situ immobilization of uranium in order to remediate soil contaminated with uranium [35]. Thus, phosphates doped with uranium have significant a role in both nuclear industry as well as environmental science.

Phosphate hosts are well studied for uranium luminescence. It has been reported that phosphate based matrices are well designed to stabilise uranyl form of uranium. Hoffman has reported  $\text{SrZnP}_2\text{O}_7$  host that stabilizes uranium as uranyl [36]. Azenha and Blasse have investigated uranium solubility in several alkaline earth phosphates and found that flexibility in crystal structure is the driving force to stabilizing uranyl, a long linear tri-

atomic molecule [37]. It has been observed that uranyl stabilization in  $Ba_3(PO_4)_2$  matrix resulted in formation of a second phase i.e.  $Ba_2UO_2(PO_4)_2$  [38]. Mohapatra et al. have reported that strontium pyrophosphate matrix incorporates uranium as uranyl at regular lattice sites of  $Sr^{2+}$  [39]. Recently, Luminescence of uranium was studied in  $SrBPO_5$  matrix by M. Kumar et al. and Rout et al. [13,20]. However, these studies have not discussed the site occupancy of uranium in details. In the present study, site occupancy and speciation of uranium in alkaline-earth-borophosphate matrix ( $MBPO_5$ , M= Ca, Sr, Ba) using photoluminescence as well as Extended X-ray absorption fine structure is discussed. Stabilization of uranium as uranate in phosphate matrix is reported here for the first time.

#### **4.2 Experimental:**

The undoped  $MBPO_5$  samples were prepared via the conventional high temperature solid state reaction route using  $MCO_3$ ,  $(NH_4)HPO_4$  and  $H_3BO_3$ . In order to prepare 'U' doped compounds, required amounts of  $UO_2(NO_3)_2 \cdot 6H_2O$  were added to the mixture of the above ingredients. After fine grinding, the mixtures were made into pellets of 10 mm diameter and 0.5 mm thickness and fired at  $600^\circ C$  in a muffle furnace for three hours. After this, the samples were thoroughly re-grinded and pelletized and heated at  $900^\circ C$  for 3 more hours.

The crystal Structure of the prepared samples were examined by powder X-ray diffraction using a Philips diffractometer (model PW 1071) with  $CuK_\alpha$  ( $\lambda = 1.5418 \text{ \AA}$ ) source. The morphology of the samples was recorded by scanning electron microscopy (SEM) model-AIS-2100, Merero Inc. All PL measurements were made using a Shimadzu RF 5301pc spectrofluorimeter equipped with a 150W continuous wave xenon lamp. For the measurements, bandwidths for the excitation and emission monochromator were set at 3

nm. A long-wavelength-pass filter (UV-35, Shimadzu), with a maximum and uniform transmittance (more than 85%) above 350 nm, was placed in front of the emission monochromator in order to reduce the scatter and second order of the incident beam into the emission monochromator. Here in this spectrofluorimeter, a provision exists to adjust for the gain of the photometric photomultiplier tube dynamically according to the changes in the Xe lamp output intensity. The PL decay times were measured by using Edinburgh F-900 time resolved fluorescence spectrometer at room temperature.

EXAFS (Extended X-ray absorption fine structure) measurements of these samples at U L<sub>3</sub> edge were carried out at the energy scanning EXAFS beam line (BL-9) in fluorescence mode with a high sensitive detector at the INDUS-2 Synchrotron Source (2.5 GeV, 100 mA) at Raja Ramanna Centre for Advanced Technology (RRCAT), Indore, India. The optical arrangement for BL-9 includes a 1.5 m horizontal pre-mirror with meridional cylindrical curvature followed by a double crystal monochromator (DCM). The collimation of the beam and rejection of higher harmonic is achieved by using the horizontal pre-mirror. The DCM is composed of a sagittal cylinder (second crystal) used for horizontal focusing as well as a Rh/Pt coated bendable post mirror facing down used for vertical focusing of the beam at the sample position. The photon energy range of the DCM is 4-25 KeV with a resolution of  $10^4$  at 10 KeV [40, 41].

The EXAFS spectra of the samples at U L<sub>3</sub> edge were recorded in fluorescence mode in the energy range 17050-17700 eV while the XANES (X-ray absorption near edge spectra) spectra have been recorded along with UF<sub>4</sub> and UO<sub>2</sub>CO<sub>3</sub> standards with energy step of 0.5 eV from 17136- 17200 eV. In the fluorescence mode of measurement, the signal ( $I_f$ ) is

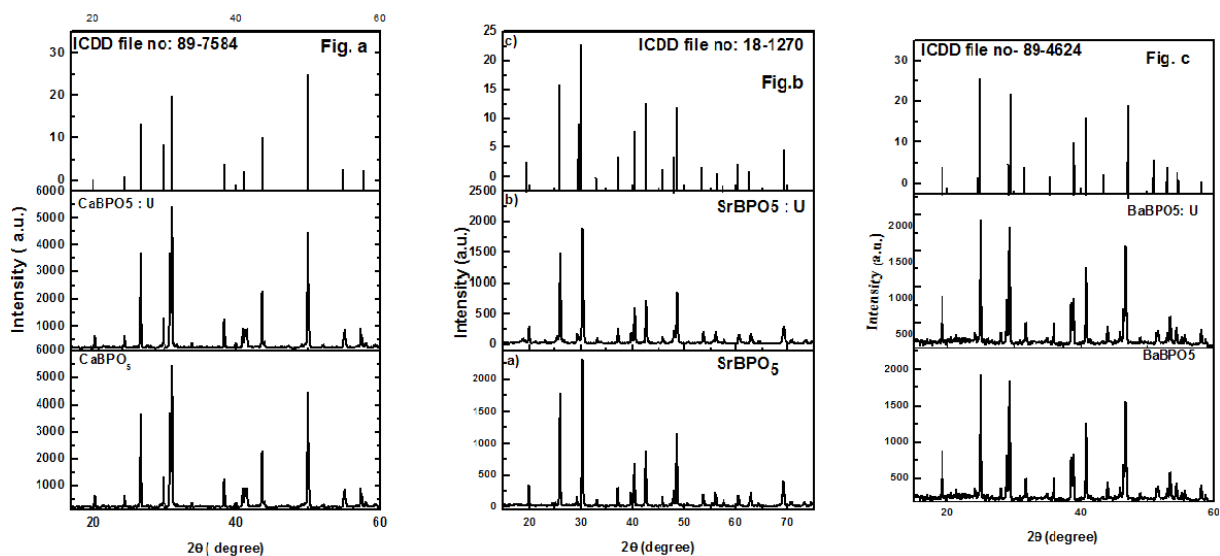
recorded by a Si drift detector placed at 90° to the incident X-ray beam. Prior to the sample, an ionization chamber detector is placed to measure the incident X-ray flux ( $I_0$ ). The absorbance of the sample ( $\mu = \frac{I_f}{I_0}$ ) is measured as a function of energy. The EXAFS spectra at Sr K edge were recorded in the transmission mode using two ionization chamber detectors in the energy range 16010-16700 eV by placing the sample in between the detectors. The incident intensity ( $I_0$ ) is measured by the first ionization chamber and the transmitted intensity ( $I_t$ ) by the second ionization chamber leading to the absorbance ( $\mu = \exp(-\frac{I_t}{I_0})$ ) recording of the sample. In order to carry out EXAFS measurements, adequate amount of powder samples were taken and mixed with cellulose powder to make a total weight of 100mg and then out of this powder, pellets of 15mm diameter were prepared.

### **4.3. Results and Discussion:**

#### **4.3.1 Crystal structure and morphology:**

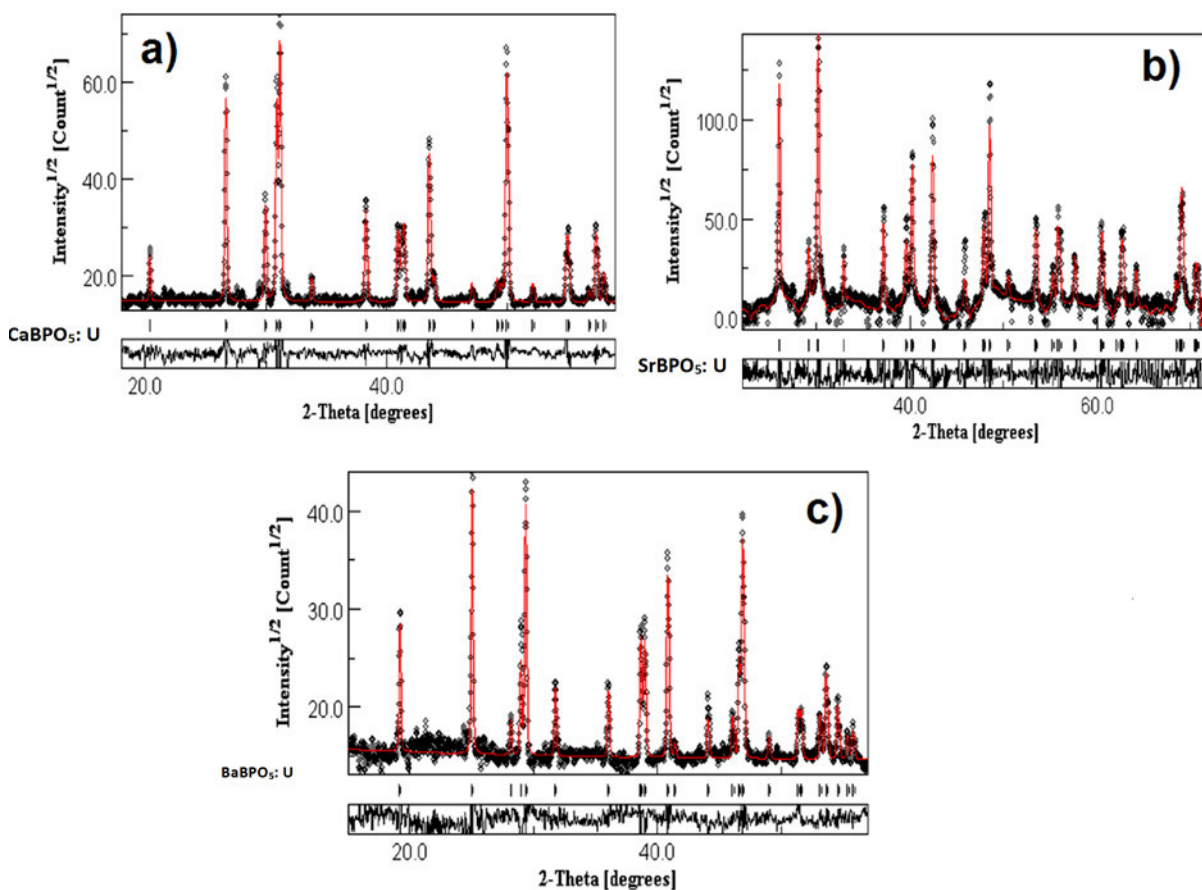
Figure.4.1 shows the X-ray diffraction patterns of MBPO<sub>5</sub> samples with and without 1 mol % uranium. Figure 4.1 (a) matches well with the standard data of CaBPO<sub>5</sub> (ICDD file no: 89-7584). The XRD pattern shows formation of single hexagonal phase in both doped and undoped samples. Figure 4.1 (b) shows a good agreement with the standard data of SrBPO<sub>5</sub> (ICDD file no: 18-1270). Figure 4.1 (c) agrees with the standard data of BaBPO<sub>5</sub> (ICDD file no: 89-4624). Rietveld analysis was carried out to confirm the phase purity and to rule out the presence of any impurity presence in uranium doped MBPO<sub>5</sub> systems [42]. In this

analysis, JAVA based Material Analysis Using Diffraction (MAUD) programme was used [43]. The instrumental resolution parameters of Philips (model PW 1071) X-ray diffraction equipment was derived from the well annealed and highly crystalline Si standard powder. The background of the intensities of XRD profiles was fitted with 4th order polynomial and refined the background and scale factor along with zero shift. The hexagonal phases of  $\text{CaBPO}_5$  (PDF file: 89-7584),  $\text{SrBPO}_5$  (PDF file: 18-1270) and  $\text{BaBPO}_5$  (PDF file: 89-4624) were taken for Rietveld calculation. The structural parameters such as unit cell parameters and positional parameters were also refined. It was observed from the Rietveld refinement that the weighted residual factor (Rwp) of 11.803%, 11.425 % and 9.330% for uranium doped  $\text{CaBPO}_5$ ,  $\text{SrBPO}_5$  and  $\text{BaBPO}_5$  respectively exhibited a better fit of reference and experimental pattern. Figure 4.2 shows the reitvield profile fitting of hexagonal phases of uranium doped  $\text{MBPO}_5$  systems and indicated that the samples were of single phase and devoid of impurity.



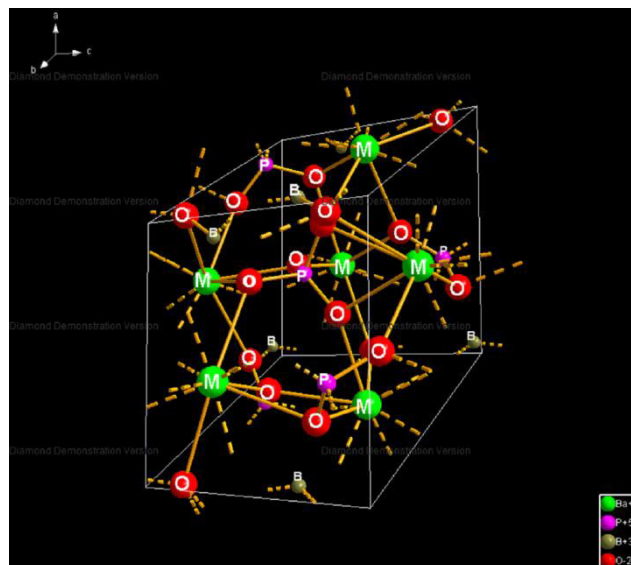
**Figure 4.1: XRD pattern of undoped and uranium doped (a)  $\text{CaBPO}_5$  (b)  $\text{SrBPO}_5$  and (c)  $\text{BaBPO}_5$ .**

Figure 4.3 shows a schematic crystal structure representation of MBPO<sub>5</sub> system. The BO<sub>4</sub> tetrahedra anionic unit actively connects to two PO<sub>4</sub> tetrahedra by its free vertices and thus a molecular motif with BPO<sub>7</sub> repeating unit is generated, where four of the O atoms are engaged in repeating the motif to afford the general formula BPO<sub>3</sub>O<sub>4/2</sub> ~ BPO<sub>5</sub>. The helical structure of BO<sub>4</sub> tetrahedra surrounds the M<sup>2+</sup> polyhedral to form a tortuous structure. In stillwellite system, the rare earth cation is coordinated to nine neighbouring oxygens whereas in MBPO<sub>5</sub> the smaller charge to ionic radii ratio of alkaline earth metal ions show eight oxygen coordination to attend structural stability [44].



**Figure 4.2: XRD Rietveld analysis of a) CaBPO<sub>5</sub>: U b) SrBPO<sub>5</sub>: U c) BaBPO<sub>5</sub>: U sintered at 900°C, 3h.**

Figure 4.4 shows SEM micrograph of the MBPO<sub>5</sub>: U system. It has been observed from statistical analysis of several micrographs that the overall particle size for these three systems is around 2 μm. All the three micrographs reveal an inhomogeneous size distribution, uneven shape, and particle agglomeration owing to its synthesis condition.



**Figure 4.3: Schematic presentation of crystal structure of MBPO<sub>5</sub> system;  
M= (Ca<sup>2+</sup>, Sr<sup>2+</sup>, Ba<sup>2+</sup>).**

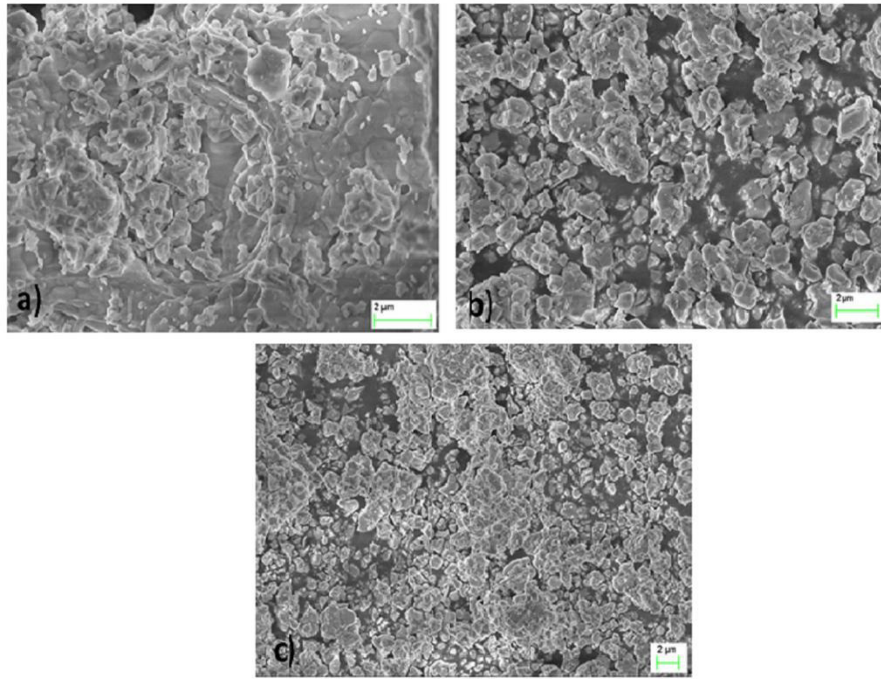


**Figure 4.4: SEM micrographs of the MBPO<sub>5</sub>: U samples; a) CaBPO<sub>5</sub>: U b) SrBPO<sub>5</sub>: U c) BaBPO<sub>5</sub>: U.**

#### **4.3.2 PL studies on U doped MBPO<sub>5</sub>:**

Figure 4.5 shows the emission spectra of Strontium, Calcium and Barium borophosphates doped with 1 mol% uranium for an excitation wavelength of 440 nm. It is seen here that uranium doped SrBPO<sub>5</sub> and CaBPO<sub>5</sub> phosphors exhibit similar emission profile which is different from that seen in case of uranium doped BaBPO<sub>5</sub>. Luminescence of uranium in SrBPO<sub>5</sub> is well documented.

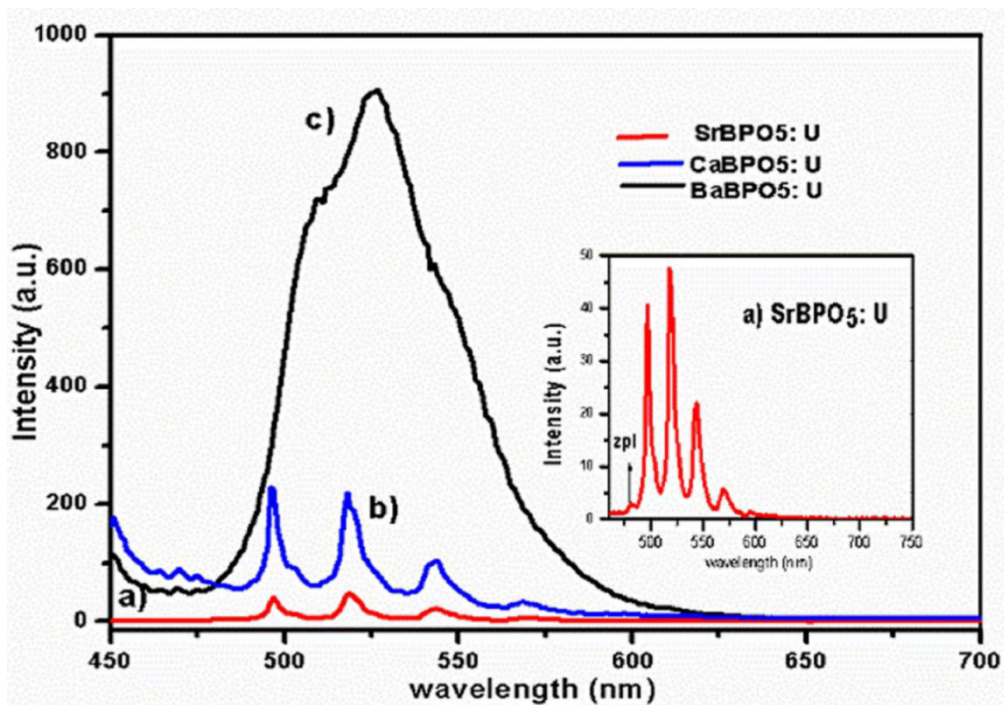


**Figure 4.5: Emission spectra of 1 mol% uranium doped in (a) SrBPO<sub>5</sub> (b) CaBPO<sub>5</sub> and (c) BaBPO<sub>5</sub> at 440 nm excitation wavelength. The inset shows a magnified (a).**

whereas luminescence of uranium particularly in CaBPO<sub>5</sub> and BaBPO<sub>5</sub> lacks literature support to the best of our knowledge. Both SrBPO<sub>5</sub>: U and CaBPO<sub>5</sub>: U hosts exhibit multiple emission peaks with peak maxima at 498, 519, 541, 565, and 595 nm. These peaks along with a small peak at 482 nm are known as the finger print of uranyl emission. The small peak at 482 nm referred as the zero point line (zpl) is due to the  $\Pi_g \rightarrow \Sigma_g^+$  electronic transition [45]. The position of zpl may vary from 460 -520 nm depending on the equatorial coordination number such as 4, 5 or 6. It has been observed that for higher co-ordination numbers zpl shows higher energy values [46, 47]. The emission peaks appeared at lower energy range represent vibrationally resolved spectra known as vibronic progression. The electronic excitation and emission process in Uranyl is explained by its complex electronic

structure [48, 49]. In uranyl, the atomic orbitals of Oxygen ( $2s2p$ ) and U ( $6s6p5f6d7s$ ) gets combined to form molecular orbitals ( $3\sigma_u$ ,  $3\sigma_g$ ,  $2\pi_u$  and  $1\pi_g$ ). The valence electrons occupy these molecular orbitals and form a totally symmetric singlet  $^1\Sigma_g^+$  ground state. The electron transition takes place from the bonding  $\sigma_u$  to nonbonding  $\phi_u$  and  $\delta_u$  molecular orbitals. In this process  $^{1,3}\Delta_g$  and  $^{1,3}\Phi_g$  excited states are generated which undergo spin orbit coupling and gets splitted in to various energy states and participate in uranyl luminescence process.

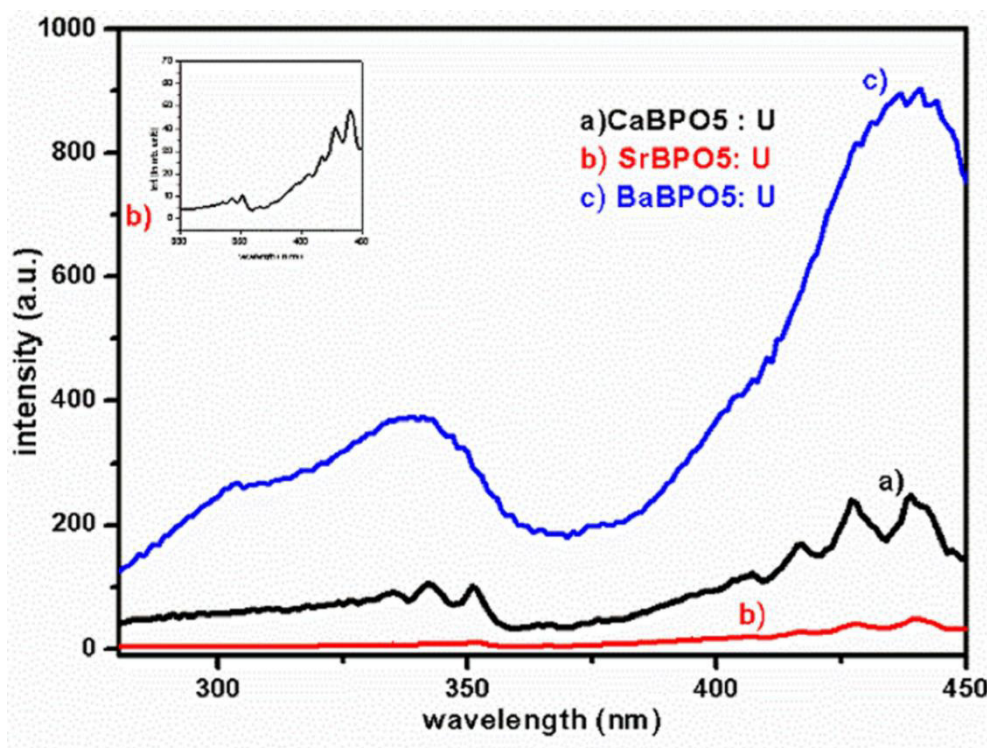


**Figure 4.6: Excitation spectra of 1 mol% uranium doped in (a) CaBPO<sub>5</sub> (b) SrBPO<sub>5</sub> and (c) BaBPO<sub>5</sub> at 519 nm emission wavelength. The inset shows a magnified (b).**

It is observed that CaBPO<sub>5</sub>: U shows comparatively more emission intensity than SrBPO<sub>5</sub>: U indicating that radiative transitions are more feasible in case of CaBPO<sub>5</sub>. The characteristic uranyl emission seen in Figure 4.5 (a and b) suggests that SrBPO<sub>5</sub> and

CaBPO<sub>5</sub> allow uranium to stabilize as uranyl in their corresponding hosts. This is further corroborated by the excitation spectra as shown in Figure 4.6. In case of SrBPO<sub>5</sub>: U and CaBPO<sub>5</sub>: U, the excitation spectra consisted of ligand-to-metal charge transfer transitions superposed with vibrational fine structures and it is reported that a maximum of twelve transitions can be elucidated from the absorption spectrum of UO<sub>2</sub><sup>2+</sup> [50,51]. Both the spectra exhibit two broad bands in the region of 315-361nm and 394-450nm with maxima at 335, 342, 350, 407, 415, 425, 434 and 446nm. These excitation peaks show an equidistant gap (vibronic progression) of 512 cm<sup>-1</sup> indicating excitation of electrons from ground state vibrational levels of uranyl to their excited electronic levels. This is typically the characteristic excitation profile of uranyl moiety. Therefore, both the excitation and emission spectra suggest that in case of SrBPO<sub>5</sub> and CaBPO<sub>5</sub> uranium is stabilized as uranyl in these matrices.

However, BaBPO<sub>5</sub>: U exhibits different PL characteristics. It shows a broad emission spectrum ranging from 470 to 620 nm with a peak maximum at 526 nm and a shoulder around 509nm (Figure 4.5). This emission being seen in the predominantly green region suggests that stabilization of uranium as UO<sub>4</sub><sup>2-</sup> is less likely as this species is known to emit in red region. Moreover, the presence of Uranyl is also less likely as the vibronic progression in this emission is absent which could be due to the weakening of the U-O triple bond caused by delocalization of bonded electrons towards neighbouring oxygens. In case of U (VI) species, the first emission originating from  $\pi_g \rightarrow \Sigma_g^+$  transition is the zero point line and here the observed shoulder around 509 nm (being positioned at higher wavelength) appears to be a weak signature of zero point line suggesting an equatorial

coordination number of 4. The broad emission band without the vibronic progression observed here for BaBPO<sub>5</sub>: U can be attributed to electronic origins. The electronic transition from oxygen (2p) dominated ground state to uranium (6d) dominated excited state is a parity allowed transition. This emission spectrum shows a close resemblance with uranates (UO<sub>6</sub><sup>6-</sup>) as reported by Blasse et al. indicating stabilization of uranium as uranate in this host and this broadened emission spectrum could be due to different types of coordination environment surrounding U (VI) ion [47]. Moreover, the excitation spectrum of BaBPO<sub>5</sub>: U is different from that of SrBPO<sub>5</sub>: U and CaBPO<sub>5</sub>: U. It exhibits a small hump like structure and two broad excitation spectra with maxima at 302, 340 and 438nm respectively. Here, the excitation spectrum is a typical charge transfer transitions from oxygen (2p) to uranium (6d) orbitals. The excitation band at higher wavelength range can be assigned to ground state electronic transition of hexavalent uranium [52]. Phosphates are well known to stabilize uranium as uranyl as is observed here in case of SrBPO<sub>5</sub> and CaBPO<sub>5</sub> hosts. However, in case of BaBPO<sub>5</sub> uranium seems to get stabilized in the form of UO<sub>6</sub><sup>6-</sup>.

All the three hosts studied here possess similar hexagonal crystal structure. However, the difference lies with the ionic radii of the constituent cations. The ionic radii for Ca<sup>2+</sup>, Sr<sup>2+</sup> and Ba<sup>2+</sup> are 1.14Å, 1.32Å and 1.49Å respectively. The uranyl moiety being a bigger molecule and assuming it substitutes at regular cation sites, Ba<sup>2+</sup> should have been a favourable site to be substituted by uranyl compared to Sr<sup>2+</sup> and Ca<sup>2+</sup> due to its higher ionic radius among the three. Consequently, the uranate luminescence signature should have been seen from SrBPO<sub>5</sub> and CaBPO<sub>5</sub>. In fact, the ionic size of all the three cations are not

sufficient to incorporate uranyl moiety. This implies that site occupancy of uranium in all these matrices needs to be investigated further.

Figure 4.7 shows the life time decay of all borophosphate hosts studied here. The PL decay curves were fitted using bi-exponential equation:  $I(t) = A_1 \exp(-t/\tau_1) + A_2 \exp(-t/\tau_2) + y_0$  where  $I(t)$  stands for intensity,  $A_1$  and  $A_2$  are scalar quantities known as pre-exponential factors, 't' is the time of measurement and  $\tau_1$  and  $\tau_2$  are emission decay times.

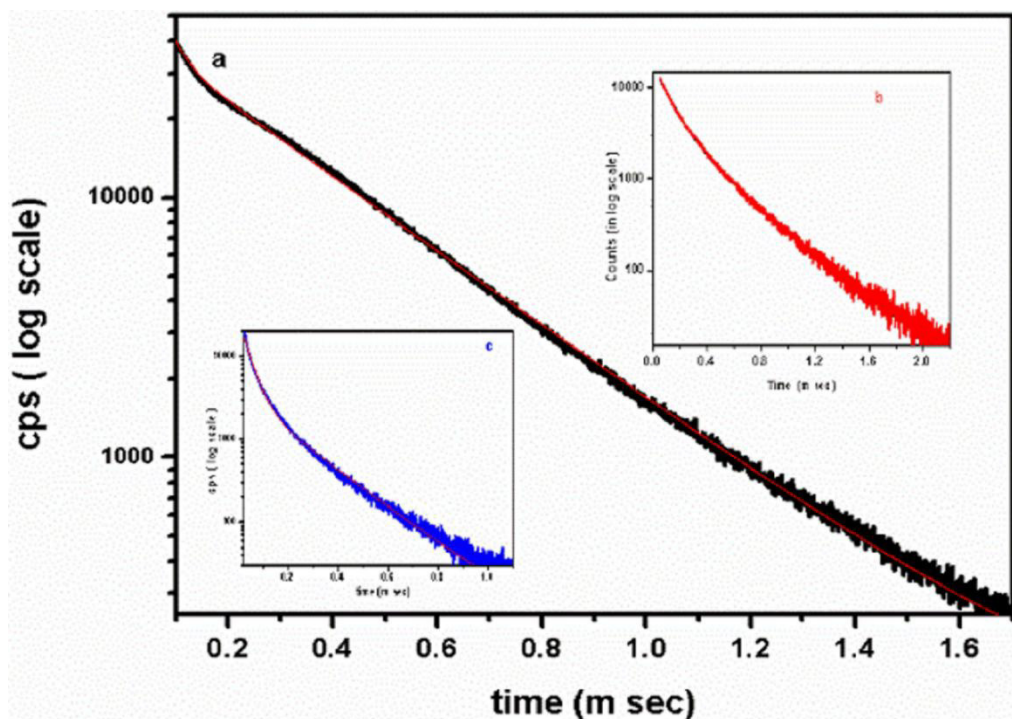


**Figure 4.7: Luminescence decay time profile of (a) BaBPO<sub>5</sub>: U (b) SrBPO<sub>5</sub>: U and (c) CaBPO<sub>5</sub>: U under 440 nm excitation and 519nm emission wavelength.**

Table 4.1 shows the decay time values of uranium in three corresponding matrices. The decay curve shows two life time values indicating stabilization of uranium in two different

environments in MBPO<sub>5</sub> systems. The presence of defect centres in the vicinity of luminescent species facilitates non-radiative decay leading to shortening of life time. The shorter decay time could be due to presence of more defect centres around uranium in one environment whereas uranium positioned away from defect centres or with less number of defects around it exhibits relatively a longer decay time.

It has been observed that uranium gives higher luminescence life time ( $\tau_1$ ) in BaBPO<sub>5</sub> host lattice whereas the lifetimes in CaBPO<sub>5</sub> and SrBPO<sub>5</sub> are comparable corroborating the fact that uranium exists as a different species in BaBPO<sub>5</sub>. The longer decay time is indicative of more symmetric site that holds parity forbidden restriction whereas shorter life time reflects asymmetric sites favouring f-f electronic transition by relaxing selection rules. The lifetime decay study suggests comparatively a more symmetric environment for uranium in BaBPO<sub>5</sub>.

**Table.4.1 Life time decay values of MBPO<sub>5</sub>: U**

Sample	$\tau_1(\mu\text{s})$	$\tau_2(\mu\text{s})$	Fitting Parameter ( $\chi^2$ )
U doped CaBPO <sub>5</sub>	185.53 (51.99 %)	32.94(48.01 %)	0.861
U doped SrBPO <sub>5</sub>	165 (65%)	54 (35%)	0.848
U doped BaBPO <sub>5</sub>	301.06 ( 87.17 %)	28.89 ( 12.83%)	0.853

### 4.3.3 EXAFS analysis:

Figure 4.8 shows the XANES spectra of MBPO<sub>5</sub>: U samples at U L<sub>3</sub> edge along with UF<sub>4</sub> and UO<sub>2</sub>CO<sub>3</sub> standards wherein U cation exists in +4 and +6 oxidation states

respectively. The absorption edges of the samples lie close to the absorption edge of  $\text{UO}_2\text{CO}_3$  standard and the features of the XANES spectra of the samples match with that of  $\text{UO}_2\text{CO}_3$  standard suggesting the presence of hexavalent uranium in these samples.

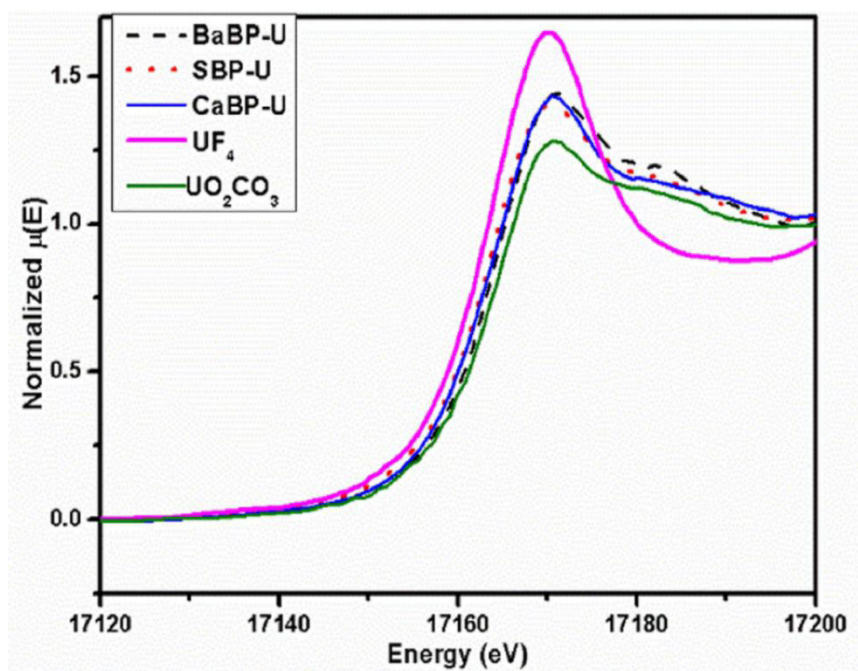
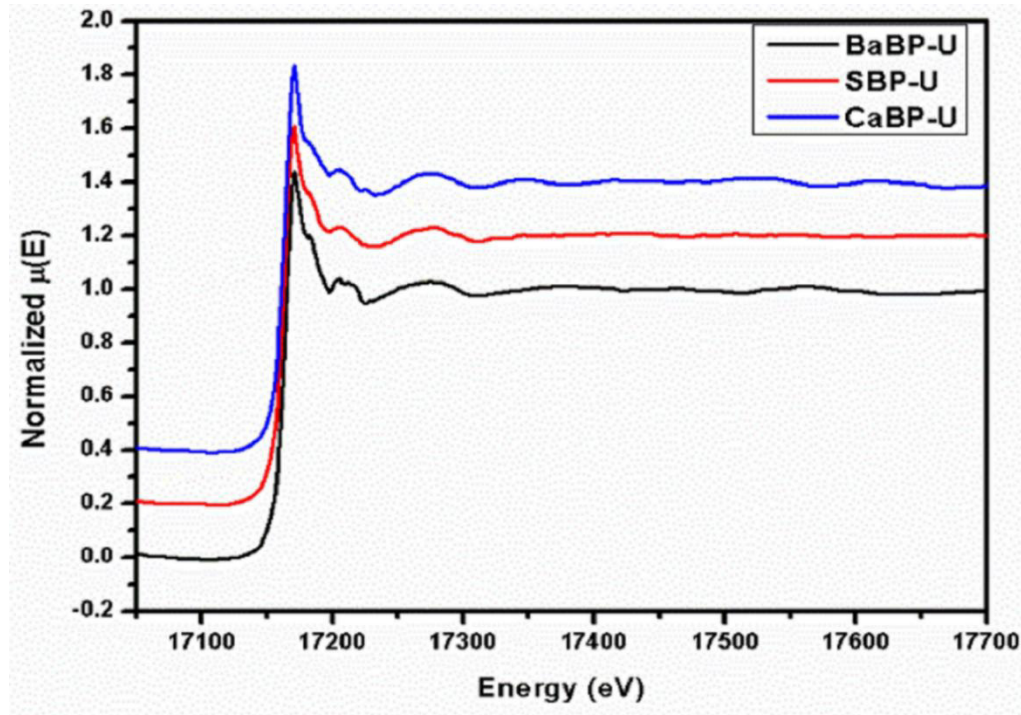


Figure 4.8: XANES spectra of MBPO<sub>5</sub>: U along with  $\text{UF}_4$  and  $\text{UO}_2\text{CO}_3$ .



**Figure 4. 9: Normalized EXAFS spectra of U doped MBPO<sub>5</sub>, at U L<sub>3</sub> edge.**

Figure 4.9 shows the experimental EXAFS ( $\mu(E)$  versus  $E$ ) spectra of the samples at U L<sub>3</sub> edge. In order to extract the oscillations present in the absorption spectra, an absorption function  $\chi(E)$  (a function of the energy dependent absorption coefficient  $\mu(E)$ ) has been introduced and it can be expressed as follows<sup>53</sup>

$$\chi(E) = \frac{\mu(E) - \mu_0(E)}{\Delta\mu_0(E_0)} \quad (1)$$

where,  $E_0$  is the absorption edge energy,  $\mu_0(E)$  gives the bare atom background value and  $\Delta\mu_0(E_0)$  represents the step in the  $\mu(E)$  value at the absorption edge. There is a need to convert the energy dependent absorption coefficient  $\chi(E)$  to the wave number dependent

absorption coefficient  $\chi(k)$ , where  $(k)$  represents the photoelectron wave number scale defined by,

$$k = \sqrt{\frac{2m(E - E_0)}{\hbar^2}} \quad (2)$$

Where  $m$  is the electron mass. The EXAFS oscillations,  $\chi(k)$  is weighted by  $k^2$  to magnify the oscillation at high  $k$  and the functions  $\chi(k)$ ,  $k^2$  are Fourier transformed using  $k$  range of 2-9.5  $\text{\AA}^{-1}$  to obtain the  $\chi(r)$  versus  $r$  spectrum which represents radial distances from the center of the absorbing atom. The experimental EXAFS data is analysed using EXAFS data analysis program offered by IFEFFIT software package [54]. The data is used to construct  $\chi(r)$  versus  $r$  spectrum and simultaneously an ideal crystallographic structure is assumed to generate a theoretical EXAFS spectra followed by fitting of the experimental data with the theoretical spectra using FEFF 6.0 code. The parameters used for the EXAFS data fitting are bond distance ( $r$ ), coordination number ( $N$ ) and Debye-Waller factor ( $\sigma^2$ ), that give the static and thermal disorder of the system and the goodness of fit is determined by the parameter  $R_{factor}$  defined<sup>53</sup> as

$$R_{factor} = \sum \frac{[\text{Im}(\chi_{dat}(r_i) - \chi_{th}(r_i))]^2 + [\text{Re}(\chi_{dat}(r_i) - \chi_{th}(r_i))]^2}{[\text{Im}(\chi_{dat}(r_i))]^2 + [\text{Re}(\chi_{dat}(r_i))]^2} \quad (3)$$

where, the experimental and theoretical values of  $\chi(r)$  are represented by  $\chi_{dat}$  and  $\chi_{th}$  respectively. The imaginary and real parts of  $\chi(r)$  are denoted by Im and Re respectively.

The experimental  $\chi(r)$  versus  $r$  spectra of the samples at U L<sub>3</sub> edge along with best fit theoretical plots carried out as above have been shown in figure 4.10 and the results of the fitting have been tabulated in Table 4.2.

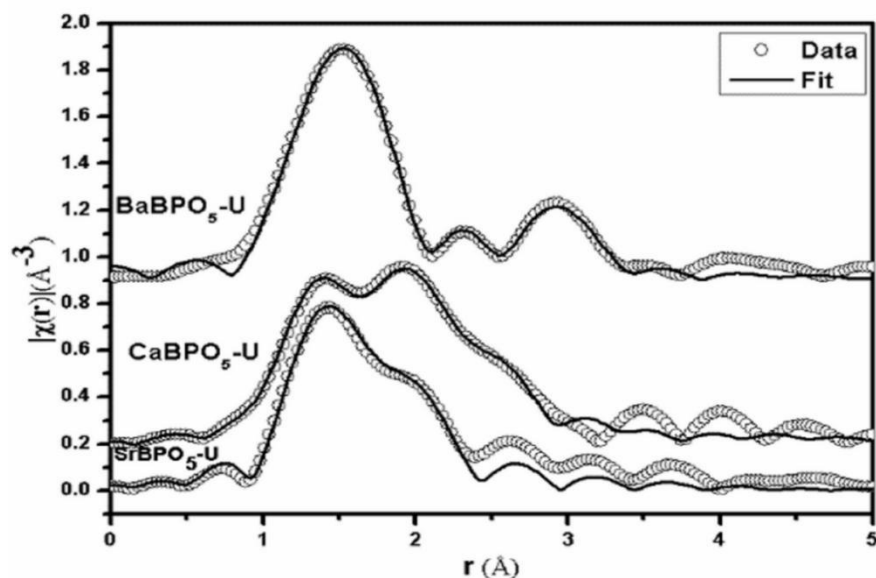


**Figure 4.10: EXAFS spectra in L space for MBPOs: U**

The  $R_{factor}$  values of all the fits are less than 0.01 which ensures goodness of the fits. It is important to note that all the presented  $\chi(r)$  versus  $r$  spectra are phase uncorrected spectra as the EXAFS software generally generate phase uncorrected spectra only but during data interpretation phase corrected datas are only used.

For the SrBPO<sub>5</sub>: U sample, the  $\chi(r)$  versus  $r$  spectrum has been fitted from 1-2.4 Å assuming the Uranyl structure with two axial oxygen bonds at 1.74 Å and four equatorial oxygen bonds at 2.47 Å. The Uranyl structure is taken from the Uranyl carbonate structure reported in the literature [55].

**Table 4.2: U L3 edge EXAFS results**

	SrBPO <sub>5</sub> : U			CaBPO <sub>5</sub> : U			BaBPO <sub>5</sub> : U		
	r(Å)	N	$\sigma^2$	r(Å)	N	$\sigma^2$	r(Å)	N	$\sigma^2$
U-O1	1.79	2	0.007	1.83	2	0.009	1.80	2	0.001
U-O2	2.38	4.2	0.009	2.45	4.1	0.003	2.28	4.9	0.008
U-O3	-	-	-	2.91	3.8	0.002	2.54	2	0.023
U-B	-	-	-	-	-	-	3.44	3	0.001
U-P	-	-	-	-	-	-	3.65	2	0.002

On the other hand, the  $\chi(r)$  versus  $r$  spectrum of the CaBPO<sub>5</sub>: U sample has been fitted from 1- 3 Å assuming three U-O shells at 1.74 Å (×2), 2.47 Å (×4) and 2.92Å (×4). The third oxygen shell is required to account for the presence of a hump between 2.5-3 Å in the  $\chi(r)$  versus  $r$  spectrum. The  $\chi(r)$  versus  $r$  spectrum of the BaBPO<sub>5</sub>: U sample has been fitted from 1-3.5 Å assuming three U-O shells at 1.74 Å (×2), 2.47 Å (×4), 2.92Å (×4), one U-B shell at 3.46 Å (×3) and one U-P shell at 3.49 Å (×2). The EXAFS analysis results show that the U-B and U-P paths corroborate well with the Ba-B and Ba-P paths as obtained from BaBPO<sub>5</sub> structure reported in literature [56]. This suggests that the Uranium cation is going into the BaBPO<sub>5</sub>: U host matrix replacing Ba cations. However, the U-O bond lengths are found to be much different than Ba-O bond lengths of the host matrix. For the SrBPO<sub>5</sub>: U and CaBPO<sub>5</sub>: U samples no peak was observed in the spectra which can correspond to

U-B or U-P shells. This may suggest that U cation is not replacing Sr and Ca regular sites in SrBPO<sub>5</sub>: U and CaBPO<sub>5</sub>: U respectively. The U-O bond lengths in CaBPO<sub>5</sub>: U system are longer than that compared to the U-O bonds in SrBPO<sub>5</sub>: U system. Also, in the SrBPO<sub>5</sub>: U, uranium has a six coordinated oxygen environment, whereas in the CaBPO<sub>5</sub>: U, uranium shows ten coordinated oxygen environment. Therefore, surrounding oxygen environment of uranium in these two matrices are different, though they show similar PL emission profile and this may contribute towards different emission intensity and life time decay values.

**Table 4.3: Sr K edge EXAFS results**

	SBP			SBP-U		
	r(Å)	N	$\sigma^2$	r(Å)	N	$\sigma^2$
Sr-O1	2.41	2	0.001	2.49	2	0.006
Sr-O2	2.59	8	0.009	2.69	8	0.014
Sr-O3	-	-	-	1.95	1.3	0.027

To get further insight into the SrBPO<sub>5</sub>: U system and to investigate if uranium is replacing Sr in the matrix or going into interstitial sites, Sr K edge EXAFS measurement has been carried out on pure SrBPO<sub>5</sub> and SrBPO<sub>5</sub>: U. The experimental  $\chi(r)$  versus  $r$  spectra of these samples at Sr K edge is shown in figure 4.11 and the results of the fitting have been tabulated in Table 4.3. The  $\chi(r)$  versus  $r$  spectrum of the SrBPO<sub>5</sub>: U sample has been fitted

from 1- 2.8 Å assuming two Sr-O shells at 2.56 Å (×2) and 2.78 Å (×8) in phase corrected spectra (figure 4.11 shows phase uncorrected spectra). Here the crystal lattice structure of SrBPO<sub>5</sub> has been taken in to account. However, the SrBPO<sub>5</sub>: U sample could not be fitted with the SrBPO<sub>5</sub> structure due to the presence of a hump at 1.9 Å (in phase corrected spectra) in the  $\chi(r)$  versus  $r$  spectrum.

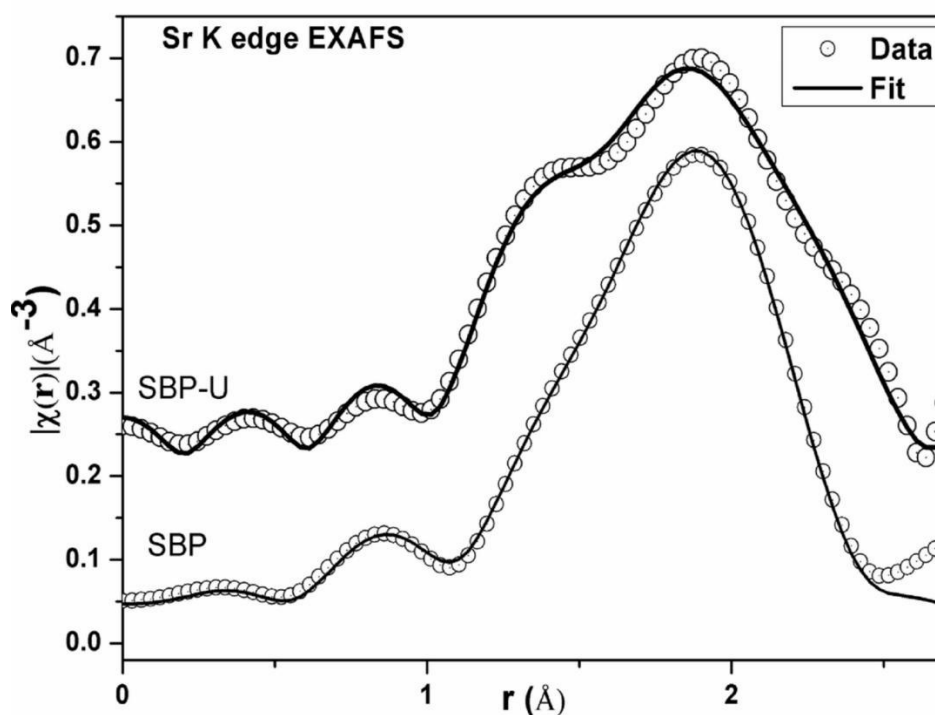


**Figure 4.11.  $\chi(r)$  vs  $r$  at Sr K edge in SrBPO<sub>5</sub>: U sample.**

To fit this spectrum, an extra oxygen path has been incorporated in the fitting model at 1.95 Å. The presence of an extra oxygen path suggests that U is not replacing Sr in the lattice, instead it may occupy some interstitial sites. The changes in the Sr environment on U doping suggests that U cations are going into the SrBPO<sub>5</sub> matrix without forming any separate phase.

The Uranyl structure is generally described by two axial U-O bonds whose bond length varies as 1.7-2.0 Å and 4-6 longer equatorial U-O bond with bond length greater than 2.0 Å. However, some Uranium compounds show symmetrical environment. These are known as Uranate structures where the axial and equatorial bond lengths are nearly equal [57]. In the present study, it is observed that the difference in bond length of the axial (U-O1) and equatorial (U-O2) uranium oxygen bonds is more for the SrBPO<sub>5</sub>: U and CaBPO<sub>5</sub>: U samples compared to the BaBPO<sub>5</sub>-U sample as can be inferred from the EXAFS analysis results tabulated in Table 4.2. The  $\chi(r)$  versus r spectra in Fig. 4.10 shows a single peak for BaBPO<sub>5</sub>-U sample and double peaks for SrBPO<sub>5</sub>: U and CaBPO<sub>5</sub>: U samples due to oxygen shells. This suggests that oxygen environment around U cation is more symmetrical in BaBPO<sub>5</sub>: U sample than that in SrBPO<sub>5</sub>: U and CaBPO<sub>5</sub>: U samples (as seen above with lifetime results). The U-O bond length values as obtained from EXAFS analysis of the BaBPO<sub>5</sub>: U sample also matches with that reported for Cesium Uranate compounds [53]. This corroborates the findings from luminescence studies that uranium stabilizes as Uranyl in SrBPO<sub>5</sub> and CaBPO<sub>5</sub> matrices, but in BaBPO<sub>5</sub> matrix the uranium stabilizes as Uranate.

#### **4.4 Conclusion:**

Uranium doped alkaline earth boro phosphates BaBPO<sub>5</sub>, SrBPO<sub>5</sub> and CaBPO<sub>5</sub> are synthesized using solid state reaction method. The PL studies indicated stabilization of uranium as uranyl in SrBPO<sub>5</sub> and CaBPO<sub>5</sub> matrices whereas the uranate form of uranium gets stabilized in BaBPO<sub>5</sub>. The life time decay values suggested a relatively asymmetric environment surrounding uranium in SrBPO<sub>5</sub> and CaBPO<sub>5</sub> and a more symmetric environment for uranium present in BaBPO<sub>5</sub>. Further investigations using EXAFS inferred

the site occupancy of uranium in all these matrices. The regular  $Ba^{2+}$  site is the preferred site for uranium in  $BaBPO_5$  whereas the interstitial sites present in  $SrBPO_5$  and  $CaBPO_5$  are responsible for uranium stabilization. The uranium stabilizes as uranate in  $BaBPO_5$  whereas it stabilizes as uranyl in  $SrBPO_5$  and  $CaBPO_5$  matrices.

#### **4.5 References:**

1. B. Lei, Q. Jing, Z. Yang, B. Zhang, S. Pan, J. Mater. Chem. C, 3(2015), 1557-1566.
2. D.Zhao, W.Cheng, H.Zhang, S. huang, Z.Xie, W.Zhang, S.Yang, Inorg. Chem., 48(2009) 6623- 6629.
3. R. Kniep, G. Gozel, B. Eisenmann, C. Rohr, M. Asbrand, M. Kizilyalli, Angew. Chem. Int. Ed. Engl., 33 [7] (1994), 749-751.
4. H. Bauer, Z. Anorg. Allg. Chem., 345 (1966) 225-229.
5. B. Han, J. Zhang, Y. Lü, Russ. J. Phy. Chem. A., 88 (7) (2014) 1209-1214.
6. M. Peng, N. Da, S. Krolikowski, A. Stiegelschmitt, L.Wondraczek, Opt. Express, 17 (23) (2009), 21169- 21178.
7. T. N Akamura, T. Takeyama, N. Takahashi, R. Jagannathan, A. Karthikeyani, G.M. Smith, P.C. Riedi, J. Lumin, 102-103 (2003), 369-372.
8. K. Sakasai, M. Katagiri, K. Toh, H. Takahashi, M. Nakazawa, and Y. Kondo, "Characteristics of a  $SrBPO_5:Eu^{2+}$  Material as a Neutron Storage Phosphor," Nuclear Science Symposium Conference Record, IEEE 1 455-459 (2002).
9. K. Sakasai, M. Katagiri, K. Toh, H. Takahashi, M. Nakazawa, Y. Kondo, Appl. Phys. A, 74 (2002) S1589–S1591.

10. Y. Lan, L. Yi, L. Zhou, Z. Tong, F. Gong, R. Wang, *Physica B*, 405 (2010), 3489–3491.
11. M. Kumar, T. K. Seshagiri, S.V. Godbole, *Bull. Mater. Sci.*, 36 (2013), 913–918.
12. M. Mohapatra, M.Kumar, V.Natarajan, S.V.Godbole, *Radiat. Phys. Chem.*, 103 (2014) 31–36.
13. M. Kumar, M. Mohapatra, V. Natarajan, *Mater. Res. Bull.*, 60 (2014), 858-863.
14. A. A. Voronkov, Yu. A. Pyatenko, *Sov. Phys. Cryst.*, 12 (1967), 258-265.
15. A. Karthikeyani, R. Jagannathan, *J. Lumin.*, 86 (2000), 79-85.
16. S. Pan, Y. Wu, P. Fu, G. Zhang, Z. Li, C. Du, C. Chen, *Chem. Mater.*, 15 (2003), 2218-2221.
17. C. Lu, S. V. Godbole, *J. Mater. Res.*, 19 [8] (2004), 2336-2342.
18. H. B. Liang, Q.Su, S. Lu, Y.Tao, T.D. Hu, T.Liu, *Mater. Res. Bull.*, 37 (2002) 1981-1989.
19. H. Liang, Y. Tao, W. Chen, X. Ju, S. Wang, Q. Su, *J. Phys. Chem. Solids*, 65 (2004), 1071-1076.
20. A. Rout, M. Mohapatra, N. Suriyamurthy, B. S. Panigrahi, *J. Lumin.*, 167 (2015), 45-50.
21. M. E. D. G. Azenha, H. D. Burrows, S.J. Formosinho, M.G.M. Mignel, A.P. Daramanyan, I. V. Khudyakov, *J. Lumin.*, 48-4 (1991), 522-526.
22. S. Maji, K.S. Viswanathan, *J. Lumin.*, 129 (2009), 1242-1248.
23. G. Blasse, K.C. Bleijenberg, D.M. Krol, *J. Lumin.*, 18-19 (1979), 57-62.

24. M. Mohapatra, B. Rajeswari, R.M. Kadam, M. Kumar, T.K. Seshagiri, N.K. Porwal, S.V. Godbole, V. Natarajan, *J. Alloys Compd.*, 611 (2014), 74–81.
25. D. R. Taikar, C.P. Joshi, S.V. Moharil, *J. Lumin.*, 153 (2014), 304-306.
26. R. U. E. 't Lam, G. Blasse, *J. Chem. Phys.*, 72 (1980), 1803–1808.
27. A. Lupei, V. Lupei, *J. Phys. C: Solid State Phys.*, 12 (1979), 1123-1130.
28. G. Blasse, G.P.M. van den Heuvel, J.J.A. van Hesteren, *J. Solid State Chem.*, 21 (1977), 99–103.
29. I. W. Donald, B. L. Metcalfe, R. N. J. Taylor, *J. Mater. Sci.*, 32 (1997), 5851–5887.
30. R.C. Ewing, W.J. Weber, J. Lian, *J. Appl. Phys.*, 95 (11) (2004), 5949-5971.
31. M. Ishimaru, Y. Hirotsu, M. Tang, J.A. Valdez, K.E. Sickafus, *J. Appl. Phys.*, 102 (2007) 063532.
32. M. L. Carter, A.L. Gillen, K. Olufson, E.R. Vance, *J. Am. Ceram. Soc.*, 92 (5) (2009), 1112- 1117.
33. E.H. Oelkers, J-M. Montel, “Phosphates and Nuclear Waste Storage,” *Elements*, 4 (2008), 113-116.
34. R.C. Ewing, L.M. Wang, 48 (2002), 673-699.
35. S. Raicevica, T. J.V. Wrightb, V. Veljkovicc, J.L. Conca, *Sci.Total Environ.*, 355 (2006), 13– 24.
36. M.V. Hoffman, *J. Electrochem. Soc.*, 117 (2) (1970), 227-232.
37. M.E. Azenha, and G. Blasse, *J. Alloys. Compd.*, 196 (1993), 81-85.
38. G. Blasse, J.P.M. van den Dungen, *J. Inorg. Nucl. Chem.*, 40 (12) (1978), 2037-

2039.

39. M. Mohapatra , A.K. Yadav , S.N. Jha , D. Bhattacharyya , S.V. Godbole, V. Natarajan, *Chem. Phys. Lett.*, 601, (2014), 81–86.
40. A. K. Poswal, A. Agrawal, A. K. Yadav, C. Nayak, S. Basu *et al.*, *AIP Conf. Proc.*, 1591 (2014), 649-651.
41. S. Basu, C. Nayak, A. K. Yadav, A. Agrawal, A. K. Poswal *et al.*, *J. Phys. : Conf. Ser.*, 493 (2014), 012032.
42. H.M. Rietveld, *Acta Crystallogr.*, 22 (1967), 151-152.
43. L. Lutterotti, MAUD Version 2.50, <http://maud.radiographema.com/> (2014).
44. F.A. Cotton, G. Wilkinson, *Advanced Inorganic Chemistry*, Inter Science Publication, MA (USA), V Edn. (1989).
45. Peter A. Tanner, Pei Zhi-Wu, Lin Jun, liu Yulong, Su Qiang, *J. Phys. Chem. Solids*, 58 (7) (1997), 1143-1146.
46. Peter A. Tanner, *J. Mol. Str.*, 405 (1997), 103-111.
47. G. Blasse, K.C. Bleijenberg, D.M. krol, *J. Lumin.*, 18/19 (1979), 57-62.
48. G. K. Liu, “Analysis of Electronic States and Energy Level Structure of Uranyl in Compounds,” *J. Phys. Chem. A*, 115 (2011), 12419-12425.
49. G. K. Liu, N.P. Deifel, C.L. Cahill, V.V. Zhurov, A.A. Pinkerton, *J. Phys. Chem. A.*, 116 (2012), 855-864.
50. V.V. Syt’ko, D.S. Umreiko, *J. Appl. Spectrosc.*, 65 (6) (1998), 857-870.
51. K. Ohwada, *Spectrochim. Actamol. Spectrosc.*, 35 (1) (1978), 99-104.

52. J. Th. W. De Hair, G. Blasse, 14 (1976), 307-323.
53. D. C. Koningsberger, and R. Prins, X ray Absorption: Principles, Applications, Techniques of EXAFS, SEXAFS and XANES. Wiley, New York, 1988, ISBN: 978-0-471-87547-5.
54. M. Newville, B. Ravel, D. Haskel, J.J. Rehr, E.A. Stern, Y. Yacoby, Physica B, 208, (1995), 154-156.
55. R. J. Finch, M. A. Cooper, F. C. Hawthorne, R. C. Ewing, Can. Mineral. 37 (1999) 929-938.
56. Y. Shi, J. Liang, H. Zhang, Q. Liu, X. Chen, J. Yang, W. Zhuang, G. Rao, J. Solid State Chem., 135 (1998), 43-51.
57. Sven Van den Berghe, M. Verwerft, J. P. Laval, B. Gaudreau, P. G. Allen, A. Van Wyngarden, J. Solid State Chem., 166 (2002), 320-329.

## **Chapter 5**

**Understanding the energy transfer mechanism  
from Uranium to Europium and Samarium in  
 $\text{SrBPO}_5$  *stillwellite* host**



## **5.1 Introduction:**

Recently, many literature reports have been published on the use of alkaline earth borophosphates (with the general formula  $MBPO_5$  ( $M=Ca, Sr, Ba$ )) as hosts for luminescent materials [1-2]. These host materials belong to the mineral type *stillwellite* and exhibit unique photoluminescence (PL) properties upon doping with suitable activators.  $SrBPO_5$  (SBP) is one such borophosphate that has attracted much attention because of its use as an X-ray and neutron storage phosphor material [3-4]. Many reports are available in the literature about the luminescence properties of lanthanides as activators in this matrix. PL properties of SBP doped with lanthanides such as Sm [5], Eu [3 and 6], Ce, Sm-Ce [7-8], Dy [9], Tb [10] and actinides such as uranium [11] have been reported earlier. In all these reports the notable thing is the forbidden nature of the f-f transitions of the lanthanide ions. Though trivalent europium is well known as a 'red' emitting ion, the forbidden nature of the 'f-f' transition leads to weak absorption coefficient and consequent weak emission leading to low quantum yield [12].

In order to circumvent this, a co-dopant ion can be used that can transfer energy efficiently to the primary activator ion (Eu). The co-dopant can be another lanthanide, transition metal or even an actinide depending on the suitability. Out of the different co-dopants, uranium has a special place. One may find many reports on the efficient energy transfer phenomena from hexavalent uranium to trivalent europium in different types of media like solution, glasses, polymers and ceramics etc. Kropp and Joshi et al. have reported energy transfer from  $UO_2^{2+}$  to  $Eu^{3+}$  in solutions and suggested that the energy transfer is accompanied by electric dipole transition and electron exchange interaction [13-14]. Later Tanner and Vargenas studied its pH dependence in aqueous perchlorate solutions

[15]. Energy transfer from  $\text{UO}_2^{2+}$  to  $\text{Eu}^{3+}$  in acidic solutions by an exchange interaction mechanism has been reported by Yamamura et al. [16]. Similarly Olken et al. observed host to guest excited state energy transfer in lamellar solids of hydrated Europium Uranyl phosphates [17]. Dai et al. had earlier proposed a static energy transfer process from  $\text{UO}_2^{2+}$  to  $\text{Eu}^{3+}$  in sol-gel glass [18]. They observed that quenching of  $\text{UO}_2^{2+}$  emission by  $\text{Eu}^{3+}$  in sol-gel glass is much less in comparison to aqueous solution which was ascribed to the mobility of the ions in the system. In borosilicate glass, transfer of energy from  $\text{UO}_2^{2+}$  to  $\text{Eu}^{3+}$  lead to a fivefold fluorescence enhancement of  $\text{Eu}^{3+}$  [19]. Okamoto et al. reported an effective energy transfer from  $\text{UO}_2^{2+}$  to  $\text{Eu}^{3+}$  in polymers based on the proximity of metal ions in ionic aggregate of these ionomers [20]. Hoffman suggested a radiation less energy transfer from  $\text{UO}_2^{2+}$  to  $\text{Eu}^{3+}$  in  $\text{SrZnP}_2\text{O}_7$  [21]. Recently, Kumar and Mohapatra had reported that both static and dynamic type mechanism is responsible for the  $\text{U} \rightarrow \text{Eu}$  energy transfer in  $\text{ZnAl}_2\text{O}_4$  spinel host [22]. It is not only Eu, uranium has proven its potential energy transfer efficiency for co-dopant samarium (Sm) also. Reisfeld et al. as has reported  $\text{UO}_2^{2+} \rightarrow \text{Sm}^{3+}$  energy transfer in phosphate glass [23]. According to this study, when the donor is excited at higher energy levels, due to stronger overlap between electronic levels of donor and acceptor the energy transfer efficiency is high. Here the sensitization of  $\text{Sm}^{3+}$  by non-radiative energy transfer from  $\text{UO}_2^{2+}$  in Zinc phosphate glass was found to be electric dipole-dipole in nature. Coordination polymers are also reported where sensitization of  $\text{Sm}^{3+}$  by  $\text{UO}_2^{2+}$  has occurred efficiently [24]. However, the dynamics of this energy transfer mechanism ( $\text{U} \rightarrow \text{Eu}$  and  $\text{U} \rightarrow \text{Sm}$ ) has not been studied in SBP matrix in spite of having plenty of literature on the individual doped systems [5, 27]. In the present

paper, the U→Eu as well as U→ Sm energy transfer mechanisms has been investigated in detail in the SBP host using PL excitation, emission and life time data.

## **5.2 Experimental:**

The undoped SBP samples were prepared via the conventional high temperature solid state reaction route using SrCO<sub>3</sub>, (NH<sub>4</sub>)<sub>2</sub> HPO<sub>4</sub> and H<sub>3</sub>BO<sub>3</sub>. For the ‘Eu’ and ‘U’ doped samples, required amounts of Eu<sub>2</sub>O<sub>3</sub> and UO<sub>2</sub>(NO<sub>3</sub>)<sub>2</sub>.6H<sub>2</sub>O were added to the mixture of the above ingredients respectively. After fine grinding, the mixtures were made into pellets of 10 mm diameter and 0.5 mm thickness and fired at 873 K in a muffle furnace for 3 hours. After this, the samples were thoroughly ground and pelletized and heated at 1173 K for 3 more hours.

The crystal Structure of the prepared samples were examined by powder X-ray diffraction using a Philips diffractometer (model PW 1071) with Cu K<sub>α</sub> ( $\lambda = 1.5418 \text{ \AA}$ ) source. All PL measurements were made using a Shimadzu RF 5301 PC spectrofluorimeter equipped with a 150 W Xenon lamp. For the measurements, bandwidths for both the excitation and emission monochromator were set at 3 nm. A long-wavelength-pass filter (UV-35, Shimadzu), with maximum and uniform transmittance (more than 85%) above 350 nm, was placed in front of the emission monochromator in order to reduce the scattering. The PL decay time measurements were carried out using an Edinburgh FLS 900 unit at room temperature.

### **5.3 Results and discussion:**

#### **5.3.1 Crystal structure analysis:**

Figure 5.1 show the X ray diffraction patterns of undoped, U (1 mol %) doped, Eu (1 mol %) doped and co-doped (U=1 mol%, Eu=1 mol %) SBP. The observed peaks were found to be in good agreement with the standard ICDD patterns (File no: 18-1270). This suggested the stabilisation of SBP in a hexagonal geometry with space group of  $P3_221$ . There was no signature of any other phase implying the formation of a single phase system. Detailed discussion regarding the crystal structure of SBP can be found elsewhere [5, 11].

Figure 5.2 shows the X ray diffraction patterns of undoped, U (1 mol %) doped, Sm (1 mol %) doped and co-doped (U =1 mol%, Sm =1 mol %) SBP. The observed peak patterns in a, b, c and d were in good agreement with the standard ICDD patterns e (File no: 18-1270). The collected XRD patterns were devoid of second phase as well as impurity peaks indicating the formation of a single phase system. Fig. 5.1 and 5.2 shows that dopant U / Sm/ Eu does not alter the crystallography of SBP system. It can be attributed to the very low concentration of the dopant ion.

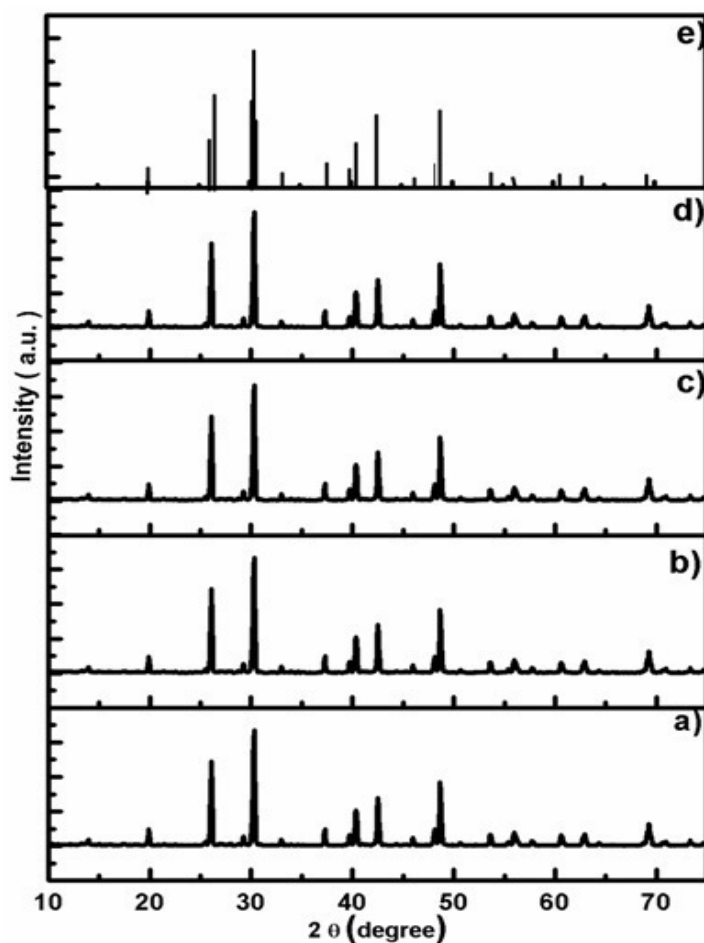


**Figure 5.1:** (a) XRD patterns for the undoped SBP, (b) Eu (1 mol%) doped SBP, (c) U (1 mol%) doped SBP, (d) U and Eu co-doped SBP, (e) Standard (ICDD) pattern no-18-1270

### 5.3.2 PL studies on Eu doped SBP:

The PL properties of Eu in SBP host are well documented [3, 10]. Figure 5.3 shows the excitation and emission profile of Eu (0.1 mol%) doped SBP. The excitation spectrum (with  $\lambda_{em} = 590$  nm) exhibits peaks at 394, 464 and 542 nm. The peak centred at 394 nm is known to be a transition from  ${}^7F_0$  ground state to  ${}^5L_6$  excited level [25]. The emission profile (with  $\lambda_{ex} = 394$  nm) shows maxima at 584, 589, 599, 612, 622, and 723 nm. These observed emission bands are the well-known  ${}^5D_0 \rightarrow {}^7F_J$  (with  $J = 0, 1, 2, 3, 4$  etc.) transitions of Eu

(III). The  ${}^5D_0 \rightarrow {}^7F_1$  transition is a magnetic dipole transition that is often reported to appear in the region 588-595 nm. In the present case, the particular transition appears to split into three emission peaks i.e. 584, 589 and 599 nm most probably due to lowering of the site symmetry around the metal ion (Stark Splitting). The band positioned at 612 nm originates from  ${}^5D_0 \rightarrow {}^7F_2$  electric dipole transition and is known to be hypersensitive towards surrounding crystal field. The crystal field strength is perturbed by site symmetry, bond length, covalency and ligand charge. Here, it is observed that  ${}^5D_0 \rightarrow {}^7F_1$  transition is more intense than  ${}^5D_0 \rightarrow {}^7F_2$  transition and the  ${}^5D_0 \rightarrow {}^7F_0$  transition is completely absent indicating more symmetric position for Eu (III) in SBP.

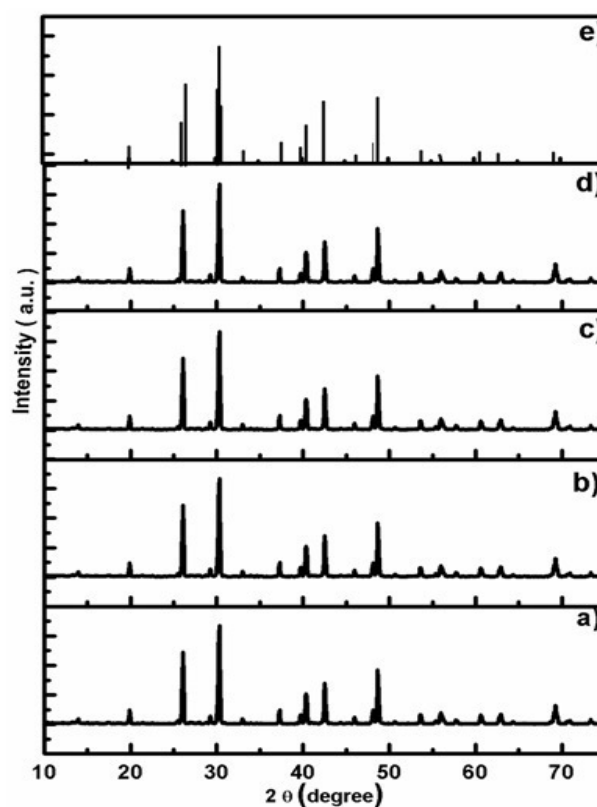


**Figure 5.2:** (a) XRD patterns for the undoped SBP, (b) Sm (1 mol%) doped SBP, (c) U (1 mol%) doped SBP, (d) U and Sm co-doped SBP, (e) Standard (ICDD) pattern no-18-1270

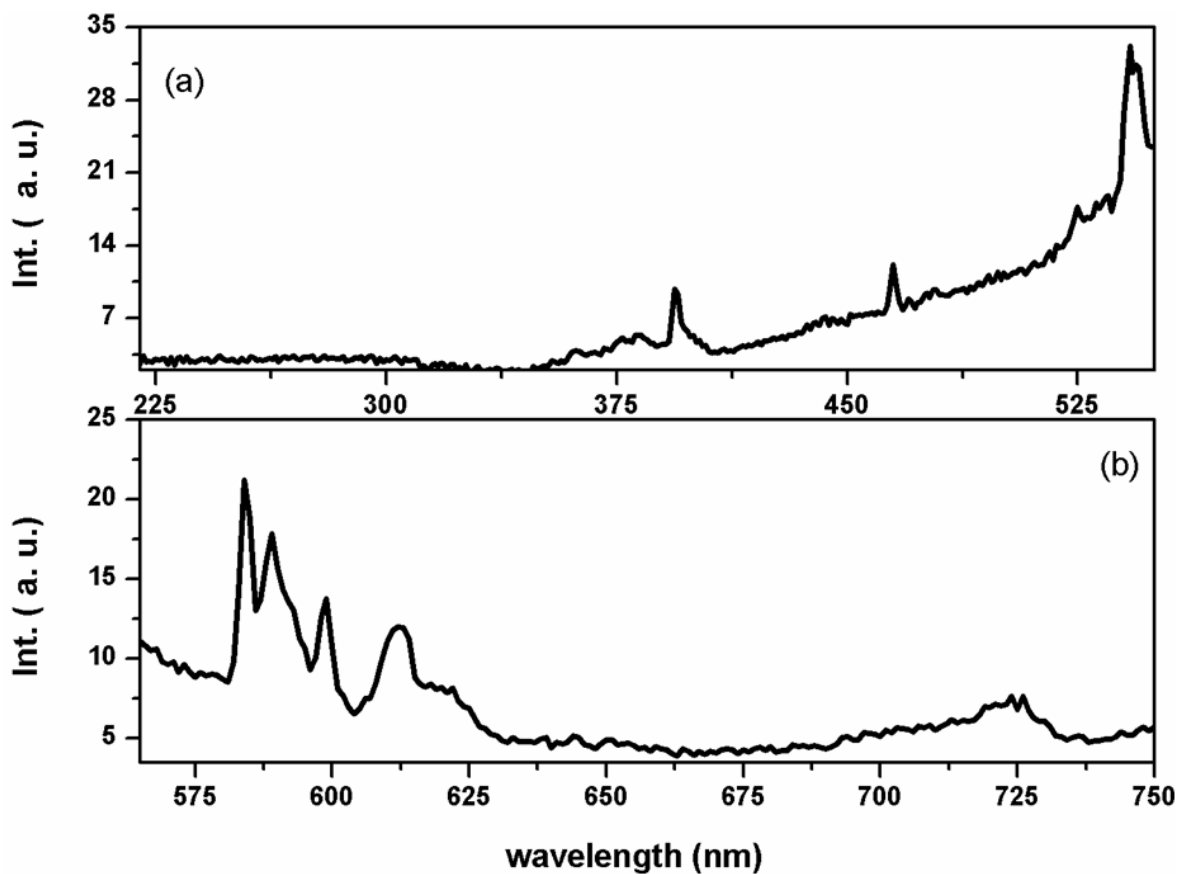


**Figure 5.3: PL (a) excitation and (b) emission spectra for the 0.1 mol% Eu doped SBP sample**

The emission peaks appeared at 622 and 723 nm correspond to transition from the  $^5D_0$  to the  $^7F_3$  and  $^7F_4$  levels, respectively. Since the main focus of the work is to understand the energy transfer mechanism, the Eu concentration throughout the work was maintained at 0.1 mol%.

### **5.3.3 PL studies on Sm doped SBP:**

Figure 5.4 shows the emission spectra of SrBPO<sub>5</sub>: Sm (1%) with an excitation wavelength of 410nm. The emission spectrum originating from  $^4G_{5/2}$  level to  $^6H_j$  levels, (where  $J= 5/2, 7/2$  and  $9/2$ ) of Sm<sup>3+</sup> are clearly observed here. The emission peak positioned at 559-566

nm is a typical magnetic dipole transition and it corresponds to  ${}^4G_{5/2} \rightarrow {}^6H_{5/2}$  transition. The  ${}^4G_{5/2} \rightarrow {}^6H_{7/2}$  emission transition is positioned at 596-608 nm. This transition is known to be a partly magnetic and partly forced electric-dipole transition [33]. The emission peak centered at 642 nm is a pure electric-dipole transition originating from  ${}^4G_{5/2} \rightarrow {}^6H_{9/2}$  transition. All of these emission peaks are associated with stark components. The presence of stark components clearly indicates that Sm is present at a site with lower symmetry.

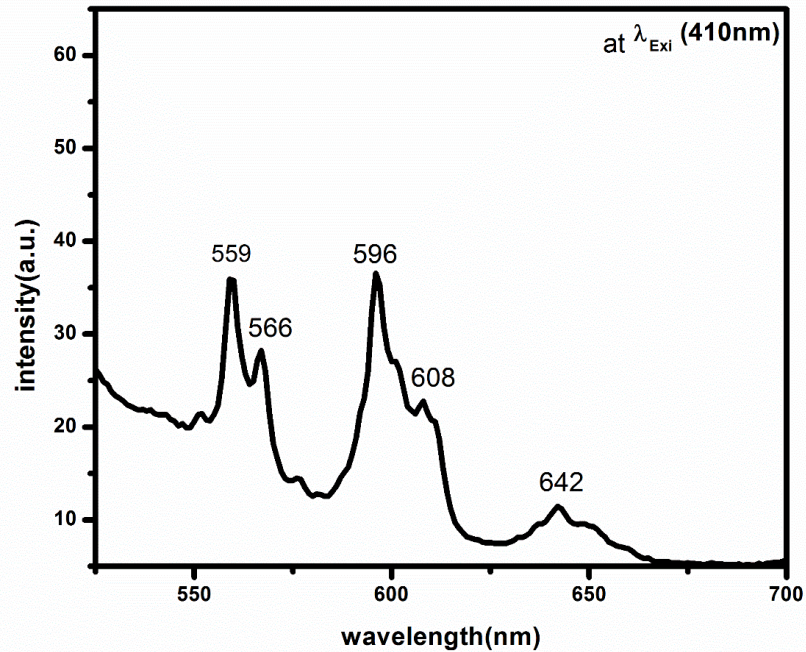


**Figure 5.4: PL emission spectrum of SBP: Sm, at an excitation wavelength of 410nm.**

The PL excitation spectrum of Sm doped SBP phosphor, monitored at a wavelength of 596 nm, is shown in Figure 5.5. The excitation bands present between 350 nm and 500 nm are representative of typical intra-4f transitions in Sm<sup>3+</sup> ions. The excitation bands centred at 346 nm, 358 nm, 373 nm, 400 nm, 417 nm, 440 nm, and 476 nm, are assigned to the  ${}^6H_{5/2} \rightarrow {}^4H_{9/2}$ ,  ${}^4D_{3/2}$ ,  ${}^4D_{1/2}$ ,  ${}^4F_{7/2}$ ,  ${}^4P_{5/2}$ ,  ${}^4I_{13/2}$  and  ${}^4I_{11/2}$  transitions of Sm<sup>3+</sup> ions, respectively [34].

Among these transitions the  ${}^6\text{H}_{5/2} \rightarrow {}^4\text{F}_{7/2}$  transition corresponding to the peak at 410 nm is the most intense and is considered for the measurement of the emission spectra of SBP:  $\text{Sm}^{3+}$  Phosphor.

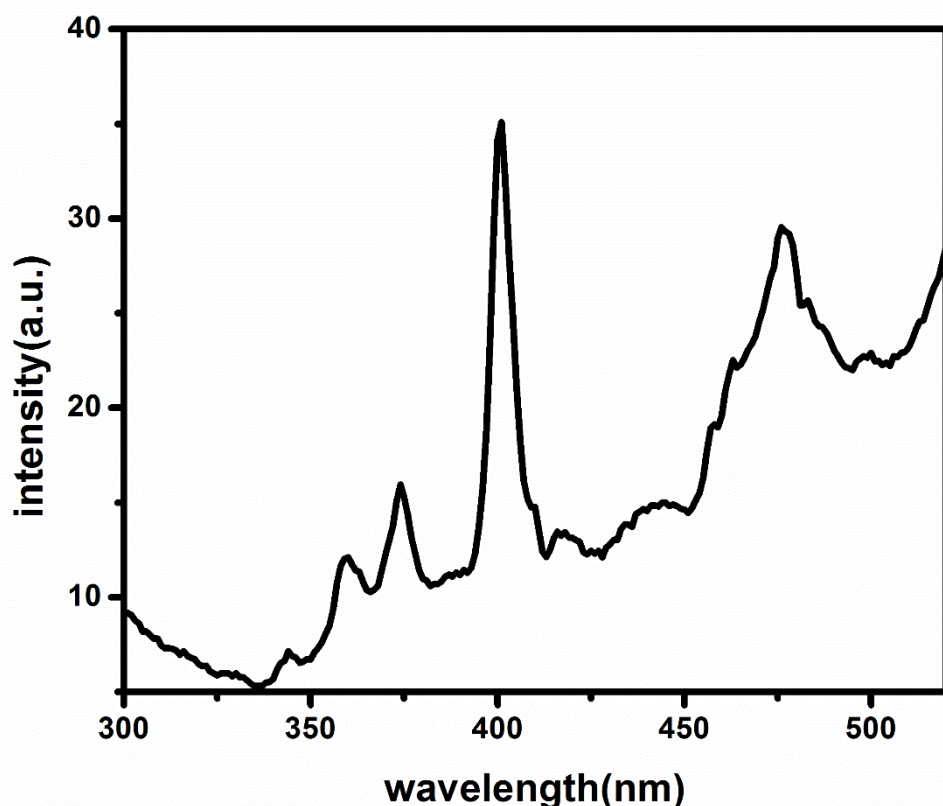


**Figure 5.5: PL excitation spectrum of SBP: Sm, at an excitation wavelength of 596 nm.**

#### **5.3.4 PL studies on U doped SBP:**

Figure 5.6 shows the excitation and emission spectra of the uranium (1 mole %) doped SBP. The excitation profile ( $\lambda_{\text{em}} = 519 \text{ nm}$ ) is characterised by the presence of a number of peaks at 335, 343, 352, 407, 417, 434, and 440 nm. Similarly, the emission spectrum shows sharp peaks at 498, 519, 541 and 565 nm with 440 nm excitation. Two rather known small

bands are also observed at 482 and 595 nm. Mohapatra and Natarajan have described the nature of excitation and emission bands of uranium in several hosts [26]. Recently, we also have discussed the PL properties of Uranium in SBP host with respect to its concentration and annealing temperature during preparation [27].

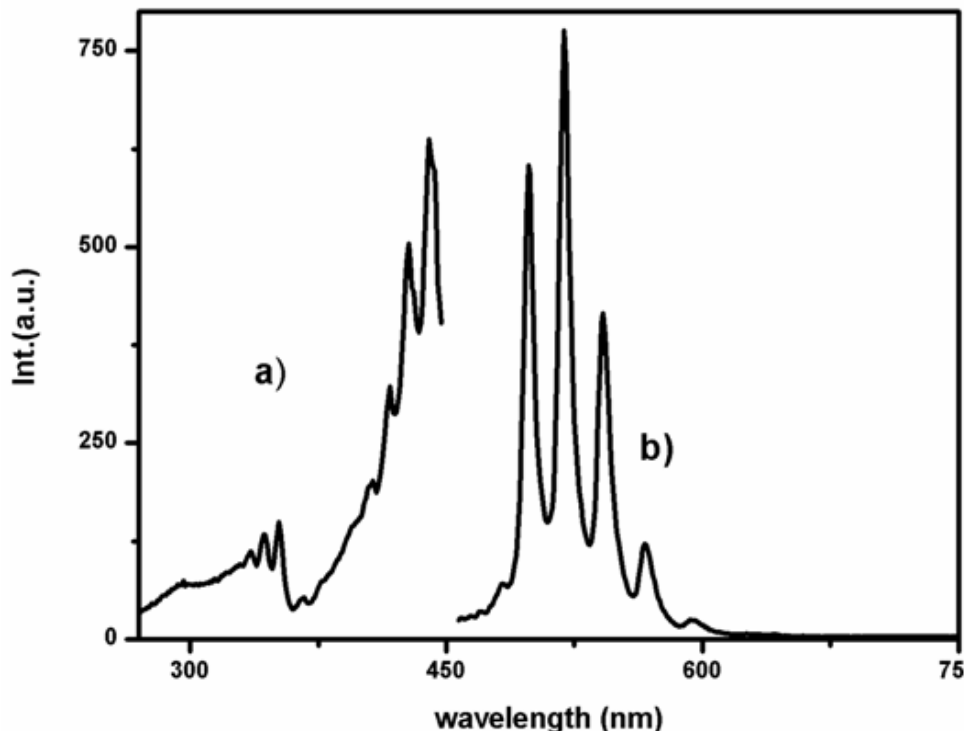


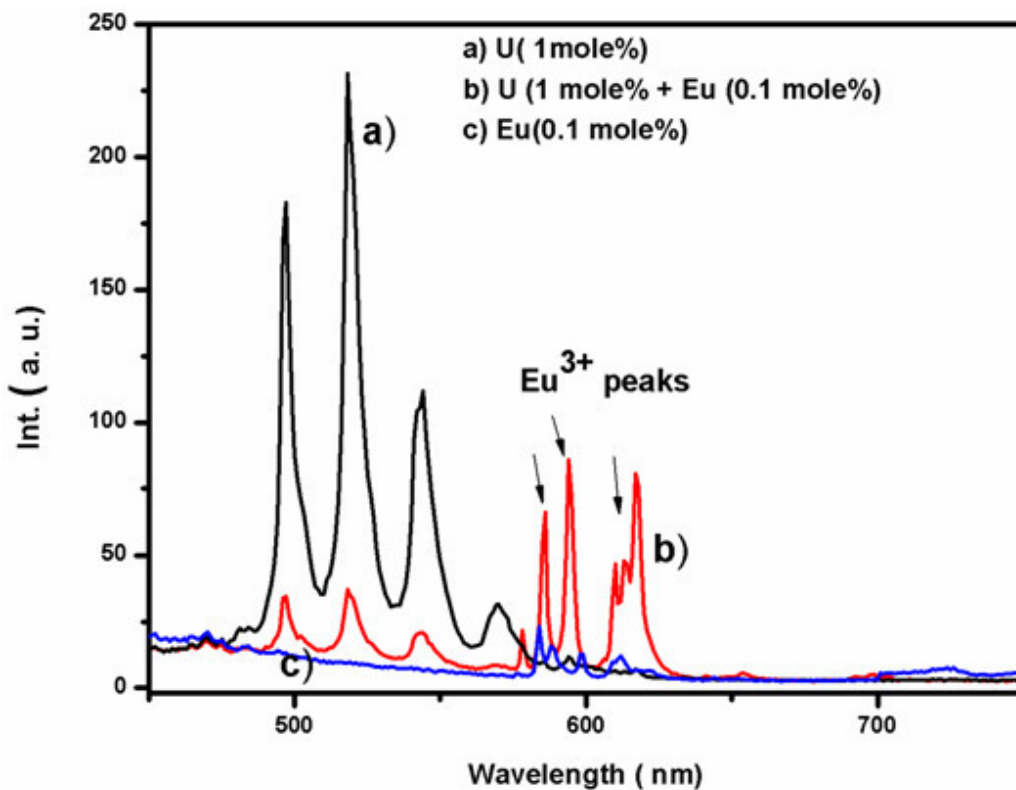
**Figure 5.6: PL a) excitation and b) emission data of uranium (1 mol %) doped SBP**

The observed spectral properties of the dopant uranium ion suggested its stabilisation as uranyl ion ( $\text{UO}_2^{2+}$ ). Here, the excitation process can be explained as an electron transition from a bonding oxygen orbital ( $\sigma_u, \sigma_g, \pi_u, \pi_g$ ) to non-bonding uranium 5f orbitals through ligand-to-metal charge transfer (LMCT) process. Although, the LMCT process follows parity forbidden rule for uranyl ion (due to its  $D_{\infty h}$  symmetry), interruption of local coordination environment lowers the symmetry and facilitates the transition. In case of the

emission spectrum, the first low intense emission peak centred at 482 nm is known as the anti-stokes band originating from the first vibrational level of the ground state whereas peaks at higher wavelength region are the vibrational progressions resulting from strong coupling of the ground state Raman active symmetric vibrational ( $\nu_1$ ) modes with the  $3\pi_u$  electronic triplet excited state. The characteristic emission profile with anti-stokes line and vibrational fine structures can be taken as fingerprint for the presence of uranium as  $\text{UO}_2^{2+}$ .

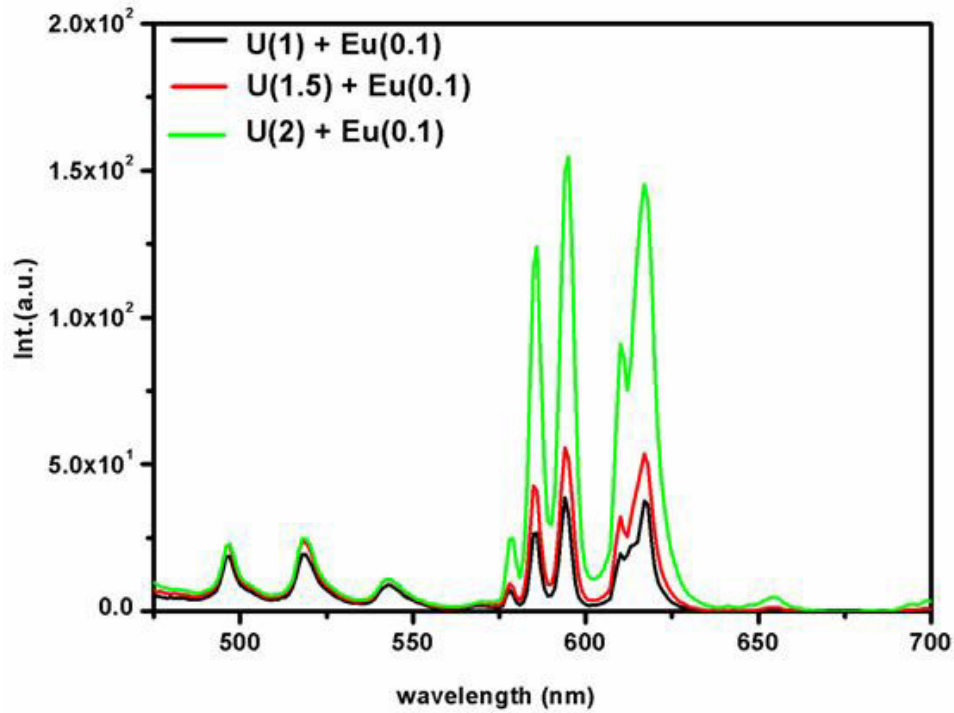
### **5.3.5 Understanding the energy transfer process from Uranium to Europium:**

Figure 5.7 shows the emission spectrum of the co-doped sample (U = 1 mol % and Eu = 0.1 mol %) with  $\lambda_{\text{ex}} = 440$  nm that corresponds to uranyl excitation. The corresponding emission spectra (with 440 nm excitation) for the single doped SBP samples (only Eu and U) are also shown in the figure for comparison under identical settings. It is evident from this figure that in the co-doped sample, upon exciting at 440 nm, the emission due to  $\text{Eu}^{3+}$  enhances (at least 4 times) with a reduction in the  $\text{UO}_2^{2+}$  emission. It is worth mentioning here that in case of the Eu-SBP sample excited at 440 nm, no signature of U was seen (figure 5.4 c).



**Figure 5.7: PL emission spectra of U, Eu and U-Eu co-doped SBP with  $\lambda_{\text{ex}} = 440 \text{ nm}$  (corresponding to uranyl excitation)**

To probe further, emission spectra were recorded for the co-doped sample by varying uranium concentration (and keeping the  $\text{Eu}^{3+}$  concentration fixed at 0.1 mol %) as shown in figure 5.8. It can be observed from the spectra that though the europium ion concentration is unchanged, its emission intensity keeps on increasing with increase in uranium concentration. On the other hand, with increase in the uranium amount, the peak intensities corresponding to uranyl ion increase marginally. In the co-doped sample, the  $\text{Eu}^{3+}$  emission was recorded by exciting at its characteristic excitation wavelength ( ${}^7\text{F}_0 \rightarrow {}^5\text{L}_6$  transition of  $\text{Eu}^{3+}$ ) of 394 nm.



**Figure 5.8: PL emission spectra of Eu (fixed at 0.1 mol %) SBP co-doped with varying Uranium concentration.**

Figure 5.9 shows emission spectra of the co-doped sample at both 440 and 394 nm. It can be observed from the figure that the emission from Eu ion is more when excited through uranyl (at 440 nm) rather than direct excitation (at 394 nm due to  ${}^7F_0 \rightarrow {}^5L_6$ ). This clearly brings out the fact that the energy transfer process from  $UO_2^{2+}$  to  $Eu^{3+}$  observed here efficiently populates the excited state of  $Eu^{3+}$  compared to that by direct excitation of  $Eu^{3+}$ .

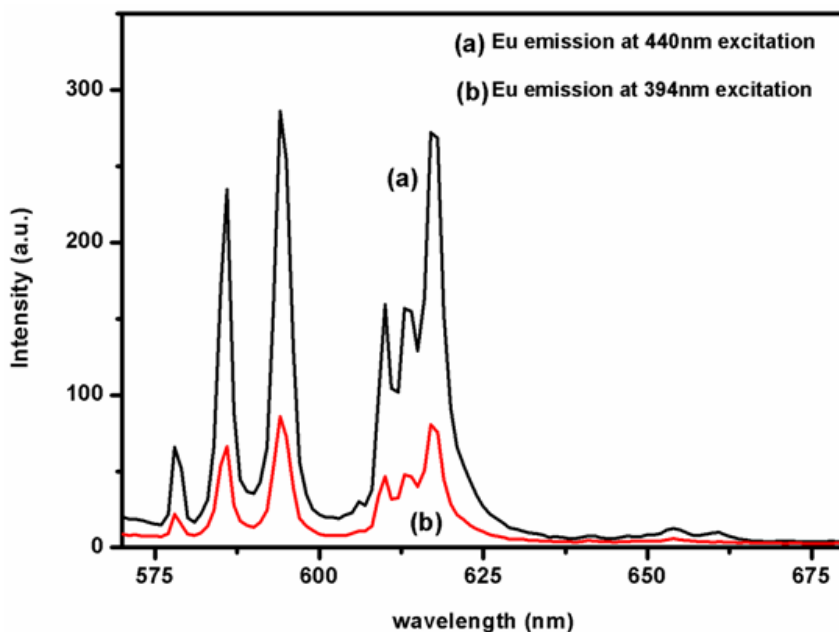


**Figure 5.9: PL emission spectra of  $\text{Eu}^{3+}$  in U- Eu co-doped SBP at (a)  $\lambda_{\text{ex}} = 440 \text{ nm}$  and (b)  $\lambda_{\text{ex}} = 394 \text{ nm}$**

Overlapping of the emission band of the donor and the excitation band of the acceptor is a prerequisite for the energy transfer to occur. In the present case the overlap between the uranyl ion emission and the europium ion excitation (in the single doped SBP samples) is shown in figure 5.10. It is obvious from this figure that there is a significant overlap between these two that drives the energy transfer.

### **5.3.6 PL decay time investigations:**

To corroborate the above mentioned static PL based investigations, PL decay time measurements were also performed on the system. Since the decay time measurements are dynamic in nature, this additional information substantiates the data obtained from the static PL excitation and emission data. Figure 5.11 shows the PL decay time curves for single doped (uranium 1 mole %) as well as the co-doped sample (uranium=1 mole % with

europium = 0.1mole %) doped samples with  $\lambda_{\text{ex}} = 440 \text{ nm}$  and  $\lambda_{\text{em}} = 521 \text{ nm}$ . The curves could be fitted in to bi-exponential decay using the following equation.

$$I(t) = A_0 + A_1 \exp(-t/\tau_1) + A_2 \exp(-t/\tau_2) \quad (1)$$

Here  $A_1$  and  $A_2$  are the pre-exponential factors and scalar quantities,  $t_i$  are the time of measurement and  $\tau_1$  and  $\tau_2$  are the decay time values.

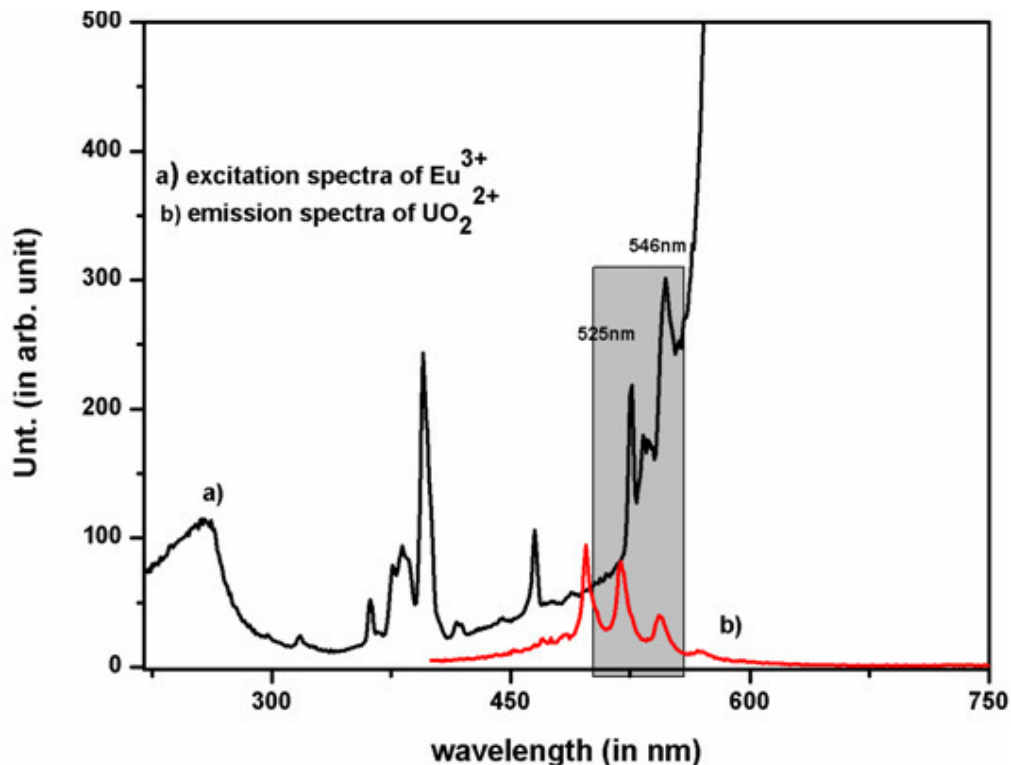


**Figure 5.10: Spectral overlap of a) excitation spectrum of SBP doped with Eu<sup>3+</sup> (0.1 mol %) and b) emission spectrum of SBP doped with U (0.1 mol%)**

The decay time values along with their respective percentage and the fitting parameters are given in table- 5.1. Based on literature data, these two life time values are attributed to the uranyl ion situated in two different environments surrounded by varying amounts of defect centres [11, 26]. It can be seen from the data that the values for both  $\tau_1$  and  $\tau_2$  reduced upon co-doping with Eu. This implies that upon co-doping with Eu, additional relaxation paths

are being created for the dissipation of the energy to the neighbouring Eu ion from the excited uranyl ion (present in two different environments).

**Table- 5.1: PL decay time values for the U and Eu-U co-doped samples with 440 nm excitation and 521 nm emission.**

Sample	$\tau_1(\mu\text{s})$	$\tau_2(\mu\text{s})$	Fitting Parameter ( $\chi^2$ )
U doped	135 (15%)	45 (85%)	1.14
U and Eu co-doped	106 (18%)	20 (82%)	1.24

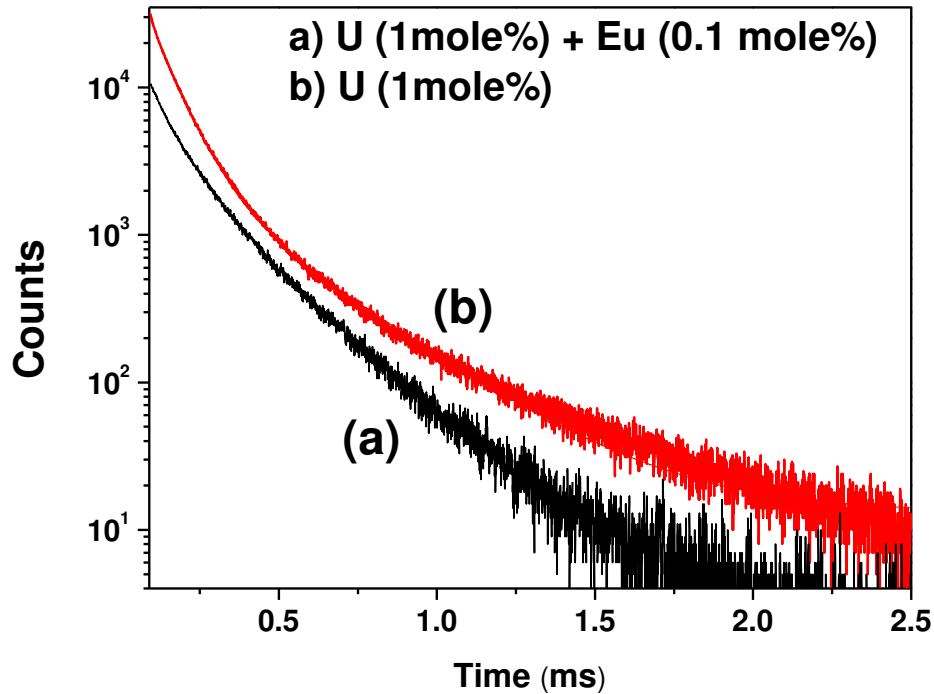


**Figure 5.11: PL decay time data for the U and Eu+U co-doped samples with  $\lambda_{\text{ex}} = 440 \text{ nm}$  and  $\lambda_{\text{em}} = 521 \text{ nm}$  (corresponding to the uranyl species)**

### **5.3.7 Calculation of the efficiency of energy transfer (optimum concentration for maximum energy transfer):**

In order to investigate the energy transfer efficiency, PL investigations were carried out on samples with varying europium concentration and a fixed uranium concentration. Figure 5.12 shows the emission spectra of co-doped samples where uranium concentration is fixed at 1 mol % and europium concentration is varied from 0.05 to 0.5 mol %.

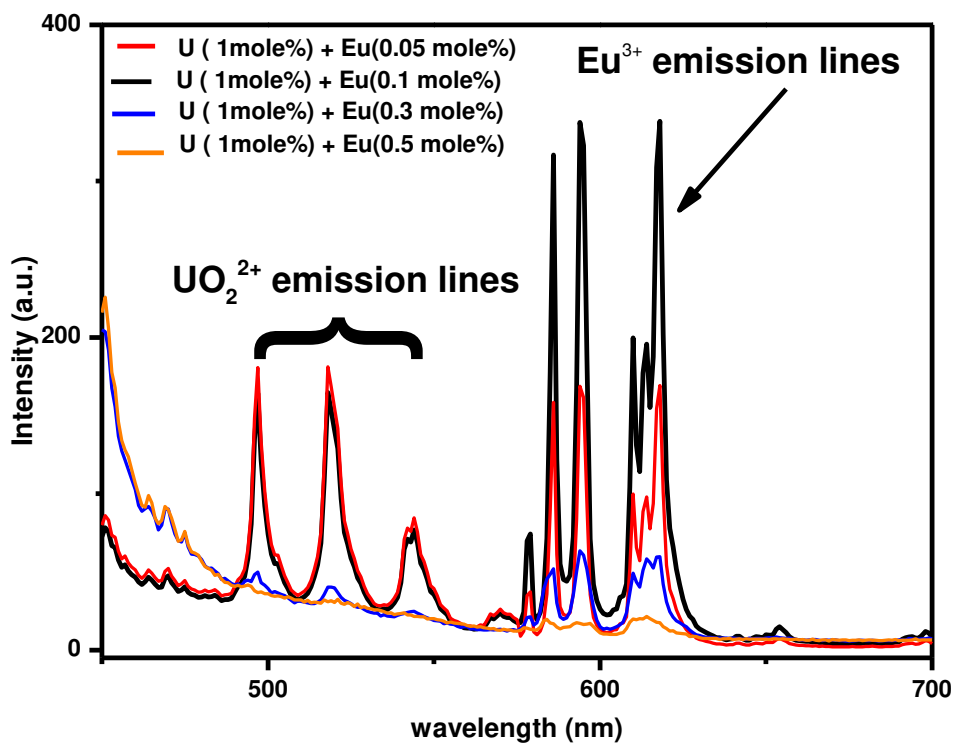


**Figure 5.12: PL emission spectra of SBP doped with U (1.0 mol %) with varying Europium concentration**

Upon excitation at 440 nm it is observed that the uranyl emission intensity decreases monotonously with the increasing europium concentration. Above 0.1 mol % of europium concentration, reduction in the  $\text{Eu}^{3+}$  emission intensity is also observed. This later phenomena can be ascribed to the concentration quenching mechanism (i.e. mutual

interaction between nearby europium ions). The above experimental results indicate that the optimum concentration of the respective dopant ions is uranyl 1 mol % and  $\text{Eu}^{3+}$  0.1 mol % for the maximum energy transfer. The efficiency for this energy transfer process ( $\eta_T$ ) can be calculated using the following expression [28].

$$\eta_T = 1 - (I_s / I_{so}) \quad (2)$$

Here  $I_s$  and  $I_{so}$  stand for the PL intensity of a sensitizer in the presence and absence of an activator, respectively. In the present system the uranyl is the sensitizer and the  $\text{Eu}^{3+}$  is the activator ion. Figure 5.13 shows the plot of ' $\eta_T$ ' as a function of  $\text{Eu}^{3+}$  concentrations. It is observed that  $\eta_T$  is increasing gradually with increasing  $\text{Eu}^{3+}$  concentration. The maximum energy transfer efficiency was observed to be ~ 80 % in the SBP *stillwellite* host.

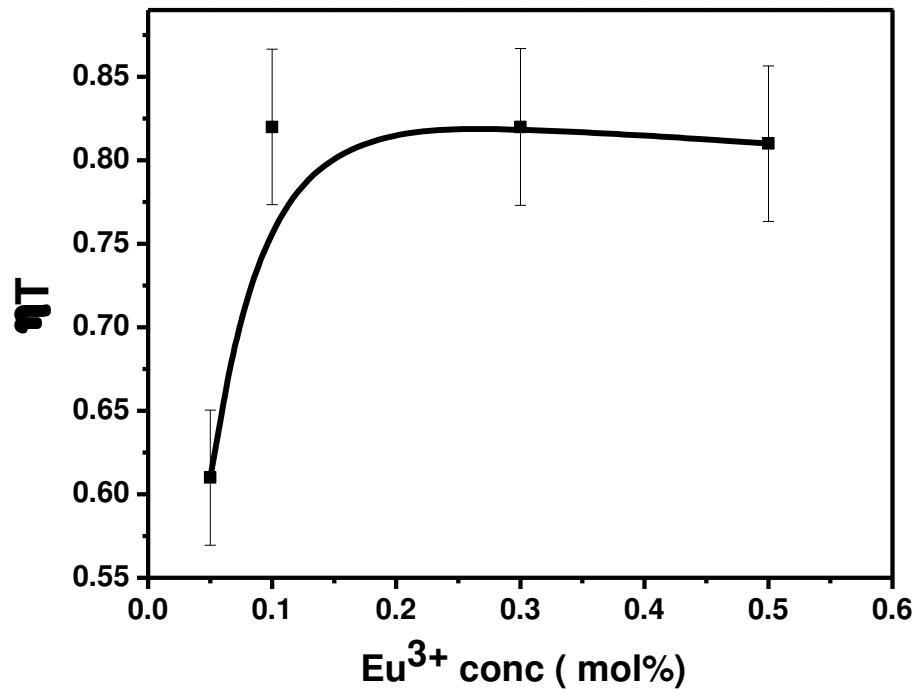


**Figure 5.13: Energy transfer efficiency ( $\eta_T$ ) of the SBP samples doped with  $\text{UO}_2^{2+}$  (1 mol %) and co-doped with varying  $\text{Eu}^{3+}$  concentration**

### 5.3.8 Mechanism for the energy transfer process:

The energy transfer mechanism follows mainly two major routes: one is the exchange interaction mechanism known as Dexter type and the other is the multi-polar interaction type or Froster resonance energy transfer (FRET) mechanism [29]. The distance between the donor and acceptor is always an important parameter in both the mechanisms. In case of FRET, the probability of energy transfer decreases at a rate of  $1/L^6$ . The critical distance ( $L_c$ ) for FRET is close to  $100\text{\AA}$ . In case of Dexter type energy transfer process the probability of energy transfer decreases as  $(\exp)^{-L}$  and here maximum typical distance is  $\leq 10\text{\AA}$ . According to Blasse, the critical distance  $R_{U-Eu}$  can be calculated using following equation [30].

$$R_{U-Eu} \approx 2[3V/4\pi XZ]^{1/3} \quad (3)$$

Here 'V' is the volume of the unit cell, 'X' is the number of uranyl and europium ions, and 'Z' is the number of formula units per unit cell. The value of X and V are obtained from XRD data. For the SBP host, the optimum concentration of uranyl and europium are estimated to be about 1 and 0.1 mol % respectively. The critical distance  $R_{U-Eu}$  is thus calculated to be  $6.9\text{\AA}$  which is shorter than  $10\text{\AA}$ , indicating that the energy transfer follows the exchange interaction mechanism. According Reisfeld's approximation, the following relations hold good for multipolar interaction in case of a Dexter type energy transfer mechanism [31].

$$(\eta_0 / \eta_s) \propto C_{U+Eu} \quad (4)$$

$$\text{and, } (\eta_0 / \eta_s) \propto C_{U+Eu}^{m/3} \quad (5)$$

Here  $\eta_0$  and  $\eta_s$  are the luminescence quantum efficiencies of uranyl in the absence and presence of Eu ion respectively. The values of  $\eta_0/\eta_s$  can be calculated approximately by the ratio of relative PL intensities ( $I_s/I_{s0}$ ); C is the sum of the concentration of uranyl and europium.

The relationship in equation 5 corresponds to the exchange interaction where  $n = 6, 8,$  and  $10$  for dipole - dipole (d-d), dipole - quadruple (d-q), and quadruple - quadruple (q-q) interactions, respectively [32]. Depending on the type of interaction one equation may show best fit for any given system.

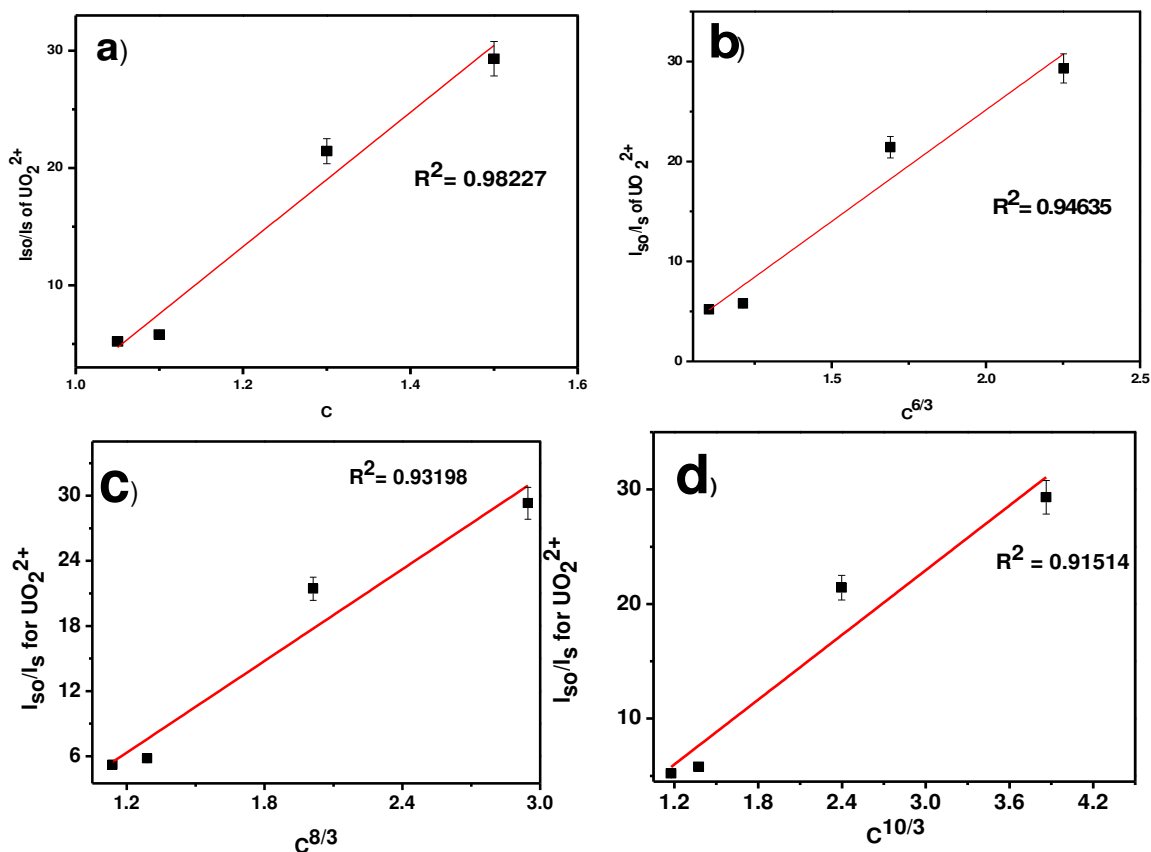


**Figure 5.14: Dependence of  $I_s/I_{s0}$  of uranyl on (a)  $C_{U+Eu}$ , (b)  $C^{6/3}_{U+Eu}$  (c)  $C^{8/3}_{U+Eu}$  and (d)  $C^{10/3}_{U+Eu}$**

The above relationships between ( $I_s/I_{so}$ ) and  $C$  were plotted using both equation 4 and 5. For equation 5, the possible values for ‘ $n$ ’ were taken as 6, 8 and 10 as shown in Figure 5.14(a) to Figure 5.14(d).

The linear relationship verified with the corresponding fitting factors  $R^2$  showed best fitting for  $\eta_0/\eta_s \propto C_{U+Eu}$  (with  $R^2 = 0.98227$ ) as shown in Figure 5.14(a). This implied that the energy transfer from  $U \rightarrow Eu$  takes place via the exchange interaction.

Based on the above discussions, the following schematic energy level diagram (Figure 5.15) can be proposed to illustrate this energy transfer process. Based on these experimental evidences, a suitable energy level scheme was proposed for both the energy transfer process.

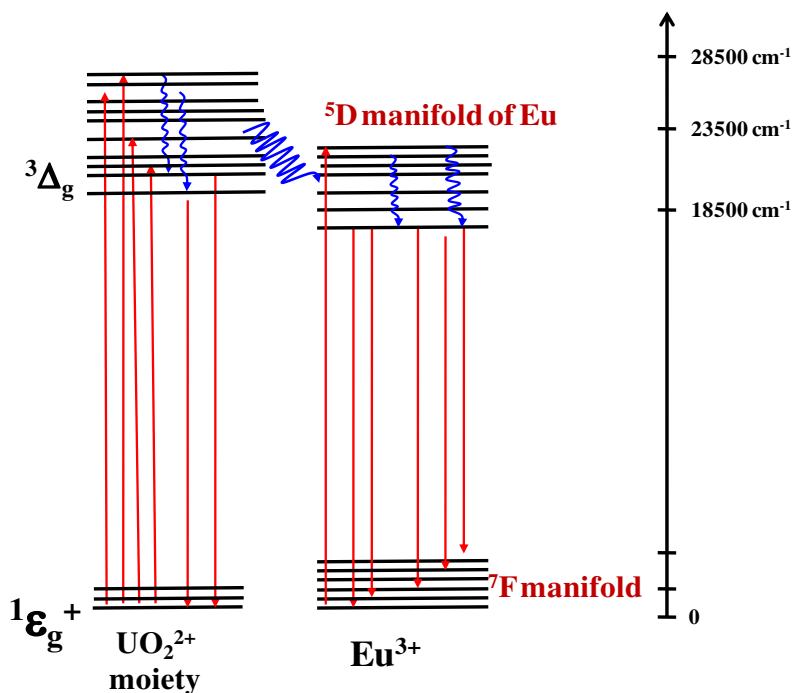


**Figure 5.15: A schematic energy level diagram explaining the energy transfer process from uranium ( $UO_2^{2+}$ ) to europium ( $Eu^{3+}$ ) in SBP host**

It was proposed that after excitation by photons, the uranate ions transfer their energy to nearby  $^5D_1$  level of  $Eu^{3+}$  ions which non-radiatively de-excites to the corresponding lower levels of  $^5D_0$ . Further this  $^5D_0$  level decays in a radiative mode to the  $^7F$  manifold giving the characteristic emission profile of trivalent Eu.

### 5.3.9 Understanding the energy transfer from uranium to samarium:

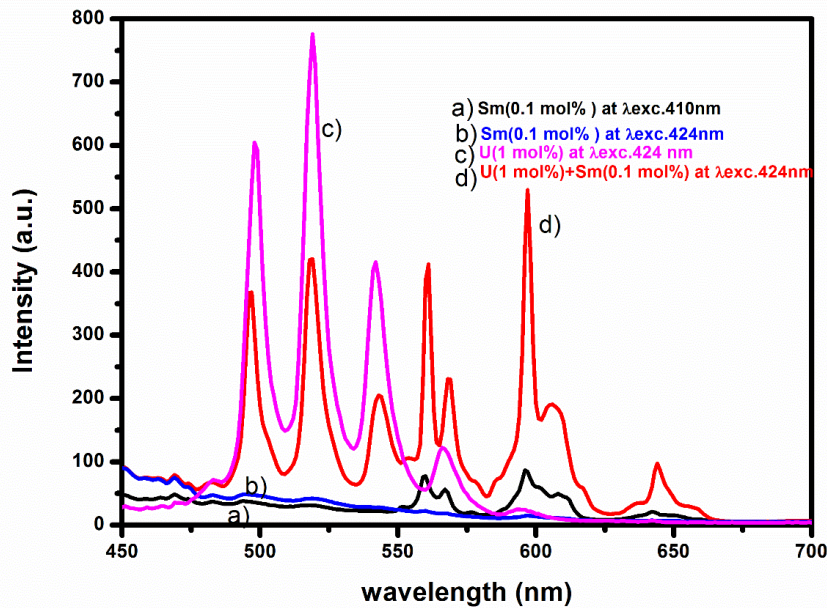


**Figure 5.16: PL emission spectra of U, Sm and U-Sm co-doped SBP at different  $\lambda_{ex}$**

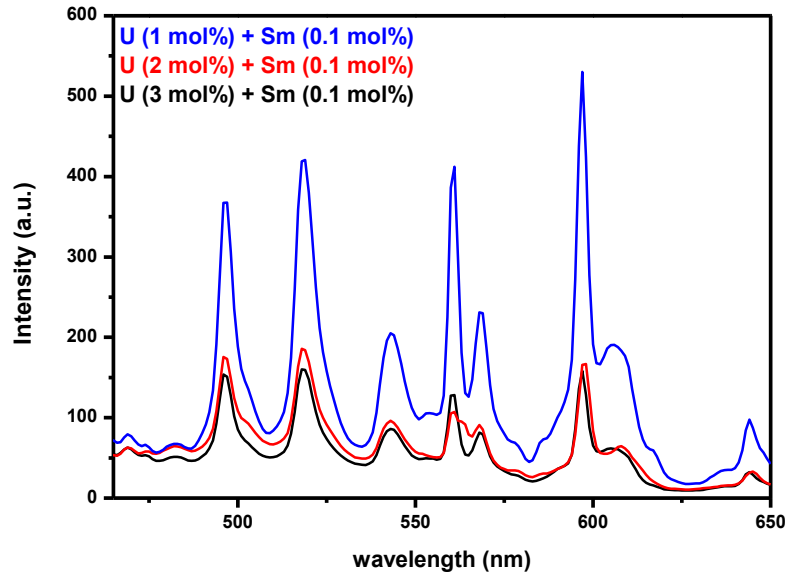
Fig. 5.16 the emission spectrum of the co-doped sample (U = 1 mol % and Sm = 0.1 mol %) with  $\lambda_{ex} = 424$  nm that corresponds to uranyl excitation. The corresponding emission spectra (with 424 nm excitation) for the single doped SBP samples (only Sm and U) are also shown in the figure for comparison under identical conditions.

Figure 5.16 (a) and (b) shows emission spectra of the Sm-SBP sample at both 410 and 424 nm respectively. . It is evident here that at uranium excitation wavelength (424

nm) Sm-SBP sample is not giving any emission whereas at 410 nm the Sm emission is due to its characteristic  ${}^6\text{H}_{5/2} \rightarrow {}^4\text{F}_{7/2}$  transition. Interestingly in the co-doped sample (figure x (d)), upon exciting at 424 nm, the emission due to  $\text{Sm}^{3+}$  enhances (~7 times) with a reduction in the  $\text{UO}_2^{2+}$  emission. It can be observed from the figure 5.16 (d) and 5.16 (a) that the emission from Sm ion is more in co-doped sample when excited through uranyl (at 424 nm) rather than direct excitation (at 410 nm due to  ${}^6\text{H}_{5/2} \rightarrow {}^4\text{F}_{7/2}$  transition). This clearly shows that the energy transfer process occur from  $\text{UO}_2^{2+}$  to  $\text{Sm}^{3+}$  efficiently and thus the excited state of  $\text{Sm}^{3+}$  gets more populated compared to that by direct excitation of  $\text{Sm}^{3+}$ .

To probe further, emission spectra were recorded at 424 nm excitation wavelength for the co-doped sample by varying uranium concentration (and keeping the  $\text{Sm}^{3+}$  concentration fixed at 0.1 mol %) as shown in figure 5.17. It can be observed from the spectra that upon increasing the uranium concentration the emission intensity of uranium decreases drastically. Although the samarium ion concentration is unchanged, but its emission intensity also decreases with increase in uranium concentration. This shows that at higher uranium concentration a concentration quenching phenomenon is taking place. Here the concentration quenching process is appeared to be dominating and it is difficult to investigate about energy transfer process from uranium to samarium unlike U (1 mol %) + Sm (0.1 mol %) doped SBP system. As it is known overlapping of the emission band of the donor and the excitation band of the acceptor is a necessary prerequisite for the energy transfer process to occur, in the present case the overlap between the uranyl ion emission and the samarium ion excitation (in the single doped SBP samples) is shown in figure 5.18. The figure shows a prominent zone i.e. centred at around 476 nm in Sm excitation range

that overlaps with the emission profile of uranium i.e. close to its zero phonon transition and thus it facilitates the energy transfer.



**Figure 5.17: PL emission spectra of Sm (fixed at 0.1 mol %) SBP co-doped with varying Uranium concentration at  $\lambda_{ex} = 424$  nm.**

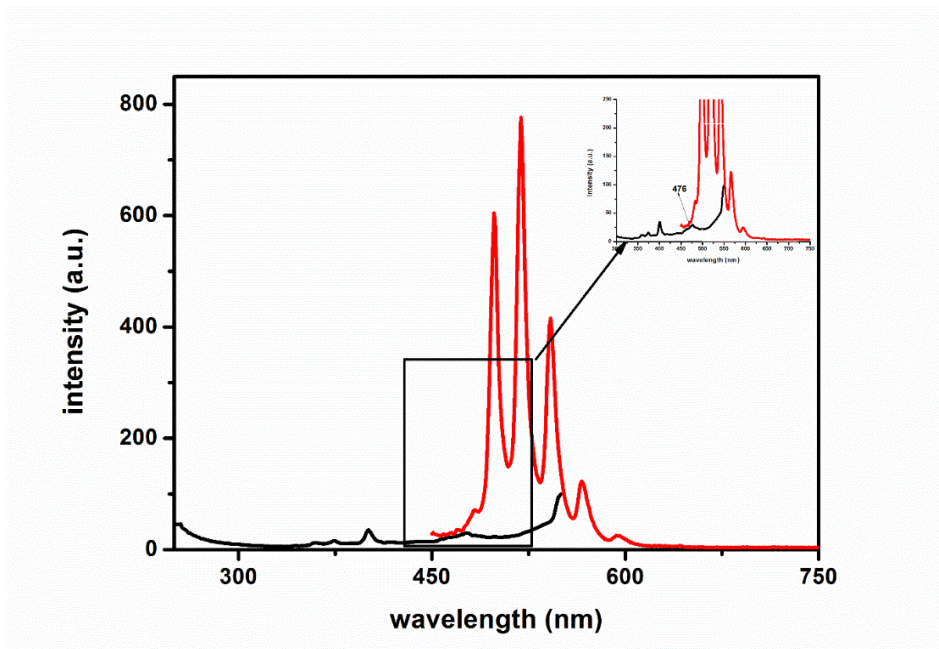


**Figure 5.18: Spectral overlap of a) excitation spectrum of SBP doped with  $\text{Sm}^{3+}$  (0.1 mol %) and b) emission spectrum of SBP doped with U (1 mol %)**

### 5.3.10 Calculation of the efficiency of energy transfer (optimum concentration for maximum energy transfer):

In order to investigate the energy transfer efficiency, PL investigations were carried out on samples with varying samarium concentration and a fixed uranium concentration. Figure 5.19 shows the emission spectra of co-doped samples where uranium concentration is fixed at 1 mol % and samarium concentration is at 0.3 mol %. It shows the effect of uranium as a sensitizer towards enhancement of emission intensity of samarium. Compared to Sm alone as well as SBP: U, Sm both excited at 401 nm, the emission intensity of Sm in SBP: U, Sm system excited at 424 nm is more and at the same time uranium in SBP: U, Sm systems excited at whether 401 or 424 nm shows a decreased emission intensity compared to SBP: U system, indicating possible energy transfer from uranium to samarium.

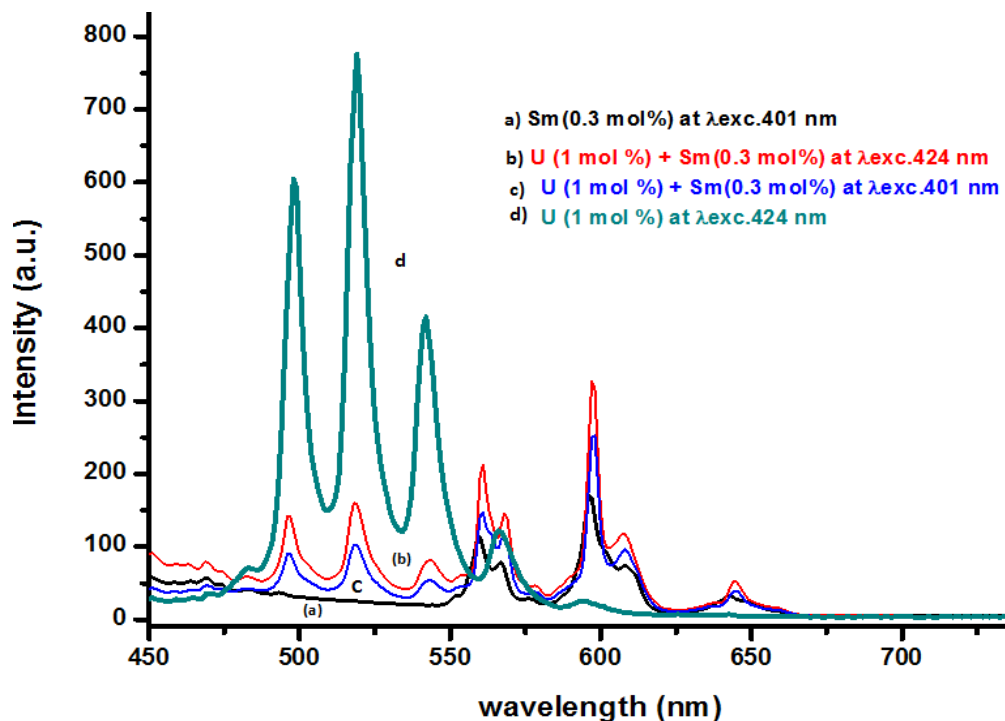


**Figure 5.19: Emission spectra of a) Sm (0.3 mol%) at  $\lambda_{exc}$ . 401 nm b) U (1 mol%) + Sm (0.3 mol%) at  $\lambda_{exc}$ . 424 nm c) U (1 mol%) + Sm (0.3 mol%) at  $\lambda_{exc}$ . 401 nm d) U (1 mol%) at  $\lambda_{exc}$ . 424 nm.**

Similarly we studied energy transfer phenomenon for SBP: U (1 mol%) + Sm (0.5 mol%) also. Fig. 5.20 shows the the emission spectra of co-doped samples where uranium concentration is fixed at 1 mol % and samarium concentration varies from 0.1 to 0.5 mol %. Upon excitation at 424 nm it is observed that the uranyl emission intensity decreases monotonously with the increasing samarium concentration. It implies that upon increase in acceptor concentration ( $\text{Sm}^{3+}$ ) more and more excited state energy of donor ion ( uranyl ion) is drained out. In this way uranyl donates or transfer energy non-radiatively to samarium and its emission intensity falls drastically. But at the same time although increased samarium concentration can withdraw more energy from uranium (fixed concentration at 1 mol %) but it is observed that above 0.1 mol % of samarium concentration, reduction in the  $\text{Sm}^{3+}$  emission intensity is observed.

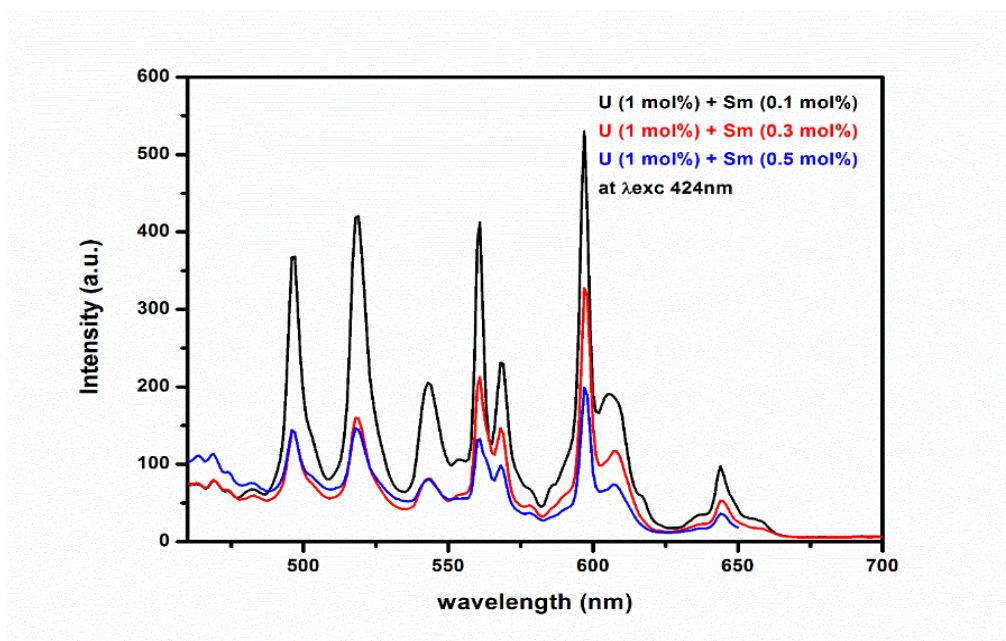


**Figure 5.20: Emission spectra of SBP: U, Sm at Constant U (1 mol%) varying Sm concentration from 0.1 mol% to 0.5 mol% at an excitation wavelength of 424 nm.**

This phenomena can be ascribed to the concentration quenching mechanism where a mutual interaction between nearby samarium ions may lead to decrease in emission intensity rather than enhancement. In this regard, SBP: U (1 mol%) , Sm (0.1 mol %) is an ideal combination where the energy transfer process as well as enhancement in Sm<sup>3+</sup> emission intensity is clearly observed. The efficiency for this energy transfer process ( $\eta_T$ ) can be calculated by using the expression

$$\eta_T = 1 - (I_s / I_{s0}) \text{ as discussed earlier [28].}$$

Here  $I_s$  and  $I_{s0}$  stand for the PL intensity of a sensitizer in the presence and absence of an activator, respectively. In the present system the uranyl is the sensitizer and the Sm<sup>3+</sup> is the activator ion. Figure 5.21 shows the plot of ' $\eta_T$ ' as a function of Sm<sup>3+</sup> concentrations. It is observed that  $\eta_T$  is increasing gradually up to 0.4 mol% with increasing Sm<sup>3+</sup> concentration. The maximum energy transfer efficiency was observed to be ~ 82 % in the SBP: U, Sm system.

As earlier discussed in SBP: U, Eu system (equation 3), here too we calculated the critical distance ( $L_c$ ) for SBP: U, Sm system. The ( $L_c$ ) was found to be 6.32 Å indicating the possible energy transfer process from uranium to samarium follows a Dexter type energy transfer process.

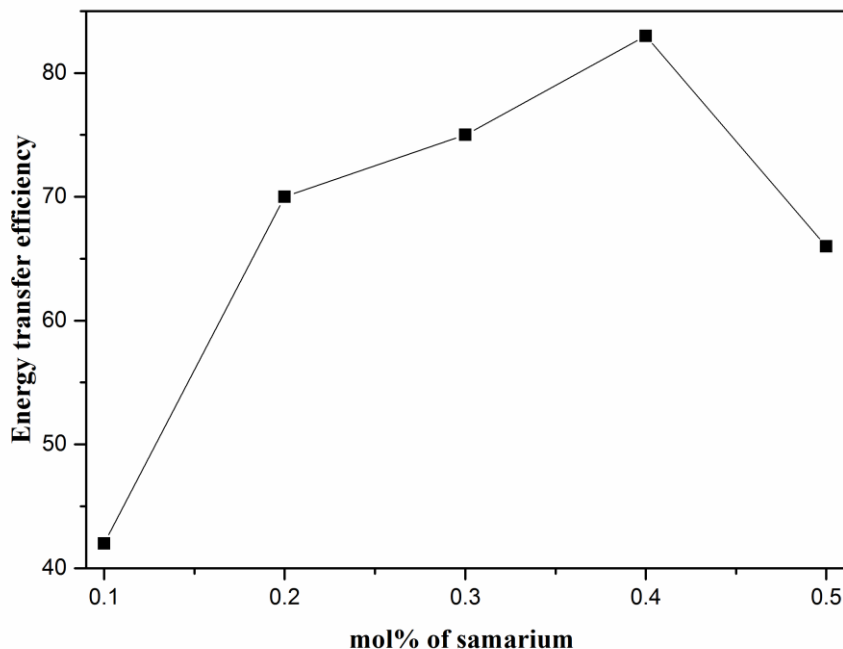


**Figure 5.21: Energy transfer efficiency vs mol% of Sm plot.**

### **5.3.11 PL decay time investigations:**

PL decay time studies were carried out on SBP: U, Sm systems to investigate more about the energy transfer process. Here the excitation wavelength was chosen to be 250 nm and emission at 596 nm for SBP: U, Sm systems in order to monitor life time of uranium. Fig 5.22 shows the life time decay curves of SBP: U, Sm systems. But interestingly at this wavelength set up the observed decay curve was a bi-exponential decay curve representing life time decay values of U as well as Sm. This is because at  $\sim 590$  nm both donor as well as acceptor ion emits. Life time decay values of Sm in SBP: Sm and SBP: U, Sm systems with 401 nm excitation and 596 nm emission were also measured. All this measurements are tabulated in Table 5.2.

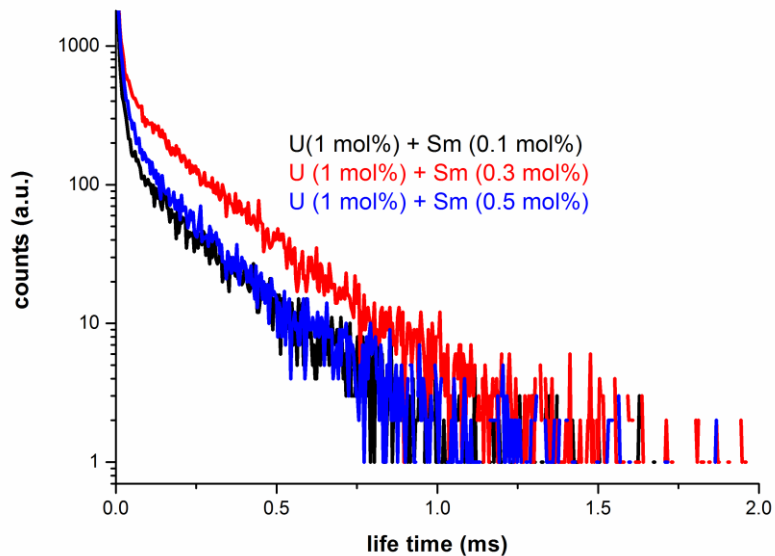


**Figure 5.22: Life time decay curves of SBP: U, Sm systems.**

**Table 5.2: Life time values of SBP: U, SBP: Sm and SBP: U, Sm systems:**

Sn	sample	Life time at 250	Life time at 401
1	u	224.59 $\mu$ s, 61.37 $\mu$ s	-
2	Sm(1)		2.4
3	U+Sm(0.1)	210 $\mu$ s, 1.99ms	2.1
4	U+sm(0.3)	181.93 $\mu$ s , 2.0ms	2.5
5	U+Sm(0.5)	86.95 $\mu$ s, 1.5ms	2.6

The life time decay studies have shown that as the Sm concentration increases the life time of U decreases (Figure 5.23). This could be attributed to increased acceptor (activator) ion concentration which facilitates a non-radiative energy loss from the excited state of

uranium. This non-radiative energy loss further facilitates energy transfer fluorescence enhancement of Sm.

Based on the above discussions, the following schematic energy level diagram (figure 5.24) can be proposed to illustrate this energy transfer process. Based on these experimental evidences, a suitable energy level scheme was proposed for both the energy transfer process. It was proposed that after excitation by photons, the uranyl ions transfer their energy to nearby  $^4G_{5/2}$  level of  $Sm^{3+}$  ions which non-radiatively de-excites to the corresponding lower levels of  $^4G_{5/2}$ . Further this  $^4G_{5/2}$  level decays in a radiative mode to the  $^6H$  manifold giving the characteristic emission profile of trivalent Sm.

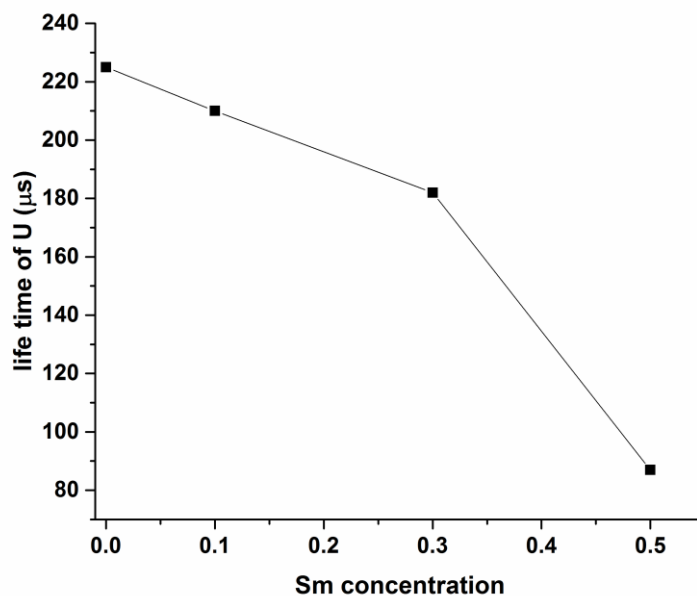


**Figure 5.23: Life time of Uranium with increased concentration of Samarium in SBP: U (1 mol %) + Sm (x mol %), x= 0.1, 0.3, 0.5**

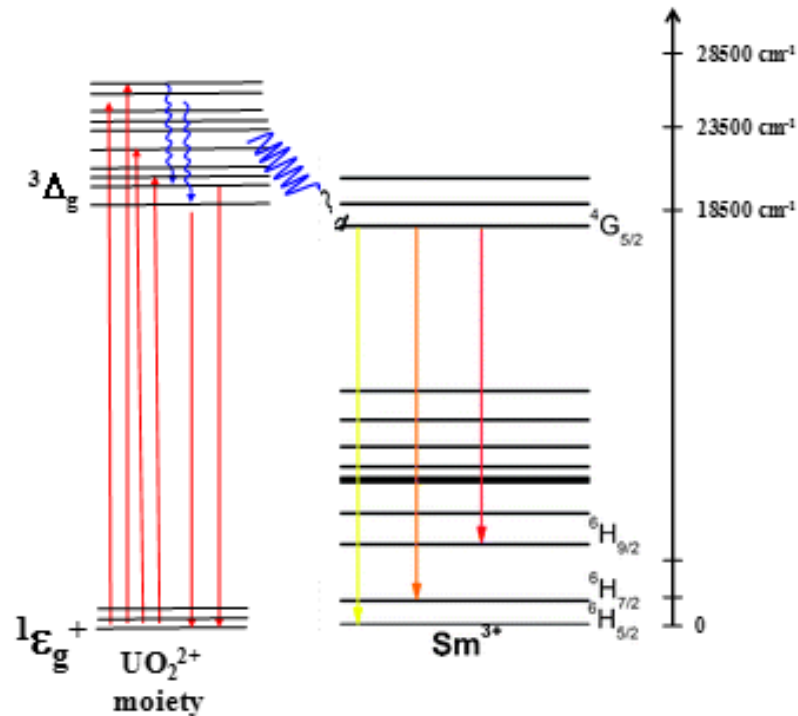


**Figure 5.24: A schematic energy level diagram explaining the energy transfer process from uranium ( $\text{UO}_2^{2+}$ ) to Samarium ( $\text{Sm}^{3+}$ ) in SBP host**

#### **5.4 Conclusion:**

In conclusion, it can be said that, PL excitation, emission and decay time investigations were carried out on U and Eu co-doped SBP as well as U and Sm co-doped SBP host prepared via solid state reaction route. The uranium ion was stabilised as uranyl whereas the Eu and Sm ion were stabilised in their respective 3+ states in the stillwellite host. In the co-doped systems, Uranyl ion was observed to be the donor whereas europium and samarium ions were observed to be acceptor ions. Optimum dopant ion concentrations were evaluated for maximising this energy transfer whose efficiency was calculated to be 80 % and 82% for SBP: U, Eu and SBP: U, Sm systems respectively.

## **5.5 References:**

1. G. Blasse, A.Brill, J.DeVries, J.Inorg. Nucl.Chem.31 (1969), 568.
2. H.B. Liang, Y. Tao, Q. Su, S.B.Wang, J. Solid State Chem. 167 (2002) 435.
3. A. Karthikeyan, R. Jagannathan, J. Lumin. 86 (2000), 79.
4. K. Sakasai, M. Katagiri, M. Matsubayashi, T. Nakamura, Y. Kondo, Nuc. Instrum. Meth. Phys. Res. A 529 (2004), 37.8
5. M.Mohapatra, M. Kumar, V.Natarajan and S.V.Godbole, Rad. Phys. Chem.,103(2014), 31-36.
6. H.B.Liang, Q.Su, Y.Tao, T.D.Hu, T.Liu, S.L.E.Shulin, J. Phys. Chem. Solids 63 (2002), 719-724.
7. Chung-Hsin Lu and S.V. Godbole, J. Mater. Res. 19 (2004), 2336-2342.
8. Mithlesh Kumar, R. M. Kadam, T. K. Seshagiri, V. Natarajan, A. G. Page, J.Radioanal.Nucl. Chem. 262 (2004), 633 – 637.
9. Bing Han, Jie Zhang, YinhuaLü, Yan Liu, Qiao Cui, Rus. J. Phys. Chem. A 88(2014), 143-148.
10. Mithlesh Kumar, T.K. Seshagiri, R.M. Kadam, S.V. Godbole, Mater Res. Bull. 46 (2011), 1359–1365.
11. Mithlesh Kumar, M. Mohapatra, V. Natarajan, Materials Research Bulletin 60 (2014), 858-863.
12. Koen Binnemans, Coordination Chemistry Reviews 295 (2015), 1–45.
13. J.L. Kropp, J. Chem. Phys. 46 (1967), 843.
14. B.D. Joshi, A.G.I. Dalvi, T.R. Bangia, J. Lumin. 10 (1975), 261-266.
15. S.P.Tanner, A.R.Vargenas, Inorg. Chem. 20(1981), 4384-86.

16. T. Yamamura, Z.Fazekas, M.Harada. H. Tomiyasu, *Phys. Chem. Chem.Phys.* 1 (1999), 3491-96.
17. M.M.Olken, C.M.Verschoor, A.B.Ellis, *Inorg. Chem.* 25 (1986), 80-82.
18. S. Dai, W.Xu, D.H.Metcalf, L.M.Toth, *Chem. Phys. Lett* 262 (1996), 315-320.
19. L.G. Deshazer, A.Y. Cabezas, *Proc. IEEE* 52 (1964), 1355.
20. Y.Okamoto, Y. Ueba, I. Nagata, E. Banks, *Macromol.* 14 (1981), 807-809.
21. M.V.Hoffman, *J. Electrochem. Soc.* 117 (1970), 227-232.
22. M. Kumar, M.Mohapatra, *Spectrochimica Acta Part A* 159 (2016), 42-47.
23. R. Reisfeld, N. Liebllich-Soffer, *J. Solid State Chem.*, 28 (3) (1979), 391-395.
24. K.E. Knope, D. T. de lill, C. E. Rowland et al., *Inorg. Chem.*, 51 (1) (2012), 201-206.
25. M. Mohapatra, Y.P.Naik, V.Natarajan, T.K.Seshagiri,S.V.Godbole, *Physica B*406 (2011), 1977–1982.
26. M.Mohapatra, V.Natarajan, *Journal of Radioanalytical and Nuclear Chemistry* 302 (2014), 1327-1332.
27. Annapurna Rout, M.Mohapatra, N.Suriyamurthy,B.S. Panigrahi, *J. Lumin.* 167 (2015), 45-50.
28. P.I. Paulose, G. Jose, V. Thomas, N.V. Unnikrishnan and M.K.R. Warriar, *J. Phys. Chem. Solids* 64 (2003), 841.
29. Dexter, D. L. *J. Chem. Phys.* 21 (1953), 836–850.
30. (a) Reisfeld, R.; Liebllich-Soffer, N. *J. Solid State Chem.* 28 (1979), 391–395;

- (b) Huang, C. H.; Chen, T. M. J. *Phys. Chem. C* 115 (2011), 2349–355.
31. Jia, Y. C.; Qiao, H.; Zheng, Y. H.; Guo, N.; You, H. P. *Phys. Chem. Chem. Phys.* 14 (2012), 3537–3542.
32. T. Smith, J. Guild, *Trans. Opt. Soc.* 33 (3) (1931), 73.
33. J. He, S. Zhang, J. Zhou et al., *Opt. Mater.*, 39 (2015), 81-85.
34. Q. Xu, D. Xu, J. Sun, *opt. Mater.*, 42 (2015), 210-214.

**Chapter 6A**  
**Luminescence approach on Speciation of  
uranium in Barium borate ( $\text{BaB}_2\text{O}_4$ )**



### **6A.1 Introduction:**

Borate based optical materials are of great interest. The main reason lies with its unique combination of large electronic band gap. In addition to this, strong nonlinear optical properties, chemical and environmental stability, mechanical robustness high transparency, exceptional optical damage threshold and low synthetic temperature also contribute towards its potential [1-5]. Recently number of borate based red-emitting luminescent materials were designed for WLEDs [6-9]. Rare earth doped  $BaB_2O_4$  were well investigated whereas there is a lack of literature support for actinide doped  $BaB_2O_4$  systems [10-12]. The present work is mainly focused on luminescence investigation of uranium when doped in  $BaB_2O_4$ .

### **6A.2 Experimental:**

The samples were prepared by a co-precipitation method. Barium nitrate hexahydrate ( $Ba(NO_3)_2 \cdot 6H_2O$ )(AR), Boric acid ( $H_3BO_3$ ), uranyl nitrate hexa hydrate ( $UO_2(NO_3)_2 \cdot 6H_2O$ ) were used as starting materials. Required amount of  $Ba(NO_3)_2 \cdot 6H_2O$  and Boric acid ( $H_3BO_3$ ) as per to the stoichiometric calculations were dissolved in de-ionized water, respectively. The required amount of ( $UO_2(NO_3)_2 \cdot 6H_2O$ ) solution was added into the  $Ba(NO_3)_2$  solution and mixed completely with continuous stirring. Then, aq solution of Boric acid was dropped in to the above mixture with a continuous magnetic stirring at  $50^\circ C$ . In this process precipitates were come out. After filtering, the precipitate was washed three times with 30 ml de-ionized water and subsequently dried in an oven at  $85^\circ C$  for 24 h. The samples were obtained after the powders were calcined at  $800^\circ C$  for 1h.

### 6A.3 Results and discussion:

#### 6A.3.1 Crystal structure:

Figure 6A.1 shows the PXRD pattern of undoped  $\text{BaB}_2\text{O}_4$ , uranium (0.5 mol %) doped  $\text{BaB}_2\text{O}_4$  and the standard reference one with ICDD file no- 24-0086. It was observed that PXRD patterns of synthesized undoped  $\text{BaB}_2\text{O}_4$  and uranium (0.5 mol %) doped  $\text{BaB}_2\text{O}_4$  dopant uranium closely resembles with the standard reference pattern of ICDD file no 24-0086 and the crystal structure come out to be monoclinic. The XRD pattern of uranium (0.5 mol %) doped  $\text{BaB}_2\text{O}_4$  is devoid of any additional peak and there is also no peak presenting impurities.

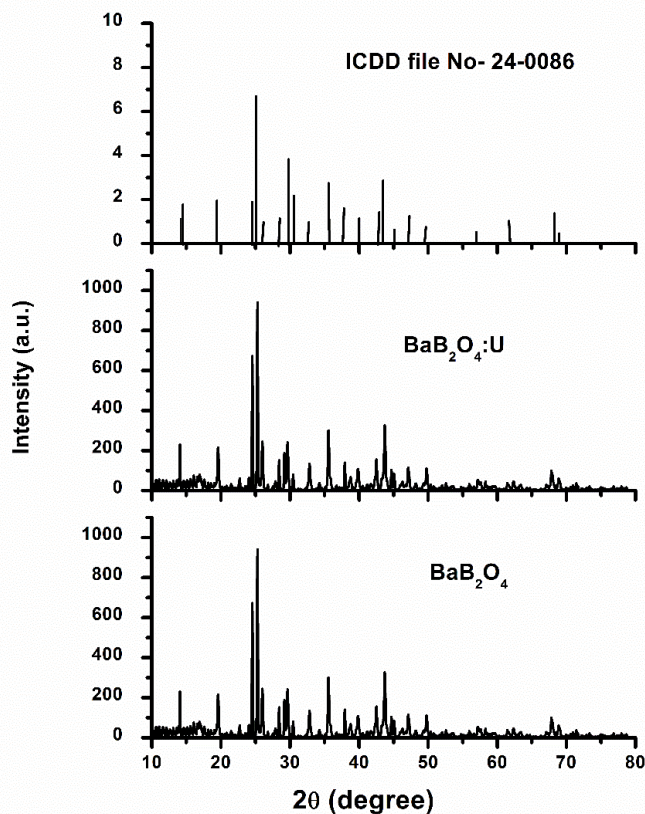


**Figure 6A.1: PXRD pattern of  $\text{BaB}_2\text{O}_4$ ,  $\text{BaB}_2\text{O}_4:\text{U}$ , standard  $\text{BaB}_2\text{O}_4$**

### 6A.3.2 Morphology:

Figure 6A.2 shows the SEM data for the BaB<sub>2</sub>O<sub>4</sub>: U synthesized via co-precipitation route. The figure shows an inhomogeneous size distribution and agglomeration of the particles in the BaB<sub>2</sub>O<sub>4</sub> system. The overall particle size for the system was found to be less than 1 μm based on the statistical analysis from several micrographs. The uneven shape of the particles observed in this case was due to the synthesis procedure.

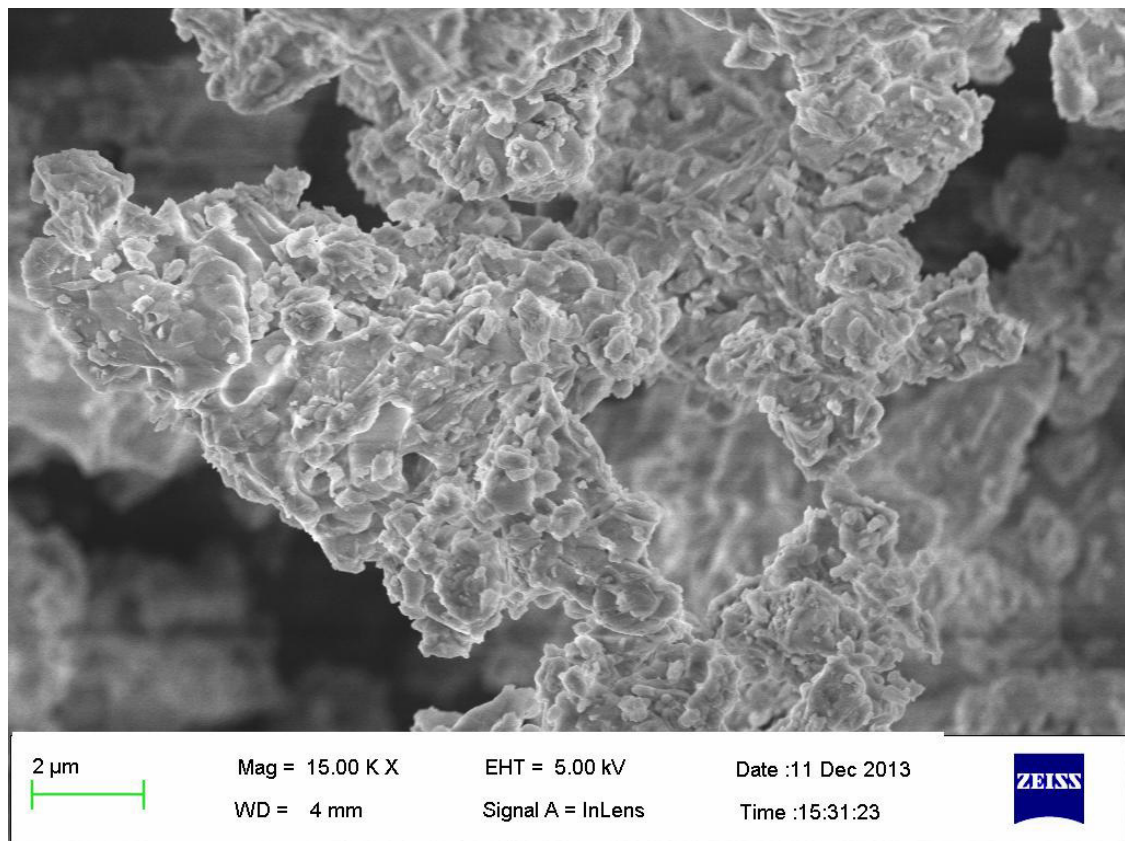


**Figure 6A.2: SEM image of BaB<sub>2</sub>O<sub>4</sub>: U system, synthesized via co-precipitation route**

### 6A.3.3 Photo luminescence (pl) investigation:

Figure 6A.3 represents the pl emission of BaB<sub>2</sub>O<sub>4</sub>: U at an excitation wavelength of 353nm. The broad spectrum revealed the superposition of strong emission peak at 550 nm and lower intensity bands at 533 nm. A small hump was also seen at 570 nm. Generally, the first emission peak of a U (VI) species is termed as the zero phonon (zp) line, that is originated by  $\Gamma_g \rightarrow \Sigma_g^+$  electron transfer transition.

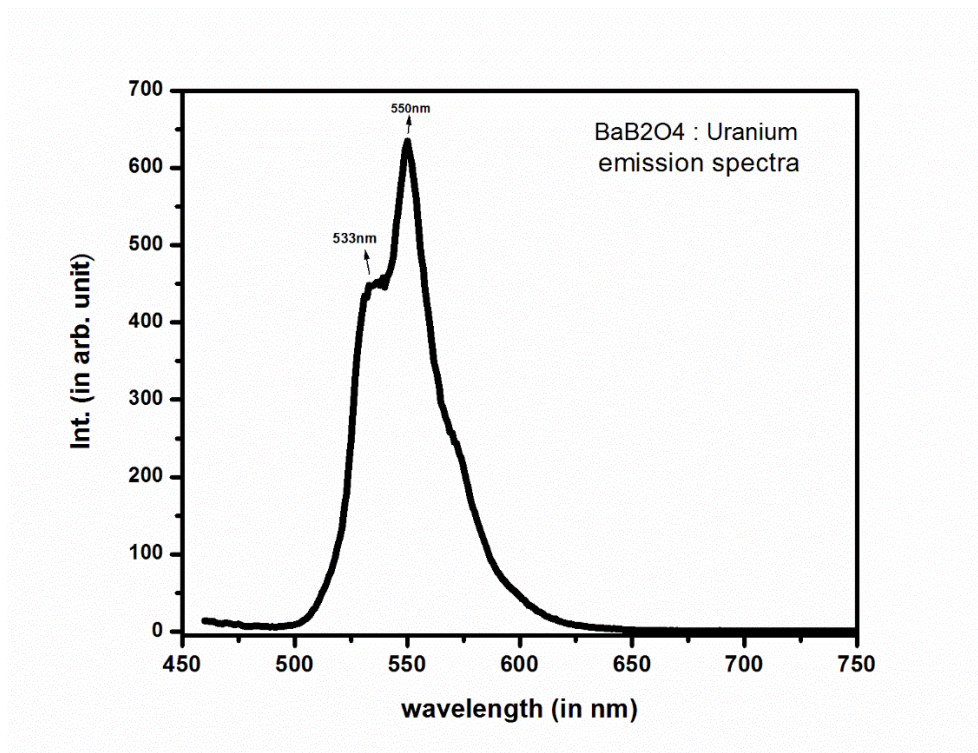
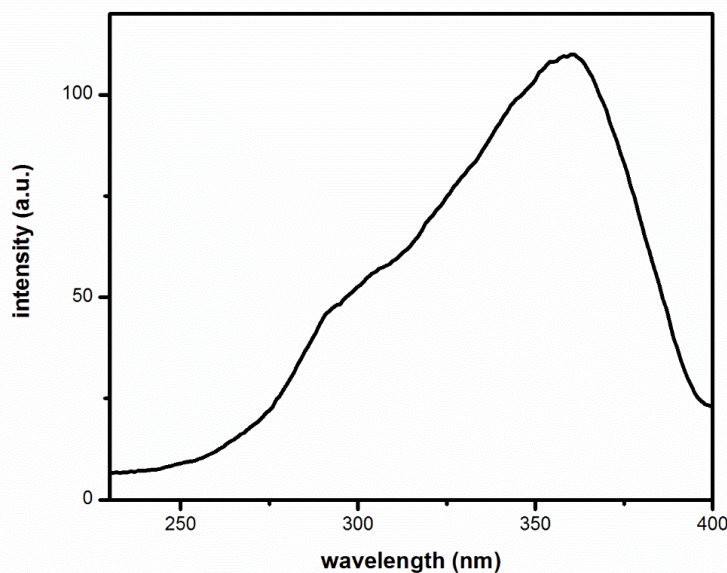


**Figure 6A.3: PL emission spectra of BaB<sub>2</sub>O<sub>4</sub>: U**

In crystalline materials, the position of the zp line normally varies from 520 to 470 nm. In the present case, the observed band starts at 500 nm. This strongly indicates that the equatorial coordination is in between 4 and 7. It is usually observed that, for uranyl species, the zp line ( $t_0$ ) is strongest peak, but for uranates, the  $t_1$  or in some case, the  $t_2$  is the most intense peak. In the present case, as it can be seen, the  $t_1$  peak is more intense. Further, the

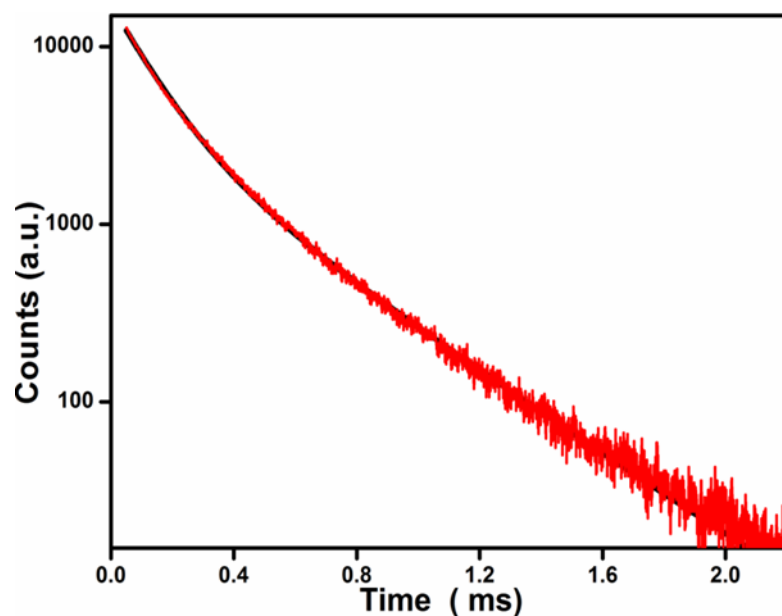
vibronic couplings, which are usually more prominent in case of uranyl species, are not clearly observed. The emission spectrum observed here also closely resembles that of uranates ( $\text{UO}_6^{6-}$ ) as reported in many literatures [13-15]. Here the emission spectrum is originated as electron transitions from orbitals derived primarily from oxygen (2p) to uranium (6d) orbitals. The transitions are thus parity allowed, but not necessarily electric dipole allowed.

Figure 6A.4 represents the pl excitation spectrum of  $\text{BaB}_2\text{O}_4:\text{U}$ . The broad excitation spectrum ranges from 250 nm to 400 nm with a maximum at 360 nm and also a small hump shape excitation at 290 nm. . Here, the excitation spectrum is a typical charge transfer transitions from oxygen (2p) to uranium (6d) orbitals. The excitation band at higher wavelength (360 nm) range can be assigned to ground state electronic transition of hexavalent uranium [16].



**Figure 6A.4: PL excitation spectra of  $\text{BaB}_2\text{O}_4:\text{U}$**

Figure 6A.5 shows the life time decay of BaB<sub>2</sub>O<sub>4</sub>: U. The PL decay curves were fitted using bi-exponential equation:  $I(t) = A_1 \exp(-t/\tau_1) + A_2 \exp(-t/\tau_2) + y_0$  where  $I(t)$  stands for intensity,  $A_1$  and  $A_2$  are scalar quantities known as pre-exponential factors, 't' is the time of measurement and  $\tau_1$  and  $\tau_2$  are emission decay times. The decay time values come out to be 6.9  $\mu$ s with  $\chi^2 = 1.058$ . The reported life time appears to be shorter as expected in the case of octahedral uranates [17]. This can be attributed to the local symmetry of uranium in BaB<sub>2</sub>O<sub>4</sub> matrix. At present host matrix there may be an asymmetric site symmetry surrounding the uranium ion and this asymmetric environment facilitates the electron transition selection rules to be relaxed and thus the forbidden transitions become partially allowed and transitions happen with shorter life time.



**Figure 6A.5: Photoluminescence decay profile of BaB<sub>2</sub>O<sub>4</sub>: U at  $\lambda_{exc} = 360$  nm**

#### 6A.3.4 Evaluation of color coordinates:

Color coordinates for BaB<sub>2</sub>O<sub>4</sub>: U was evaluated adopting standard procedure [18]. The CIE (Commission Internationale de l'éclairage) chromaticity coordinates are useful to determine a light emitting materials performance on color luminescent emission. A (x, y) co-ordinate in the color space determines the color of any light source. The spectral power distribution (SPD) of the light source and the CIE color matching functions are the required parameters to determine the (x, y) coordinate. The chromaticity coordinates x, y, z can be obtained from tristimulus value X, Y and Z as follows:

$$x = X/X+Y+Z, y = Y/X+Y+Z \text{ and } z = Z/X+Y+Z$$

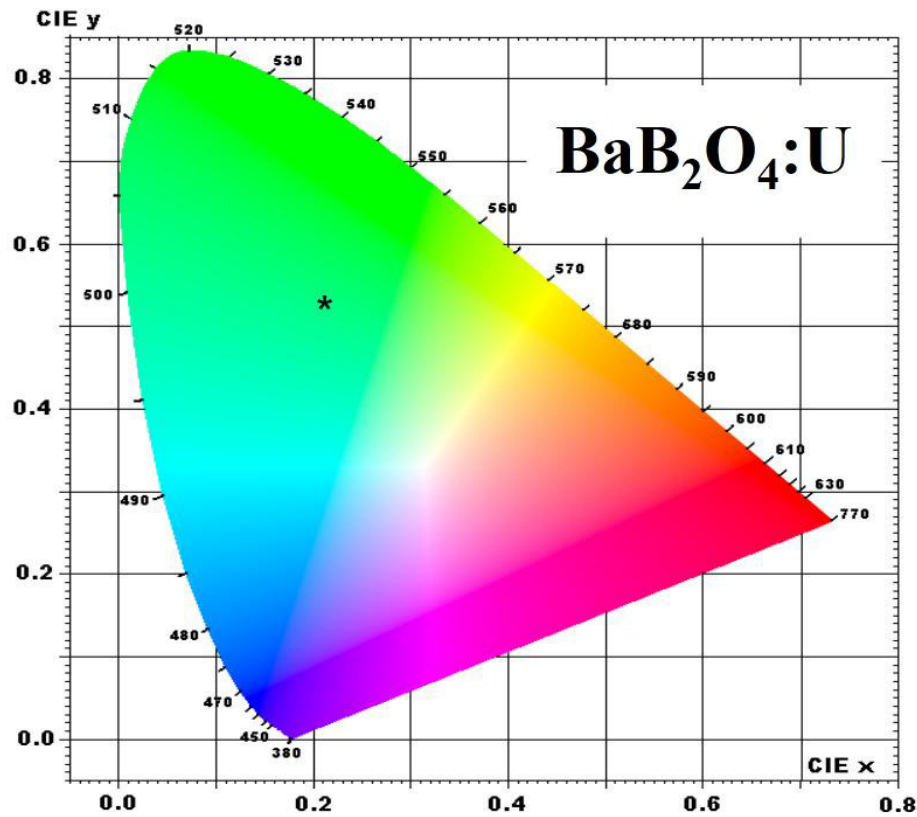


Figure 6A.6: CIE chromaticity diagram for the BaB<sub>2</sub>O<sub>4</sub>: U system, the coordinates are demarked by an asterisk

The predominating wavelength from a light source is evaluated using CIE chromaticity diagram. This wavelength is an interception point of a straight line drawn from one of the CIE white illuminants, through the (x, y) coordinates up to the extent, where it touches the outer locus of points along the spectral edge of the 1931 CIE chromatic diagram. In BaB<sub>2</sub>O<sub>4</sub>: U the calculated values of x and y coordinates were found to be 0.228 and 0.521 respectively indicated as an asterisk mark (\*) in the figure 6A.6. The CIE index values show that the present compound is a 'Green' emitting phosphor.

#### **6A.4 Conclusion:**

Uranium doped BaB<sub>2</sub>O<sub>4</sub> samples were prepared via co-precipitation route. XRD studies confirmed the formation of single phase upon doping of uranium in to BaB<sub>2</sub>O<sub>4</sub> matrix. SEM studies indicated the presence of uneven, agglomerated particles with less than 1 μm individual particle size. PL studies confirmed the stabilisation of uranium as UO<sub>6</sub><sup>6-</sup> in the system. The life time decay studies revealed a shorter single life time value, indicating asymmetric site symmetry surrounding the uranium ion in BaB<sub>2</sub>O<sub>4</sub>. The CIE indices for this system suggested that the material is a potential green emitting phosphor.

#### **6A.5 References:**

1. E.V. Koporulina, N.I. Leonyuk, D. Hansen, J. Cryst. Growth, 191 (1998), 767.
2. N. Liu, D. Zhao, L. Yu, K. Zheng, W. Qin, Colloid Surf., A 363 (1–3) (2010), 124–129.
3. F. Lucas, S. Jaulumes, M. Quattron, J. Solid State Chem., 150 (2000), 404.
4. Q.R. Zhao, X. Zhu, X. Bai, H.H. Fan, Y. Xie, Eur. J. Inorg. Chem., 13 (2007), 1829–1834.

5. S.T. Durmanov, O.V. Kuzmin, G.M. Kuzmicheva, *Opt. Mater.*, 18 (2001), 243.
6. F. Yang, Y. Liang, M. Liu, X. Li, M. Zhang, N. Wang, *Opt. Laser Technol.*, 46 (2013), 14–19.
7. R. Zhang, X. Wang, *J. Alloys Compd.*, 509 (2011), 1197–1200.
8. W.R. Liu, C.C. Lin, Y.C. Chiu, Y.T. Yeh, S.M. Jang, R.S. Liu, *Opt. Express*, 18 (2010), 2946–2951.
9. W.B. Dai, S. Ye, E.L. Li, P.Z. Zhuo, Q.Y. Zhang, *J. Mater. Chem.*, C 3 (31) (2015), 8132–8141.
10. X. Feng, A. Tang, H. Huang, *Optik - International Journal for Light and Electron Optics*, 172 (2018), 714–720.
11. J. Liu, X. Wang, Z. Wu, S. Kuang, *Spectrochimica Acta Part A*, 79 (2011), 1520–1523.
12. W. G. Zou, M. Lu, F. Gu, Z. Xiu, S. Wang, G. Zhou, *Optical Materials*, 28 (2006), 988–991.
13. P.A. Tanner, P.Z. Wu, L. Jun, L. Yulong, S. Qiang, *J. Phys. Chem. Solids*, 58 (1997), 1143–1146.
14. K.C. Bleijenberg, *Struct. Bond.*, 42 (1980), 97–128.
15. G. Blasse, K.C. Bleijenberg, D.M. Krol, *J. Lumin.*, 18 (19) (1979), 57–62.
16. J. Th. W. De Hair, and G. Blasse, “Luminescence of the Octahedral Uranate Group,” *J. Lumin.*, 14 (1976), 307–323.
17. J. Vandenborre, R. Drot, E. Simoni, *Inorg. Chem.*, 46 (2007), 291–296.
18. T Smith, J Guild, *Trans. Opt. Soc.*, 33 (3) (1931–32), 73–134.



**Chapter 6B**  
**Investigation of Photo luminescence and site  
occupancy of uranium in  $\text{BaAl}_2\text{B}_2\text{O}_7$**



### **6B.1 Introduction:**

Recently, alkaline-earth aluminium borates have gained much attention owing to its potential in designing efficient luminescent materials [1, 2]. Emergence of this material is associated with its low synthesis temperature, high UV transparency, high luminescence brightness, good thermal stability and also non-linear optical properties that make the material useful for application in plasma display panels (PDPs), UV devices and non-linear optical materials [3, 4, 5]. This matrix is well known as an ideal host to several rare earths and contributes towards developing WLED (white light emitting diodes) materials [6, 7, 8, 9]. Among the alkaline-earth aluminium borates,  $\text{BaAl}_2\text{B}_2\text{O}_7$  has evolved as a potential phosphor material. The most fascinating about Alkaline-earth aluminum borate ( $\text{BaAl}_2\text{B}_2\text{O}_7$ ) being a host is its crystal structure that was first described by Hubner and latter it was studied in details by Ye et al. [10, 11]. The whole structure of  $\text{BaAl}_2\text{B}_2\text{O}_7$  resembles to be rhombohedral where the Ba ions are sandwiched between layers consisted of  $\text{AlO}_4$  tetrahedra and  $\text{BO}_3$  triangles in large cavities formed by six oxygen atoms at the vertices of an octahedron and six more distant oxygen atoms also with an octahedral arrangement. The well occupied Ba ion sites seem to be ideal host sites for many guest ions. Pekgozlu et al. have reported blue emission from  $\text{Pb}^{2+}$  doped  $\text{BaAl}_2\text{B}_2\text{O}_7$  [12]. Camardello et al. have studied optical spectroscopy, thermal quenching and electron-vibrational interaction of  $\text{BaAl}_2\text{B}_2\text{O}_7: \text{Eu}^{2+}$  [13]. Recently, an abnormal reduction of  $\text{Eu}^{3+}$  to  $\text{Eu}^{2+}$  in oxidizing environment under UV excitation is also observed in  $\text{BaAl}_2\text{B}_2\text{O}_7$  matrix [5]. However, incorporation of actinides in alkaline-earth aluminum borate lacks literature support. At present, solid host matrices doped with uranium are being studied in order to

investigate suitable matrices for long term storage of radioactive waste [14-19]. Although many works has been carried out on uranium doped borates but uranium doped alkaline-earth aluminum borate is still an untouched one [20-22]. In the present investigation, luminescence of uranium in  $\text{BaAl}_2\text{B}_2\text{O}_7$  host matrix has been carried out. As it is known that solubility and site occupancy of uranium in solid matrices, being a heavy metal ion is always challenging so it is interesting to study  $\text{BaAl}_2\text{B}_2\text{O}_7 : \text{U}$  system. Uranium shows various oxidation states i.e. from trivalent to hexavalent and interestingly each of these state shows their characteristic optical spectroscopic properties [23-29]. The uranium in hexavalent state appears in different forms such as  $\text{UO}_4^{2-}$ ,  $\text{UO}_6^{6-}$  or  $\text{UO}_2^{2+}$ . So, the form of stabilization or speciation is also an important factor for investigation and towards this end luminescence technique is very useful. The present study is intended to probe  $\text{BaAl}_2\text{B}_2\text{O}_7 : \text{U}$  system and extract information regarding speciation of uranium, its photophysical properties as well as its site occupancy in  $\text{BaAl}_2\text{B}_2\text{O}_7$  host matrix.

### **6B.2. Experimental:**

The uranium doped and undoped samples were prepared via solution combustion technique. All the chemicals used were of Analytical Reagent (AR) grade. Stoichiometric proportions of  $\text{Ba}(\text{NO}_3)_2$ ,  $\text{Al}(\text{NO}_3)_3 \cdot 9\text{H}_2\text{O}$ ,  $\text{H}_3\text{BO}_3$  (5 mol % excess), and  $\text{UO}_2(\text{NO}_3)_2 \cdot 6\text{H}_2\text{O}$  were ground together thoroughly in an Agate Mortar, adding little amount of double distilled water to obtain an aqueous homogeneous solution. In the first phase, the aqueous solution was transferred into a china basin and slowly heated at lower temperature of  $70^\circ\text{C}$  in order to remove the excess water. The heated solution is known as precursor solution. Then the precursor solution was introduced into a preheated muffle furnace maintained at

600°C. The solution boils and foams appears and suddenly it ignites to burn with flame and finally a voluminous, foamy precursor powder was obtained. The whole combustion process was over in about 5 min. The well-mixed precursor powders were pressed into pellets. The pellets were then placed in an alumina crucible and heated in a muffle furnace for 3 hrs at 900°C in air and quenched to room temperature.

The crystal Structure and phase purity of the prepared powders were examined through powder X-ray diffraction using a Philips diffractometer (model PW 1071) operating with monochromatic  $\text{CuK}_\alpha$  ( $\lambda = 1.5418\text{\AA}$ ) radiation. Photo luminescence (PL) excitation and emission measurements were made using a Shimadzu RF 5301pc spectrofluorimeter with 150W CW (continuous wave) xenon lamp as the excitation source. A long-wavelength-pass filter (UV-35, Shimadzu), with a maximum and uniform transmittance (more than 85%) above 350 nm, was placed in front of the emission monochromator in order to reduce the scatter of the incident beam into the emission monochromator. In the RF 5301pc spectrofluorimeter, the gain of the photometric photomultiplier tube is dynamically adjusted to correct for the changes in the Xe lamp output intensity using a monitoring photomultiplier. The PL decay time measurements were carried out using an Edinburgh FLS-900 time resolved fluorescence spectrometer at room temperature.

X-ray absorption (XAS) measurements, which include both X-ray near edge structure (XANES) and Extended X-ray absorption fine structure (EXAFS) measurements, have been done on the U doped  $\text{BaAl}_2\text{B}_2\text{O}_7$  sample at Ba and U  $L_3$  edge at the Energy Scanning EXAFS Beamline (BL-9) at the Indus-2 Synchrotron Source (2.5 GeV, 200 mA) at the Raja

Ramanna Centre for Advanced Technology (RRCAT), Indore, India. The details of the beam line is given elsewhere [30, 31].

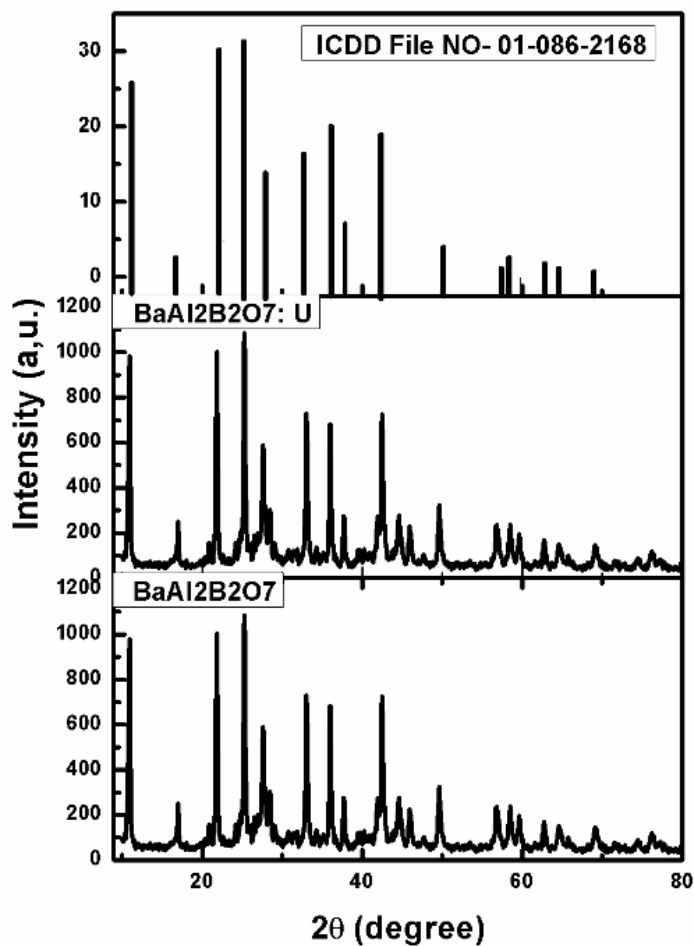
EXAFS measurement at U L<sub>3</sub> edge has been carried out in the fluorescence mode, the sample was placed at 45° to the incident X-ray beam and the fluorescence signal ( $I_f$ ) is detected using a Si drift detector placed at 90° to the incident beam. An ionization chamber placed prior to the sample measures the incident beam ( $I_0$ ) and in this case the X-ray absorption co-efficient of the sample is determined by  $\mu = I_f / I_0$ . EXAFS measurements at Ba L<sub>3</sub> edge, on the other hand, have been done in transmission mode where the sample is placed between two ionisation chamber detectors. The first ionization chamber measures the incident flux ( $I_0$ ) and the second ionization chamber measures the transmitted intensity

( $I_t$ ) and the absorbance of the sample is obtained as ( $\mu = \exp(-\frac{I_t}{I_0})$ ).

### **6B.3 Results and discussion:**

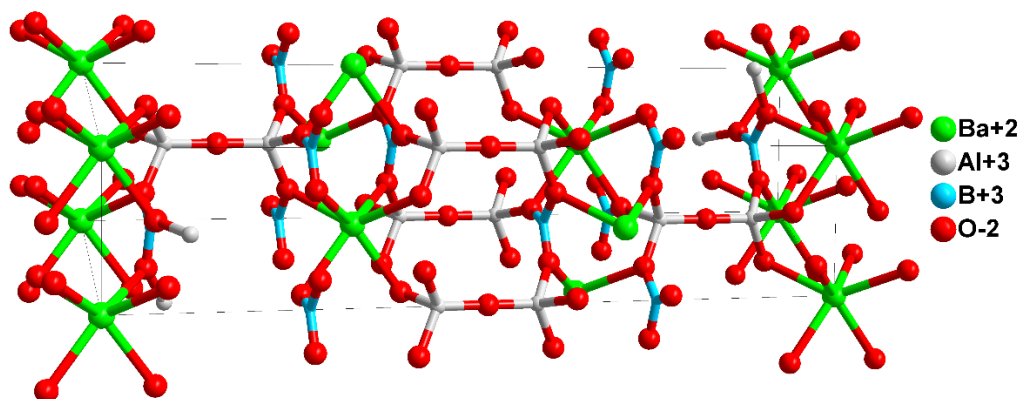
#### **6B.3.1 Crystal structure and morphology:**

Figure 6B.1 represents the powder X-ray diffraction (XRD) patterns of uranium doped and undoped BaAl<sub>2</sub>B<sub>2</sub>O<sub>7</sub>. The XRD patterns are in good agreement with the standard data in JCPDS file no. 01-086-2168. BaAl<sub>2</sub>B<sub>2</sub>O<sub>7</sub> matrix shows rhombohedral crystal structure and it has been observed that, incorporation of uranium does not disturb the original structure. The BaAl<sub>2</sub>B<sub>2</sub>O<sub>7</sub> system is composed of BO<sub>3</sub> triangles, BaO<sub>6</sub> octahedra and AlO<sub>4</sub> tetrahedra units (Figure 6B.2).



**Figure 6B.1: XRD patterns of undoped and uranium doped BaAl<sub>2</sub>B<sub>2</sub>O<sub>7</sub> with a reference of standard ICDD 86-2168 pattern.**

The independent triangular BO<sub>3</sub> ions are connected alternatively by Al–O–Al bridges and Ba atoms resulting in a rigid framework of corner-shared AlO<sub>4</sub> tetrahedra and BO<sub>3</sub> triangles. In present case, the uranium doped host lattice has two possible regular lattice sites i.e. Ba<sup>2+</sup> and Al<sup>3+</sup> for incorporation of uranium. The ionic radius of hexavalent uranium (0.87 Å) is greater than the ionic radius of Al<sup>3+</sup> (0.51 Å) but less than that of Ba<sup>2+</sup> (1.34 Å). Therefore, it is interesting to probe the site occupancy of uranium in BaAl<sub>2</sub>B<sub>2</sub>O<sub>7</sub>.



**Figure 6B.2: Schematic presentation of crystal structure of BaAl<sub>2</sub>B<sub>2</sub>O<sub>7</sub> system**

### **6B.3.2 PL investigations:**

Uranium (1mol %) doped BaAl<sub>2</sub>B<sub>2</sub>O<sub>7</sub> shows a broad emission spectrum (Figure 6B.3). The emission spectrum ranges from 475 to 650 nm with a maximum at 550 nm upon excitation at wavelength of 285nm. Here the range of emission wavelength indicates the absence of U (III), U (IV) and U (V) form of uranium. It is because the emission maxima of U (III), U (IV) and U (V) are known to appear at higher wavelength regions than observed in the present case [24-26, 28]. So, the next possibility indicates towards U (VI) emission. In case of stabilization as U (VI), there are possibilities that uranium may get stabilized as uranyl group (UO<sub>2</sub><sup>2+</sup>), tetrahedral (UO<sub>4</sub><sup>2-</sup>) or octahedral uranium groups (UO<sub>6</sub><sup>6-</sup>, and U<sup>6+</sup> and UO<sub>9</sub><sup>12-</sup>). The observed emission profile corresponds to green emission thus presence of uranium in the form of tetrahedral (UO<sub>4</sub><sup>2-</sup>) group, that emits in red region is not valid [32, 33]. The probability of presence of uranyl form also fades away as the broad emission spectra of BaAl<sub>2</sub>B<sub>2</sub>O<sub>7</sub>: U is a structure less one i.e. devoid of vibronic progression lines. In uranyl the equidistant vibronic progressions are originating from strong coupling of the

ground state Raman active symmetric vibrational ( $\nu_1$ ) mode with the  $3\pi_u$  electronic excited state. In addition to this the zero point line i.e. the electron transfer transition from oxygen to one of the non-bonding uranium orbital ( $\pi_g \rightarrow \Sigma_g^+$ ) is a prominent marker for uranyl emission [34] and occurs in the range between 471-520 nm. In present case the emission profile lacks of all these uranyl emission characteristics. Thus the presence of uranium in the form of uranyl is ruled out. So, now the broadened emission spectrum is an indicative of uranium ions experiencing a range of coordination geometries and environments and may stabilize in the form of  $UO_n$  ( $n$ = number of oxygen present at equatorial as well as axial position). Here, the coordination number at equatorial position is more likely to be 4 (as in  $UO_6^{6-}$ ) and/or lower than 7 (as in  $UO_9^{12-}$ ). However, the observed spectra closely resembles to  $UO_6^{6-}$  as reported in various literature [35-37]. Although uranium faces f-f parity forbidden charge transfer transition issues but the involvement of vibronic coupling of 5f-t<sub>1u</sub> with ungerade vibrational modes of  $UO_6^{6-}$  octahedron facilitates relaxation.

The excitation spectrum of the  $BaAl_2B_2O_7: U$  monitored at 550 nm emission is shown in Figure 6B.4. The spectrum exhibits a broad band in the region 220–300 nm peaking at 285 nm, which is ascribed to charge transfer from oxygen (2p) to uranium (6d) orbitals. In addition to this, excitation peak at around 434 nm is due to hexavalent uranium. Although the PL studies confirms the stabilization of uranium in the form of  $UO_6^{6-}$  but there is no strong clue about the site occupancy. As, Ba exists as an octahedra  $BaO_6$  in  $BaAl_2B_2O_7$  moiety, uranium may prefer to reside in Ba regular sites rather than  $Al^{3+}$  sites which remains as  $AlO_4$  tetrahedra structure. As discussed earlier the ionic radii of host ions ( $Ba^{2+}$ ,  $Al^{3+}$ ) are also not in good agreement with ionic radii of dopant ion ( $U^{(vi)}$ ). There is a huge

difference in the oxidation states of host ions and dopant ion too. In this regard luminescence decay time studies are of great importance.

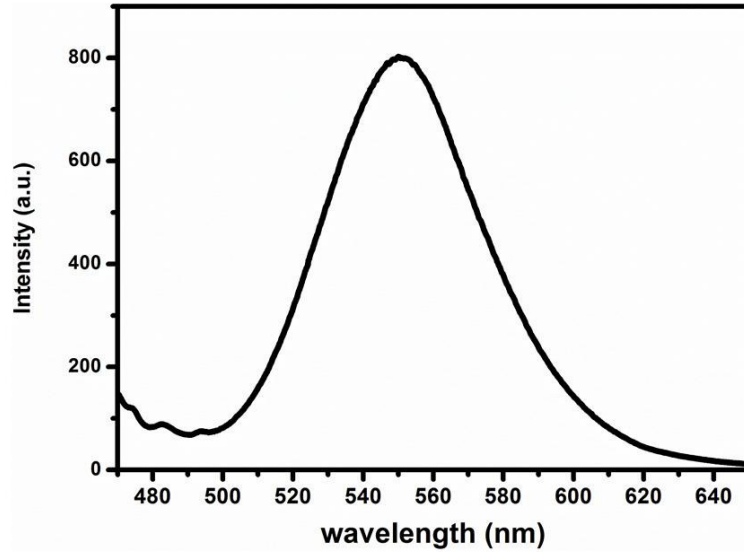


**Figure 6B.3: PL emission spectra of the BaAl<sub>2</sub>B<sub>2</sub>O<sub>7</sub>: U system at an excitation wavelength of 285nm**

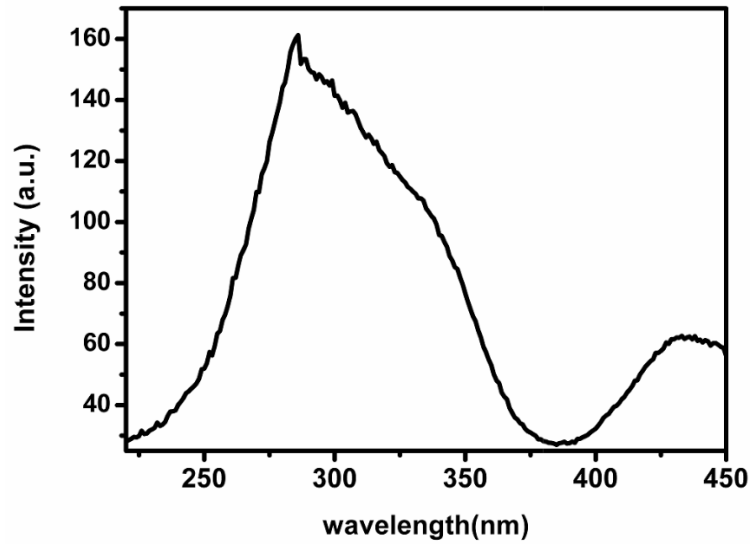


**Figure 6B.4: PL excitation spectra of the BaAl<sub>2</sub>B<sub>2</sub>O<sub>7</sub>: U system at an emission wavelength of 550nm**

### **6B.3.3 PL decay time studies:**

Here luminescence decay time measurements were carried out by exciting the sample at 285 nm and monitoring emission at 550 nm. The life-time/decay curve is shown in Figure 6B.5 and it was observed that the curve could be fitted as bi-exponential decay:  $I(t) = A_1 \exp(-t/\tau_1) + A_2 \exp(-t/\tau_2) + y_0$  where  $A_1$  and  $A_2$  are pre-exponential factors and are scalar quantities, 't' is the time of measurement and  $\tau_1$  and  $\tau_2$  are the decay time values. The PL decay time values for  $\text{BaAl}_2\text{B}_2\text{O}_7: \text{U}$  were observed to be  $\tau_1 = 24 \mu\text{s}$  (65%) and  $\tau_2 = 86 \mu\text{s}$  (35 %). The double decay time values suggest the presence of uranate ions at sites with two different types of surrounding environment. Here there are two possibilities. First one is the uneven distribution of defect centres around the uranium ion i.e. the one surrounded with more defect centres may result in smaller decay time values through non radiative relaxation. Secondly the double decay time may be presenting two different lattice sites occupied by uranium i.e. regular lattice sites of Al and Ba ions. As Ba ion possesses an octahedral geometry, uranium may experience a better symmetric coordination environment compared to tetrahedral environment of Al ion and thus uranium placed at Ba site may decay slower than the uranium placed at Al site owing to symmetry forbidden rules. Information from PL and PL decay time studies are not corroborating each other and thus investigation of site occupancy of uranium in  $\text{BaAl}_2\text{B}_2\text{O}_7$  remains interesting for further studies.

#### 6B.4. EXAFS studies on BaAl<sub>2</sub>B<sub>2</sub>O<sub>7</sub>: U

##### 6B.4.1 Ba L<sub>3</sub> edge:

Figure 6B.6 shows the XANES spectra of the BaAl<sub>2</sub>B<sub>2</sub>O<sub>7</sub> and U doped BaAl<sub>2</sub>B<sub>2</sub>O<sub>7</sub> samples at Ba L<sub>3</sub> edge. The XANES spectra do not show any significant change except a small increase in the white line intensity for the U doped BaAl<sub>2</sub>B<sub>2</sub>O<sub>7</sub> sample. The EXAFS oscillations have been extracted from the absorption spectra following the standard procedure [38, 39]. The  $\chi(k)$  function is weighted by  $k^2$  to amplify the oscillations at high  $k$  and the functions  $\chi(k)k^2$  are Fourier transformed in  $r$  space to generate the  $\chi(r)$  versus  $r$  plots (or FT-EXAFS spectra) in terms

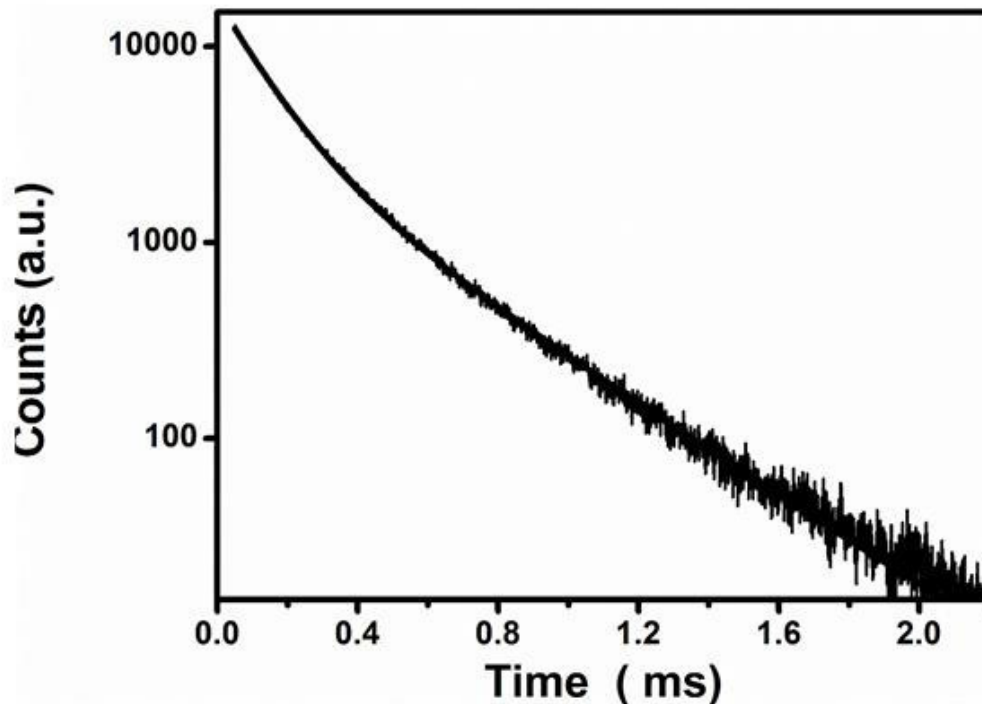
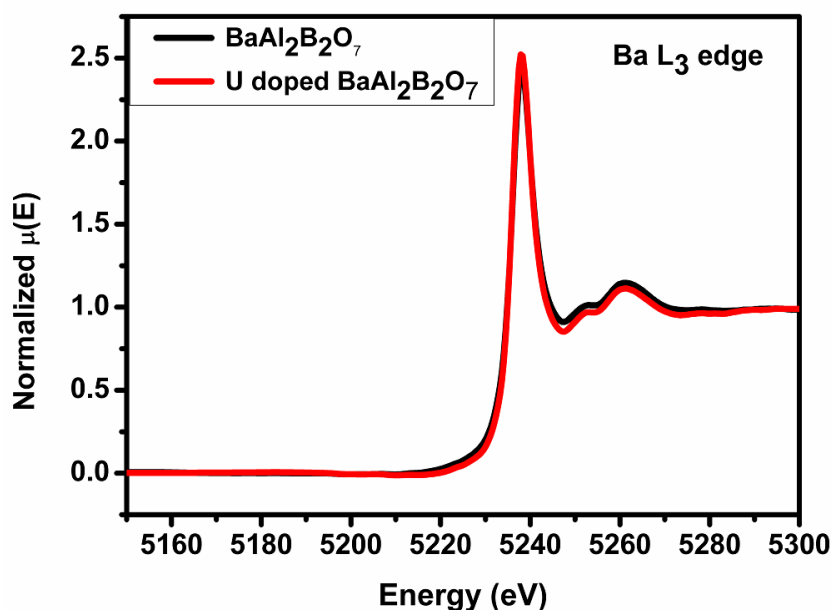


Figure 6B.5: PL decay curve of the BaAl<sub>2</sub>B<sub>2</sub>O<sub>7</sub>: U system at an  $\lambda_{\text{emission}}$  of 550 nm and  $\lambda_{\text{excitation}}$  of 285 nm

of the real distances from the center of the absorbing atom. The  $k$  range used for Fourier Transform is 2-8.5  $\text{\AA}^{-1}$ , the short  $k$  range is due to the appearance of Ba  $L_2$  edge at 5624 eV which is at a difference of 377 eV from the  $L_3$  edge (5247 eV). EXAFS Data Analysis program Athena and Artemis in the Demeter software package has been used for data processing and data fitting respectively [40].



**Figure 6B.6: XANES spectra of the  $\text{BaAl}_2\text{B}_2\text{O}_7$  and U doped  $\text{BaAl}_2\text{B}_2\text{O}_7$  samples at Ba  $L_3$  edge**

The  $\chi(r)$  versus  $r$  plots of the  $\text{BaAl}_2\text{B}_2\text{O}_7$  and U doped  $\text{BaAl}_2\text{B}_2\text{O}_7$  samples at Ba  $L_3$  edge have been shown in Figure 6B.7. The  $\chi(r)$  versus  $r$  data has been fitted from 1.5- 2.8  $\text{\AA}$  assuming two Ba-O paths at 2.75  $\text{\AA}$  ( $\times 6$ ) and 3.25  $\text{\AA}$  ( $\times 6$ ) following the crystal structure of  $\text{BaAl}_2\text{B}_2\text{O}_7$  [41]. The theoretical fits following this procedure has been plotted in Fig. 7 and the fitting results have been tabulated in Table 6B.1. From the results, it can be observed that the Ba-O bond length decreases on U doping. From figure 6B.7 it is also evident that

the intensity of the peak near 3.2 Å (phase uncorrected) which corresponds to Ba-Al coordination shell at 3.75 Å according to BaAl<sub>2</sub>B<sub>2</sub>O<sub>7</sub> crystal structure, increases on U doping. The increase in the intensity

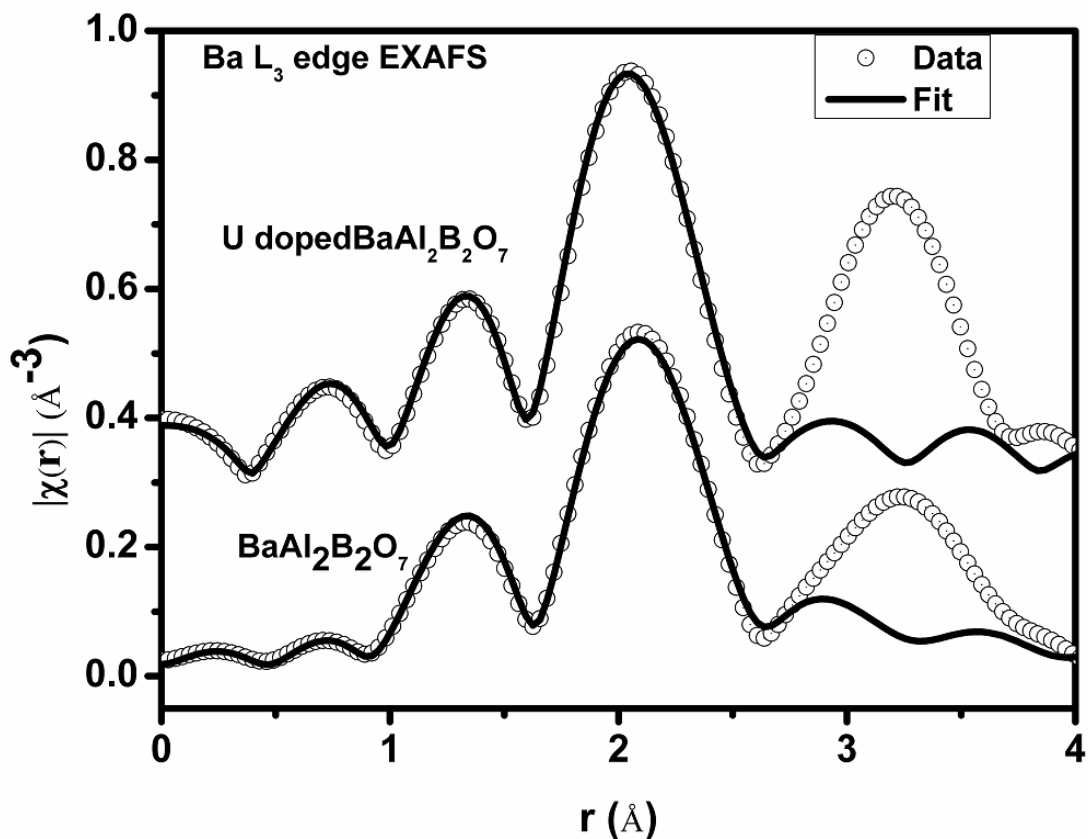


**Figure 6B.7:**  $\chi(r)$  versus  $r$  plots of BaAl<sub>2</sub>B<sub>2</sub>O<sub>7</sub> and U doped BaAl<sub>2</sub>B<sub>2</sub>O<sub>7</sub> samples at Ba L<sub>3</sub> edge

of this peak may be attributed to the replacement of Al with U. Since the atomic number of U (92) is much higher than that of Al (13), therefore the scattering amplitude of U is much higher compared to Al which may result in an increase of peak intensity. Also, the ionic radius of U (0.87 Å) is higher than that of Al (0.675 Å), therefore the replacement of Al with a larger ion like U may result in shortening of nearby bonds as has been observed for

Ba-O bonds. It should be noted that due to the short  $k$  range ( $2-8.5 \text{ \AA}^{-1}$ ) of the data, the  $\chi(r)$  versus  $r$  data has been fitted only up to the first shell.

**Table 6B.1: EXAFS Results of Ba L<sub>3</sub> edge**

	<i>BaAl<sub>2</sub>B<sub>2</sub>O<sub>7</sub></i>			<i>U doped BaAl<sub>2</sub>B<sub>2</sub>O<sub>7</sub></i>		
	$r(\text{\AA})$	$N$	$\sigma^2$	$r(\text{\AA})$	$N$	$\sigma^2$
<i>Ba-O1</i>	$2.78 \pm 0.02$	$6.0 \pm 0.1$	$0.0125 \pm 0.0008$	$2.71 \pm 0.02$	$6.8 \pm 1.2$	$0.0125 \pm 0.0005$
<i>Ba-O2</i>	$3.17 \pm 0.01$	$6.0 \pm 0.1$	$0.0225 \pm 0.0005$	$3.12 \pm 0.03$	$5.3 \pm 0.8$	$0.0223 \pm 0.0007$

**6B.4.2 U L<sub>3</sub> edge:**

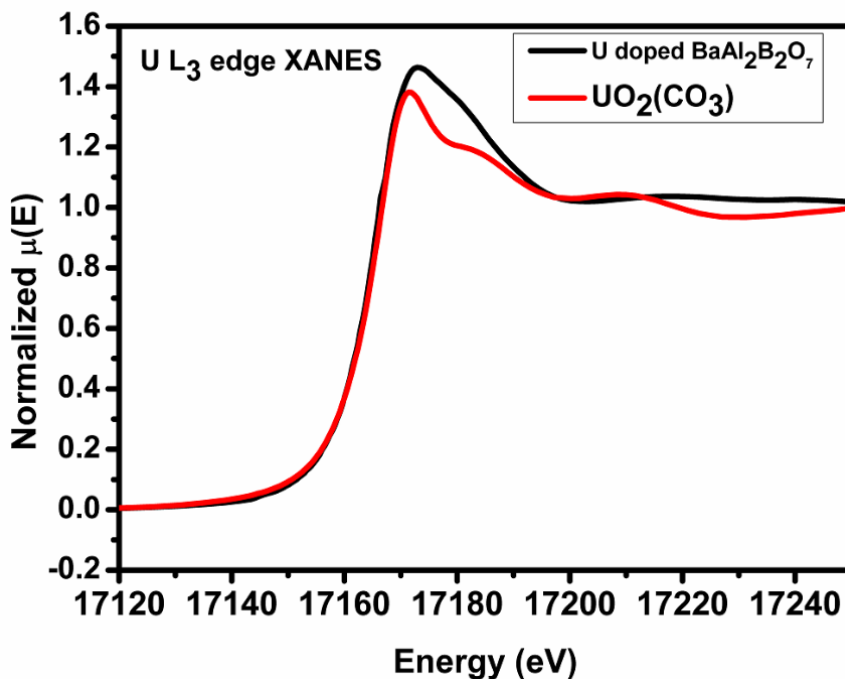


**Figure 6B.8: XANES spectra of the U doped BaAl<sub>2</sub>B<sub>2</sub>O<sub>7</sub> sample at U L<sub>3</sub> edge along with UO<sub>2</sub>CO<sub>3</sub> standard**

Figure 6B.8 shows the XANES spectra of the U doped  $\text{BaAl}_2\text{B}_2\text{O}_7$  sample at U  $L_3$  edge along with  $\text{UO}_2\text{CO}_3$  standard where U cations exist in +6 oxidation state. From the XANES spectra it is evident that U cations exist in +6 oxidation state in the U doped  $\text{BaAl}_2\text{B}_2\text{O}_7$  sample. Figure 6B. 9 shows the  $\chi(r)$  versus  $r$  plots (or FT-EXAFS spectra) of the U doped  $\text{BaAl}_2\text{B}_2\text{O}_7$  sample at U  $L_3$  edge. The FT-EXAFS spectrum is extracted from the EXAFS spectra using the Fourier transform  $k$  range of  $2\text{-}9 \text{ \AA}^{-1}$  and is fitted in the  $r$  range of  $1\text{-}2.5 \text{ \AA}$  using an axial U-O shell with coordination 2 and an equatorial U-O shell with coordination of 4 following the Uranate structure as predicted from Photoluminescence measurements done on the samples.

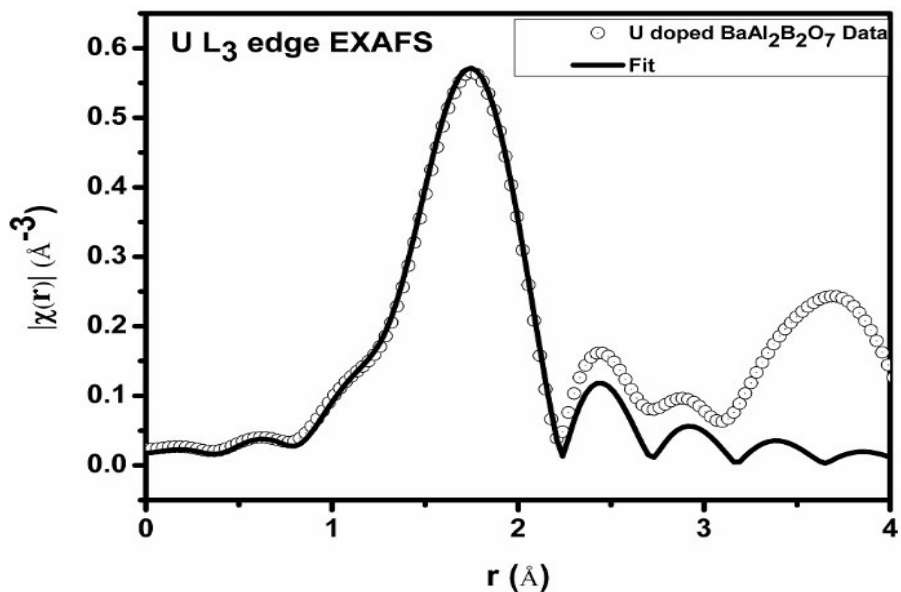


**Figure 6B.9:**  $\chi(r)$  versus  $r$  plots (or FT-EXAFS spectra) of the U doped  $\text{BaAl}_2\text{B}_2\text{O}_7$  sample at U  $L_3$  edge

**Table 6B.2: EXAFS Results of U L<sub>3</sub> edge**

U doped BaAl <sub>2</sub> B <sub>2</sub> O <sub>7</sub>			
	r(Å)	N	σ <sup>2</sup>
U-O <sub>ax</sub>	1.89±0.02	2	0.0095±0.0008
U-O <sub>eq</sub>	2.27±0.01	4.1±0.1	0.0022±0.0006

The coordination number of the axial U-O path is kept fixed, while all other parameters of the axial and equatorial U-O paths are varied during the fitting. The experimental data along with the best theoretical fit following the above mentioned procedure have been plotted in Fig. 6B.9 and the EXAFS fitting results are tabulated in Table 6B.2. From the EXAFS fitting results (Table 6B.2) it is evident that the two axial oxygen atoms exist at a bond distance of 1.89 Å and four equatorial oxygens exist at a distance of 2.27 Å around U cations which is consistent with Uranate structure [42, 43]. So, it is evident From the EXAFS results that there is a possibility of U replacing Al in the BaAl<sub>2</sub>B<sub>2</sub>O<sub>7</sub> lattice. However, the U L<sub>3</sub> edge EXAFS results suggest that U cations exists in distorted octahedral geometry as Uranate in the lattice. Therefore, from the EXAFS analysis at both Ba and U L<sub>3</sub> edge, it appears that though U replace the tetrahedral coordinated Al, but it rearranges its local environment as distorted octahedral geometry of the Uranate structure.

### **6B.5 Conclusion:**

Uranium doped BaAl<sub>2</sub>B<sub>2</sub>O<sub>7</sub> is successfully synthesized by solution combustion synthesis method and it is validated by PXRD studies. The PL studies have shown that BaAl<sub>2</sub>B<sub>2</sub>O<sub>7</sub> host matrix is an ideal matrix for uranium luminescence studies as uranium gets stabilized

in this host as uranate ( $\text{UO}_6^{6-}$ ). This host matrix offers two different environments (with respect to defect centres) for uranium stabilization which is understood from PL life time measurement indicating two lifetime values of 24  $\mu\text{s}$  (65%) and 86  $\mu\text{s}$  (35 %). Further investigations using EXAFS inferred the site occupancy of uranium in  $\text{BaAl}_2\text{B}_2\text{O}_7$ . The regular  $\text{Al}^{3+}$  site is the preferred site for uranium in this matrix.

### **6B.6 References:**

1. J.S. Benitez, A. Andres, M. Marchal, E. Cordoncillo, M.V. Regi, P.J. Escribano, *J. SolidState Chem.* 171 (2003) 273-277.
2. T.R.N. Kutty, *Mater. Res. Bull.* 25 (1990) 343–348.
3. L. Tian, B.Y. Yu, C.H. Pyun, H.L. Park, S. Mho, *Solid State Commun.* 129 (2004) 43–46.
4. D. A. Keszler, *Curr. Opinion Solid State Mater. Sci.* 1, (1996) 204-211.
5. R.S. Palaspagar, A.B. Gawande, R.P. Sonekar, S.K. Omanwar, *Optik* 126 (2015) 5030–5032.
6. F. Lucas, S. Jaulmes, M. Quarton, T.L. Mercier, F. Guillen, C.J. Fouassier, *SolidState Chem.* 150 (2000) 404–409.
7. H. You, G. Hong, *Mater. Res. Bull.* 32 (1997) 785–790.
8. R. Jagannathan, R.P. Rao, T.R.N. Kutty, *Mater. Res. Bull.* 27 (1992) 459–466.
9. Z. Ren, C. Tao, H. yang, S. Feng, *Mater. Lett.* 61 (2007) 1654-1657.
10. K.H. Hubner, *N. Jb. Miner. Abh.* 112 (2) (1970) 150
11. N. Ye, W.R. Zeng, B.C. Wu, X.Y. Huang, C.T. Chen, *Z. Kristallogr. NCS* 213 (1998) 452.

12. İ. Pekgözlü, S. Seyyidoğlu, S. Taşcıoğlu, J. Lumin. 128 (2008) 1541–1543.
13. S.J. Camardello, P.J. Toscano, M.G. Brik, A.M. Srivastava, Opt. Mater. 37 (2014) 404–409.
14. A.E. Ringwood, S.E. Kesson, N.G. Ware, W. Hibberson, A. Major, Nature 278 (1979) 219–223.
15. K.E. Sickafus, H. Matzke, T. Hartmann, K. Yasuda, J.A. Valdez, P. Chodak III, M. Nastasi, R.A. Verrall, J. Nucl. Mater. 274 (1999) 66–77.
16. S.V. Stefanovsky, A.G. Ptashkin, O.A. Knyazev, S.A. Dmitriev, S.V. Yudintsev, B.S. Nikonov, J. Alloys Compd. 444–445 (2007) 438–442.
17. K.E. Sickafus, R.W. Grimes, J.A. Valdez, A. Cleave, M. Tang, M. Ishimaru, S.M. Corish, C.R. Stanek, B.P. Uberuaga, Nat. Mater. 6 (2007) 217–223.
18. R.C. Ewing, W.J. Weber, J. Lian, J. Appl. Phys. 95 (2004) 5949–5971.
19. M.L. Carter, A.L. Gillen, K. Olufson, E.R. Vance, J. Am. Ceram. Soc. 92 (2009) 1112–1117.
20. P. A. Tanner, P.Zhi-Wu, L. Jun, L. Yulong, S. Qiang, J. Phys. Chem. Solids 58 (7) (1997) 1143–1146.
21. T.K.Seshagiri, M.Mohapatra, T.K.GunduRao, R.M.Kadam, V.Natarajan, S.V.Godbole, J. Phys. Chem. Solids 70 (2009) 1261–1266.
22. M. Mohapatra, B. Rajeswari, R.M. Kadam, M. Kumar, T.K. Seshagiri, N.K. Porwal, S.V. Godbole, V. Natarajan, J. Alloys Compd. 611 (2014) 74–81.
23. G. Blasse, K.C. Bleijenberg, D.M. Krol, J. Lumin. 18/19 (1979) 57–62.
24. R.N. Shehelokov, G.T. Bolotova, G.T. Soviet, J. Coord. Chem. 4 (1978) 343–349.

25. M. E. Azenha and G. Blasse, *J. Alloys Compd.* 196 (1993) 81-85.
26. P.A. Tanner, *J. Mol. Struct.* 355 (1995) 299–302.
27. A.F. Leung, L. Hayashibara, J. Spadaro, *J. Phys. Chem. Solids* 60 (1999) 299–304
28. C.D. Flint, P.A. Tanner, *Mol. Phys.* 53 (1984) 801–811.
29. A Lupei and V Lupei, *J. Phys. C: Solid State Phys.*, Vol. 12, (1979) 1123-1130.
30. A. K. Poswal, A. Agrawal, A. K. Yadav, C. Nayak, S. Basu, S. R. Kane, C. K. Garg, D. Bhattacharyya, S. N. Jha and N. K. Sahoo. *AIP Conf. Proc.* 1591 (2014) 649.
31. S. Basu, C. Nayak, A. K. Yadav, A. Agrawal, A. K. Poswal, D. Bhattacharyya, S. N. Jha and N. K. Sahoo. *J. Phys.: Conf. Ser.* 493 (2014) 012032.
32. H. Gobrecht, W. Weiss, *Z. Phys.* 140(1955)139.
33. G. Blasse, *J. Electrochem. Soc.* 115(1968)738.
34. P.A. Tanner, *Spectrochim. Acta* 46A (1990) 1259–1262.
35. G. Blasse, K.C. Bleijenberg, D.M. Krol, *J. Lumin* 18 (19) (1979) 57–62.
36. K.C. Bleijenberg, *Struct. Bond.* 42 (1980) 97–128.
37. M.E. Azenha, D.V. Voort, G. Blasse, *J. Solid State Chem.* 101 (1992) 190–194.
38. Konigsberger, D.C., and R. Prince. *X ray Absorption: Principles, Applications, Techniques of EXAFS, SEXAFS and XANES.* Wiley, New York, 1988.
39. S.D. Kelly, D. Hesterberg, B. Ravel, 2008. Analysis of soils and minerals using X-ray absorption spectroscopy, in *Methods of Soil Analysis, Part 5–Mineralogical methods*; A.L. Ulery, L.R. Drees, Eds.; Soil Science Society of America: Madison, WI, USA,

2008; 367.

40. B. Ravel and M. Newville. *Journal of Synchrotron Radiation* 12 (2005) 537–541.

41. N. Ye, W. R. Zeng, B. C. Wu, X. Y. Huang and C. T. Chen. *Zeitschrift fuer Kristallographie - New Crystal Structures* 213 (1998), 452.

42. Sven Van den Berghe, M. Verwerft, J. P. Laval, B. Gaudreau, P. G. Allen and A. Van Wyngarden. *Journal of Solid State Chemistry* **166** (2002), 320-329

43. Loopstra B. O.; Rietveld H. M. The Structure of Some Alkaline-Earth Metal Uranates. *Acta Crystallogr.* 1969, B25, 787–791.



# **Chapter 7**

## **Summary and Conclusions**



## **7.1 Introduction**

This chapter presents a summary of all the works discussed in preceding chapters. This concluding chapter also discusses the future perspectives which stem out from this research work. This thesis presents luminescence studies of uranium in various solid matrices. These solid matrices include alkaline earth borophosphates, barium borate and barium aluminium borate matrices. All these matrices (doped and undoped) were characterized in order to observe the phase purity as well as morphology studies. The luminescence studies were carried out with an aim to observe the PL characteristics of dopant ion (uranium) such as excitation, emission and decay time values that indirectly informs about the feasibility of photo luminescence process in that particular matrix as PL process is associated with both radiative as well as non-radiative decay processes. The life time decay values of uranium ion in different systems were studied carefully in order to probe the effect of surrounding lattice as well as defects. The analysis of PL spectra were used for speciation of uranium in different matrices. EXAFs studies were carried out and found very useful in order to determine the site occupancy of uranium. This also gives an insight in to the local coordination environment of uranium. All these studied matrices were found to be ideal phosphors for uranium luminescence.

## **7.2. Summary and Conclusions**

The alkaline earth borophosphates were found to be potential enough for accommodating uranium in their host lattice. The conventional solid state synthesis route was followed for synthesis of both uranium doped and undoped alkaline earth borophosphate samples. The PXRD datas confirmed the correct phase formation. Photo luminescence studies including

lifetime decay studies revealed the oxidation state as well as form of stabilization of uranium in corresponding matrices.

In case of SrBPO<sub>5</sub>: U system, Photoluminescence (PL) studies confirmed the stabilisation of uranium as uranyl ion (UO<sub>2</sub><sup>2+</sup>) in the system. Based on the PL emission data concentration quenching was observed beyond 7 mol% of the uranyl ion concentration. The critical distance ( $L_c$ ) was estimated to be 3Å suggesting Dexter type of energy transfer mechanism responsible for the quenching. The life time decay studies indicated the presence of two different types of environment around Uranyl ion. The effect of annealing temperature was also studied. On annealing at temperatures beyond 900°C the PL emission and decay time reduced drastically. It was concluded that on annealing at temperatures beyond 900°C, defect centres get agglomerated around the metal ion providing non radiative pathways for the energy to get dissipated thereby reducing the PL emission and decay time. Color coordinates were evaluated for the 7 mol% uranium doped sample annealed at 900°C and it was found that SrBPO<sub>5</sub>: U is a potential green emitting phosphor. The various oxidation state as well as different forms of stabilization of uranium fascinated us to explore different host lattices i.e. other alkaline earth (calcium, strontium and barium) based borophosphates. XRD measurements confirmed the single phase formation of uranium doped alkaline earth boro phosphate samples. The PL of uranium in calcium and barium borophosphate is studied for the first time. Photoluminescence studies indicated presence of uranium as Uranyl in SrBPO<sub>5</sub> and CaBPO<sub>5</sub> matrices whereas in case of BaBPO<sub>5</sub> the indication was for uranate species. The life time data corroborated presence of a different uranium species in SrBPO<sub>5</sub>, CaBPO<sub>5</sub> and BaBPO<sub>5</sub>. The site occupancy of uranium

was further probed using EXAFS which confirmed that in case of SrBPO<sub>5</sub> and CaBPO<sub>5</sub>, uranium enters as Uranyl whereas in BaBPO<sub>5</sub>, uranium enters in to the host as uranate irrespective of greater ionic radii of Ba<sup>2+</sup> ion.

In order to understand the luminescence behaviour of uranium with its co-dopant i.e. rare earths like europium and samarium, phosphors like SrBPO<sub>5</sub>: U, Eu and SrBPO<sub>5</sub>: U, Sm were investigated. It was observed that while 'Eu and Sm' were stabilised in its trivalent state and uranium was stabilised as the uranyl ion (UO<sub>2</sub><sup>2+</sup>) in this host. Detailed mechanism for the observed energy transfer from uranium to europium and samarium were studied separately using emission, excitation and photoluminescence decay time measurements. In the co-doped systems, Uranyl ion was observed to be the donor whereas europium and samarium ions were observed to be acceptor ions. In these systems the energy transfer process was found to be of Dexter type. Optimum dopant ion concentrations were evaluated for maximising this energy transfer whose efficiency was calculated to be 80 % and 82% for SBP: U, Eu and SBP: U, Sm systems respectively.

Borate matrices were also investigated for uranium luminescence. Uranium doped BaB<sub>2</sub>O<sub>4</sub> samples were prepared via co-precipitation route. XRD studies were carried out to find the phase purity of synthesized samples. It was observed that dopant uranium did not affect the crystal structure of BaB<sub>2</sub>O<sub>4</sub> system significantly. Synthesis through co-precipitation route resulted with a morphology of uneven, agglomerated particles with less than 1 μm individual particle size, which was observed in SEM analysis. PL studies confirmed the stabilisation of uranium as UO<sub>6</sub><sup>6-</sup> in the system. The life time decay studies revealed a shorter single life time value, indicating asymmetric site symmetry surrounding the

uranium ion in  $\text{BaB}_2\text{O}_4$ . The CIE indices for this system suggested that the material is a potential green emitting phosphor.

Uranium doped  $\text{BaAl}_2\text{B}_2\text{O}_7$  phosphors were synthesized through solution combustion synthesis method. The luminescence studies indicated suitability of this alumino borate matrix to stabilize uranium as uranate ( $\text{UO}_6^{6-}$ ). The uranium life time values suggested uranium to be surrounded by two different environments with varied/different defect concentrations. The site occupancy of uranium in  $\text{BaAl}_2\text{B}_2\text{O}_7$  was probed through EXAFS studies. It was observed that the preferred sites for uranium incorporation is the  $\text{Al}^{3+}$  regular lattice sites, irrespective of greater ionic radii of  $\text{Ba}^{2+}$  sites.

### **7.3 Scope of future work:**

Based on the information obtained from the present studies, the borophosphate as well as alumino borate matrices can be further studied for incorporation of radioactive wastes. In addition to this different types of ceramic as well as glass matrices can be explored for uranium luminescence. Towards this following studies can be carried out.

- 1) Probing the effect of radiation damage on the structure of  $\text{MBPO}_5: \text{U}$ ,  $\text{BaAl}_2\text{B}_2\text{O}_7: \text{U}$  systems.
- 2) Investigation of uranium luminescence in phosphate based glasses.
- 3) Luminescence studies of uranium in oxide based ceramics.
- 4) Investigation of uranium luminescence and its site occupancy in silicates with apatite-related structure.
- 5) Temperature dependent photo luminescence properties of uranium in  $\text{MBPO}_5: \text{U}$ ,  $\text{BaAl}_2\text{B}_2\text{O}_7: \text{U}$  and  $\text{BaB}_2\text{O}_4: \text{U}$  systems.

## Glossary

<b>Abbreviation</b>	<b>Full name</b>
PL	Photo Luminescence
WLED	White Light Emitting Diodes
EXAFS	Extended X-ray Absorption Fine Structure
DCM	Double Crystal Monochromator
LMCT	Ligand to Metal Charge Transfer
NLO	Nonlinear Optical Material
XAS	X-ray Absorption Structure
XANES	X-ray Near Edge Structure
SEM	Scanning Electron Microscope